STUDIES OF EXTRA FRAGMENTS OF THE CYTOCHROME *BC*$_1$ COMPLEX FROM *RHODOBACTER SPHAEROIDES* AND THE INTERACTION BETWEEN CYTOCHROME CAA$_3$ AND F$_1$F$_0$-ATP SYNTHASE FROM ALKALIPHILIC *BACILLUS PSEUDOFIRMUS* OF$_4$

XIAOYING LIU

Bachelor of Science
Lanzhou University
Lanzhou, Gansu, China
1996

Master of Science
Lanzhou University
Lanzhou, Gansu, China
1999

Submitted to the Faculty of the Graduate College
of the Oklahoma State University in partial
fulfillment of the requirements for the
DEGREE OF DOCTOR OF PHILOSOPHY
May, 2006

STUDIES OF EXTRA FRAGMENTS OF THE CYTOCHROME BC_1 COMPLEX FROM *RHODOBACTER SPHAEROIDES* AND THE INTERACTION BETWEEN CYTOCHROME CAA_3 AND F_1F_0-ATP SYNTHASE FROM ALKALIPHILIC *BACILLUS PSEUDOFIRMUS* OF_4

Thesis Approved:

Chang-an Yu
Thesis advisor

Linda Yu

Eldon C. Nelson

Richard C. Essenberg

Robert L. Burnaps

A. Gordon Emslie

Dean of the Graduate College

Acknowledgements

I would like to express my sincere appreciation to my advisor, Dr. Chang-An Yu for his intelligent supervision and guidance. I am also thankful to Dr. Linda Yu for her encouragement and motivation to my pursuit of knowledge in science. My appreciation extends to my other committee members Dr. Eldon C. Nelson, Dr. Richard Essenberg, Dr. Robert Burnap, whose guidance, assistance, encouragement are also invaluable. I would like to thank Dr. Di Xia (NIH) for his support.

Finally, I would like to give my very special appreciation to my parents, sister and my husband for their wonderful love, understanding, support, encouragement and guidance during my Ph.D study.

Table of Contents

List of Tables

List of Figures

Abbreviations

ADP	Adenosine diphosphate
ATP	Adenosine triphosphate
BSA	Bovine serum albumin
cyt	cytochrome
dam	DNA adenine methylation
DM (LM)	Dodecyl β-maltoside
DSC	Differential scanning calorimetry
E. coli	*Escherichia coli*
EPR	Electron paramagnetic resonance
HRP	Horseradish peroxide
ICM	Intra-cytoplasmic membrane
ISP	Rieske iron-sulfur protein
kDa	kilodaltons
kb	Kilo base pair
LB	Lennox L. Broth
MALDI-TOF	Matrix-assisted laser desorption ionization time-of flight
NAD	Nicotinamide adenine dinucleotide, oxidized form
NADH	Nicotinamide adenine dinucleotide, reduced form
NADP	Nicotinamide adenine dinucleotide phosphate, oxidized form

NADPH	Nicotinamide adenine dinucleotide phosphate, reduced form
Ni-NTA	Nickel-nitrilotriacetic acid
PAGE	Polyacrylamide gel electrophoresis
PCR	Polymerase chain reaction
PMSF	Phenylmethylsulfonyl fluoride
ppt	precipitate
psi	Pound per square inch
Q	ubiquinone
QH_2	ubiquinol
$Q_0C_{10}BrH_2$	2,3-dimethoxy-5-methyl-6-(10-bromodecyl)-1,4-benzoquinol
$Q_0C_{10}H_2$	2,3-dimethoxy-5-methyl-6-decyl-1,4-benzoquinol
QCR	Ubiquinol-cytochrome *c* reductase, bc_1 complex, complex III
rpm	Revolution per minute
R. sphaeroides	*Rhodobacter sphaeroides*
SDS	Sodium dodecyl sulfide
Tris	Tris (hydroxymethyl) aminomethane
UHDBT	5-n-undecyl-6-hydroxy-4,7-dioxobenzothiazole

Chapter I

Introduction

Cytochrome *bc* complexes in Respiration and Photosynthesis

Ubiquinol-cytochrome *c* oxidoreductase, also known as complex III or cytochrome bc_1 complex, which belongs to the superfamily of '*bc* complexes', is present in the inner membrane of the mitochondria (Fig. 1) or in the cytoplasmic membrane of many bacteria (1-5). Cytochrome bc_1 complex, the central component of the energy-conserving electron transfer pathway for their respiration or photosynthesis, catalyzes electron transfer from ubiquinol to soluble *c*-type cytochromes (cyt*c* in mitochondria, cytc_2 in some bacteria) with concomitant generation of a proton gradient and membrane potential, which is referred to as proton motive force (pmf). The proton motive force is the driving force for synthesis of ATP by the complex V (F_1F_0-ATP synthase) (Fig. 1) in the inner mitochondria membrane.

All cytochrome bc_1 complexes contain three core subunits, cytochrome *b*, cytochrome c_1, and Reiske iron-sulfur protein (ISP), which house two *b*-type hemes (b_L and b_H), one *c*-type heme (heme c_1), and a high potential [2Fe-2S] cluster (6), respectively.

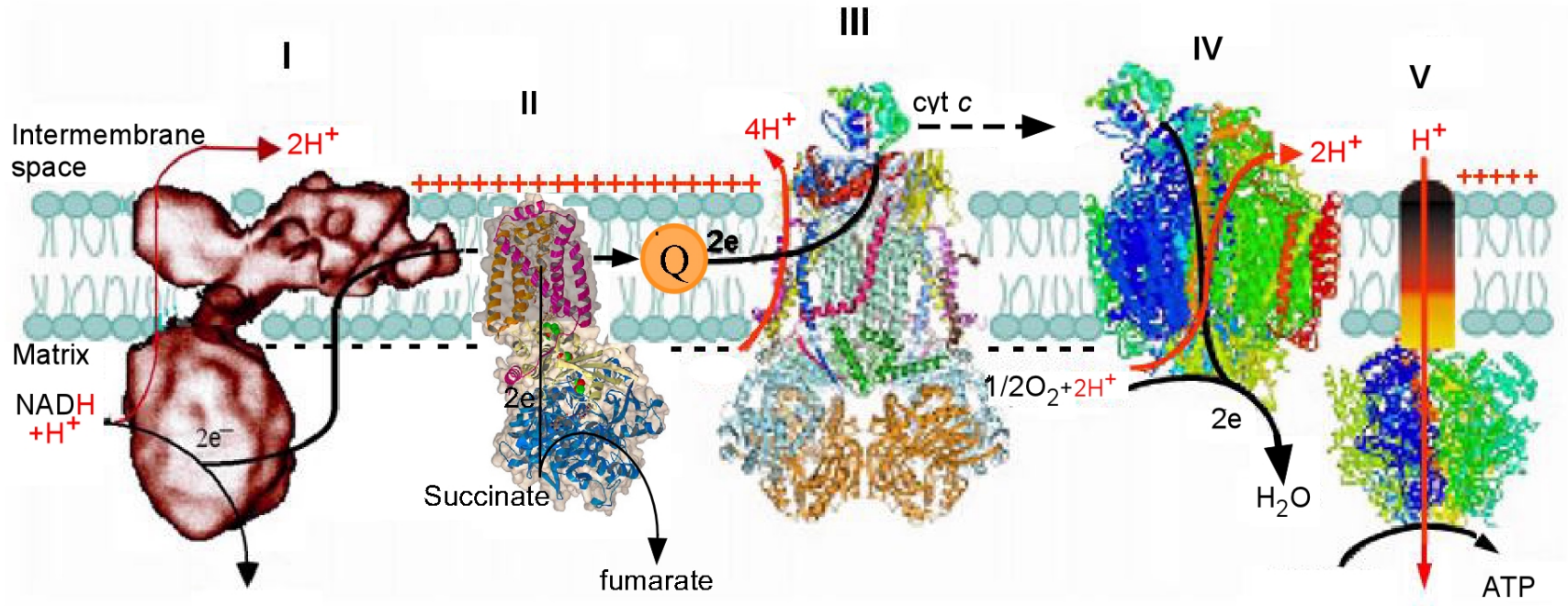

Fig.1. Mitochondrial electron transfer chain.

In mitochondria, the cytochrome bc_1 complex is a part of the respiratory electron transport chain. The electrons derived from glucose and fatty acids oxidation are transferred to the NAD^+ and FAD to form NADH and $FADH_2$ in the reactions catalyzed by the glycolytic enzymes, β-oxidation enzymes and the citric acid cycle enzymes (Fig.2.). The electrons, from reoxidation of NADH and $FADH_2$, pass through the electron-transport chain, composed of four complexes: NADH-ubiquinol reductase (complex I) (7) (Fig.1.), succinate-ubiqinol reductase (complex II), ubiquinol-cytochrome *c* reductase (complex III or cytochrome bc_1 complex), and cytochrome *c* oxidase (complex IV), to generate the pmf as mentioned above.

In addition to the respiratory system, the cytochrome bc_1 complex is also found in the electron transport system of purple photosynthetic bacterium. In the facultative photosynthetic purple nonsulfur bacterium *Rhodobacter sphaeroides*, the first steps of the conversion of light into chemical energy are accomplished by a cyclic electron transfer system, which generates a proton gradient across the chromatophore membrane. Photo-induced cyclic electron transfer involves two large transmembrane multiprotein complexes, the reaction center (RC) and the cytochrome bc_1 complex, functionally connected through redox reactions of quinone in the lipid phase and of a water soluble protein (cytochrome c_2) in the periplasmic phase (8). Absorption of one photon leads to photo-oxidation of the primary electron donor, P870 (a bacteriochlorophyll), of the RC, which delivers an electron through a bacteriopheophytin to the primary quinone acceptor Q_A. The electron is then transferred inside the reaction center to the secondary quinone acceptor Q_B, which, equilibrates with the Q-pool in the membrane following its full reduction and protonation to QH_2 after accepting two electrons. The QH_2 now serves as

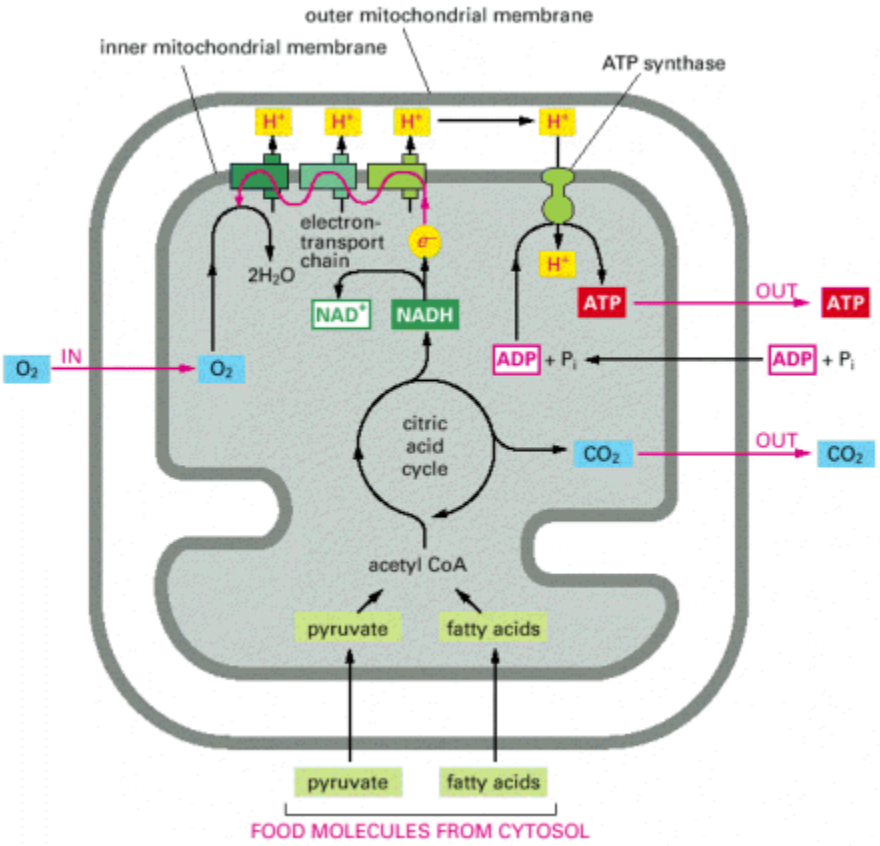

Fig.2. A summary of energy-generating metabolism in mitochondria(9).

the substrate for the cytochrome bc_1 complex reaction. Same as in the mitochondrial bc_1 complex, for every mole of QH_2 that is oxidized, two moles of cytochrome c_2 are reduced, and four moles of proton are translocated across the membrane. The cycle is completed by re-reduction of the photo-oxidized P870 by reduced cytochrome c_2 (10). In many other purple bacteria, like *Rhodopseudomonas viridis*, a RC-bound tetraheme cytochrome c, containing two high-potential and two low-potential hemes, acts as the immediate electron donor to P870 (10) (Fig. 3). Therefore, in the cyclic pathway, there is no exogenous electron donor or a final electron acceptor. Electrons continuously recycle between the reaction center and the bc_1 complex with light energy serving as the driving force, resulting protons pumped across the membrane to form the proton motive force.

The cytochrome b_6f complex, plastoquinol-plastocyanin oxidoreductase, which also belongs to superfamily of *bc* complex, functions in the electron transport chains of oxygenic photosynthesis carried out by algae, *Chlamydomonas reinhardtii* (11), thermophilic cyanobacteria, *Mastigocladus laminosus* (12) and higher plants. The multisubunit b_6f membrane protein complex mediates electron transfer between the photosystem II, in which H_2O is the electron donor, and the photosystem I. Consistent with a basic paradigm of membrane energy transduction (13), electron transfer through the b_6f complex is coupled to proton translocation across the membrane. The transfer of protons across the b_6f complex, utilizing oxidation and reduction of lipophilic quinone, establishes a proton electrochemical potential gradient across the membrane that is negative on the stromal side and positive on the thylakoid lumenal side (14-18). The chloroplast b_6f complex is a dimer and comprised of 8–9 subunits (4–5 large and 3–4 small subunits) (20), with its four "large" subunit being cytochrome *f*, which contains

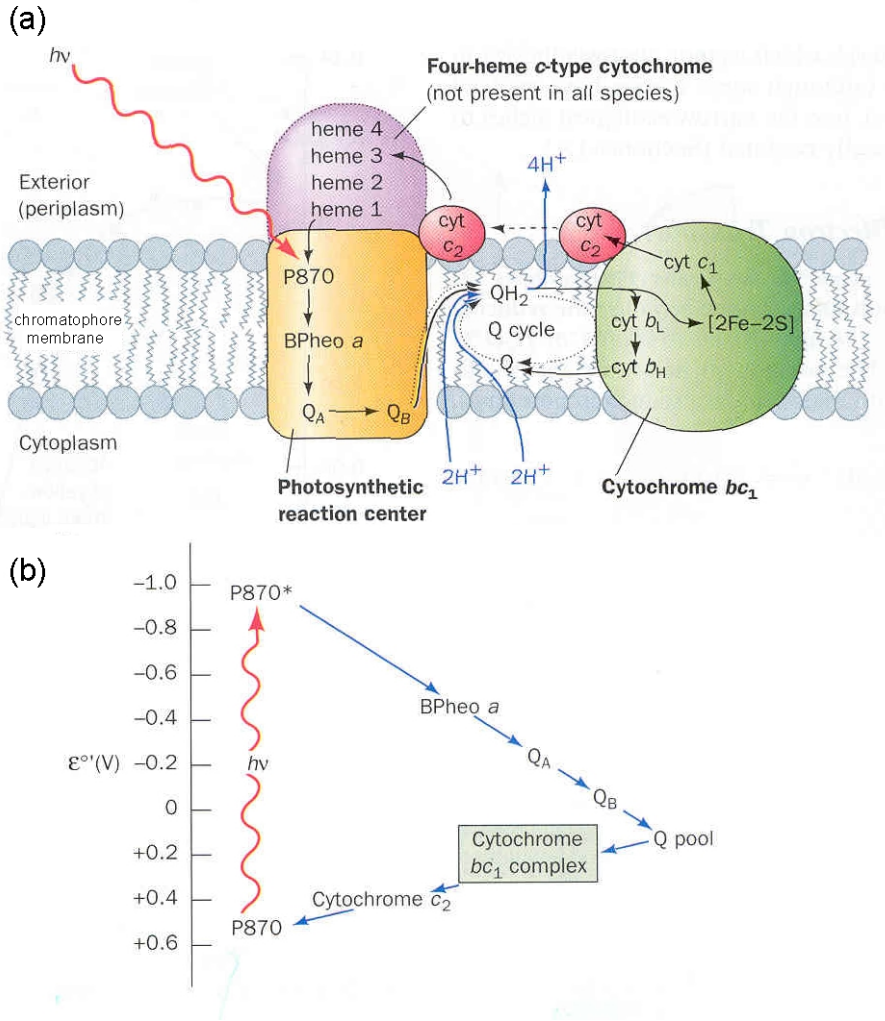

Fig.3. Photosynthetic electron-transport system of purple photosynthetic bacteria. (a) A schematic diagram indicating the arrangement of the system components in the bacterial plasma membrane and the flows of electrons (black arrows) and protons (blue arrows) that photon ($h\upsilon$) absorption promotes through them. (b) The approximate standard reduction potentials of the photosynthetic electron-transport system's various components (19).

one *c*-type heme, cytochrome b_6, which contains two *b*-type hemes, subunit IV, and a Rieske iron-sulfur protein which contains one [2Fe-2S] cluster. The cytochrome *b* of mitochondrial complex III is a fusion of chloroplast cytochrome b_6 and subunit IV. The cytochrome *b* subunit of the cytochrome b_6f complex corresponds to the N-terminal heme-bearing part of bc_1 complex's cytochrome *b* subunit, while a sequence similar to the C-terminal part presents in subunit IV (21,22). The Rieske iron-sulfur proteins in the two complexes are homologous and structurally similar. However, cytochrome *f* is unrelated to its counterpart in complex III, cytochrome c_1 although both are *c*-type cytochromes (19). Moreover, there are at least three small subunits in higher plant cytochrome b_6f, called PetA, PetM and PetL subunit (23-26).

The photosynthetic pathway occurring in chloroplast with cytochrome b_6f complexes is very complicated. There are two photosynthetic systems in this pathway, photosystem I (PSI) and photosystem II (PSII), the latter is equivalent to the reaction center in *R. sphaeroides*. In chloroplast, water is the electron donor for the photosynthesis. Electrons are released from a water splitting reaction mediated by a Mn-containing protein complex, and O_2 is also generated in this reaction. Plastoquinol (PQ), equivalent to ubiquinol, which is reduced in photosystem II, transfers an electron through the cytochrome b_6f complex to plastocyanin (PC), functional analog of cytochrome *c*. The reduce PC then transfers the electron to photosystem I, whose redox potential is low enough to reduce $NADP^+$. After being excited by light energy, photosystem I transfers the electron to $NADP^+$ and produces NADPH via an NADP reductase. Therefore, a strong electron donor (NADPH) is produced by this pathway in addition to generating the proton motive force. Alternatively, the electron may be returned to the cytochrome b_6f

complex in a cyclic process that only translocated protons into the thylakoid lumen (Fig.4.).

Proton-motive Q cycle

The proton-motive Q-cycle model (27, 28), which was first proposed by Mitchell (27) and modified later (7, 29, 30), has been favored for describing electron transfer, the proton translocation, the 2:1 H^+/e^- ratio and the "oxidant-induced reduction of cytochrome *b*" in the cytochrome bc_1 complex. There are two features for this Q-cycle mechanism (7, 29, 31, 32) (Fig.5.). (1) The presence of two separate ubiquinol/ubiquinone binding sites; an ubiquinol oxidation site (Qo) near the P (inter-membranes space) side of the mitochondrial inner membrane, and a ubiquinone reduction site (Qi) near the N (matrix) side. (2) The bifurcated electron transfer at the Qo site. The mechanism of ubiquinol oxidation at Qo site involves a divergent oxidation in which the ubiquinol at the Qo site is oxidized by ISP and cytochrome b_L (4, 33) either in a concerted mechanism (34-37) or in a sequential mechanism (38-42). In the concerted mechanism, oxidation of ubiquinone requires that both the iron-sulfur protein and cytochrome b_L be oxidized and that cytochrome b_L reduction precedes iron-sulfur protein reduction of cytochrome c_1 (36). In the sequential mechanism, the iron-sulfur protein oxidizes the quinol to semiquinone, which then reduces cytochrome b_L (Fig.5B). However, the presence of such semiquinone has not been detected (35, 43).

In both mechanisms, two protons are released into the positive side of the membrane when the quinol is oxidized. The first electron is transferred to cytochrome *c*

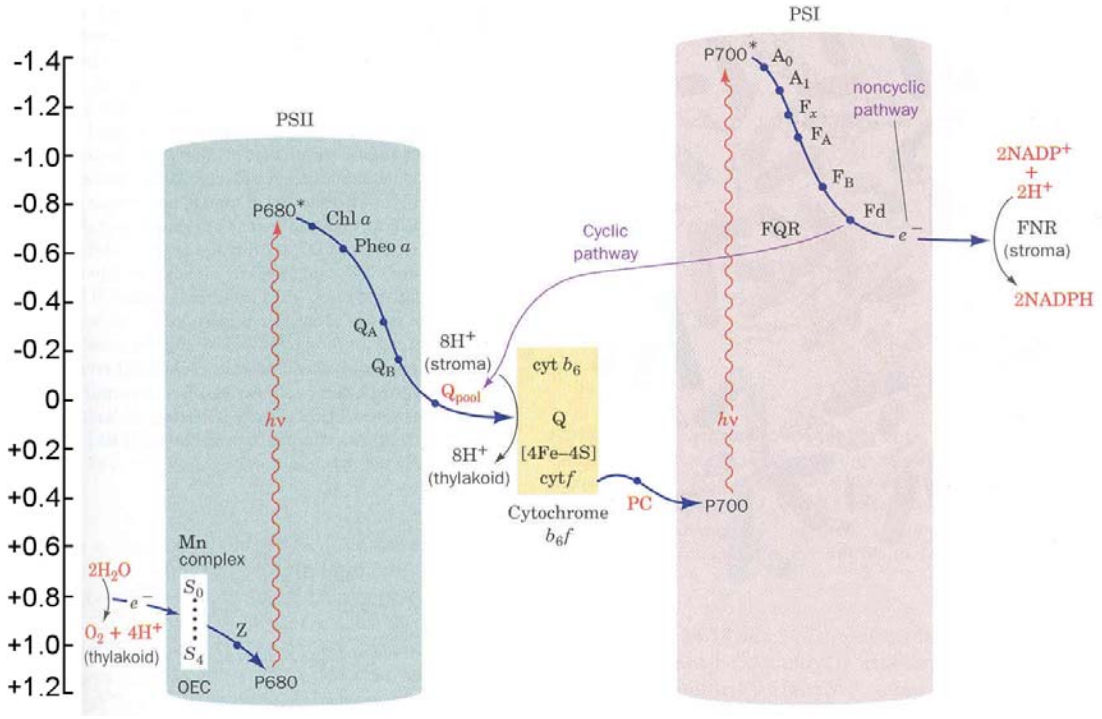

Fig.4. Detailed diagram of the photosynthesis. OEC, oxygen evolving complex; FQR, ferredoxin-plastoquinone reductase; FNR is ferredoxin-NADP+ reductase (44).

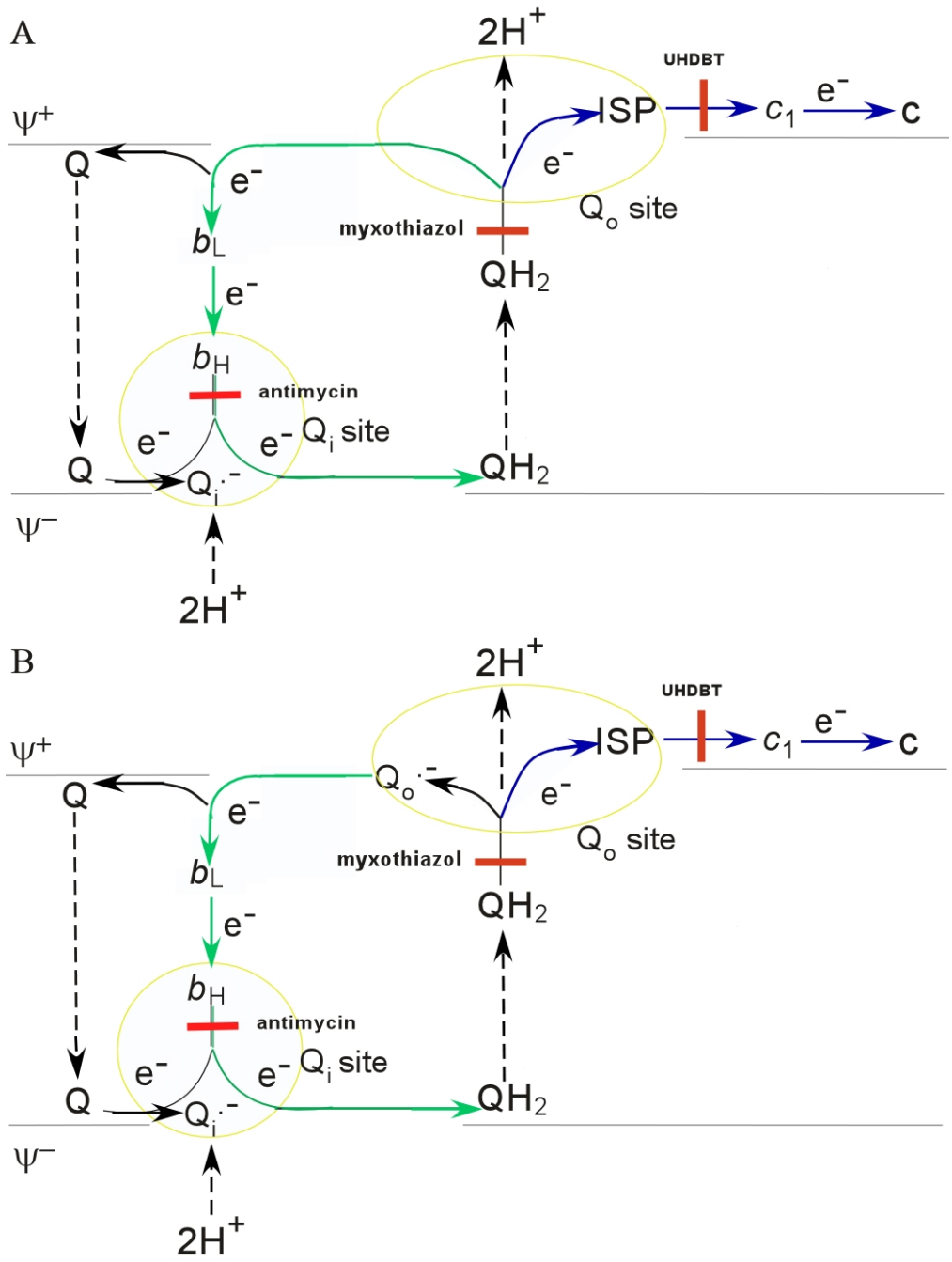

Fig.5. The proton motive Q cycle with (A) concerted and (B) sequential bifurcated reaction at Qo site.

through the high potential chain, which has been transferred to ISP, heme c_1 and then to heme c (c_2 in bacteria). The other electron is transferred through the low potential chain, which has been transferred to heme b_L and heme b_H. At the Qi site, a ubiquinone (Q) accepts an electron from the b_H heme to form a relatively stable ubisemiquinone ($Q^{\cdot P-}$). At this point, the reaction is only half complete, with only one of the two electrons from the ubiquinol being transferred to cytochrome c. In the second half of the Q cycle, all steps are repeated: one ubiquinol is oxidized, one cytochrome c is reduced, two protons are deposited into the positive side of the membrane, and the b_H heme is reduced via the b_L heme. At the Qi site, the ubisemiquinone, which is generated in the first half of the Q cycle, accepts another electron from the b_H heme and uptakes two protons from the negative side of the membrane to form ubiquinol (QH_2) and complete one Q cycle. The net result of one complete Q cycle generates one molecule of oxidized ubiquinone, two molecules of reduced cytochrome c, uptake two protons from the negative side of the membrane, and deposits four protons to the positive side of the membrane,

$$QH_2 + 2 \text{ cyt } c^{3+} + 2H^+_{\text{(N-side)}} \longrightarrow Q + 2 \text{ cyt } c^{2+} + 4H^+_{\text{(P-side)}}$$

The proton motive Q-cycle mechanism is supported by many biophysical and biochemical experimental results:

a) It accounts for the oxidant-induced cytochrome b reduction phenomenon.

   A pulse of oxygen induces oxidation of cytochrome c and c_1, which is accompanied by a transient reduction of cytochrome b. Rapid oxidation of the c-type cytochromes and ISP accelerated ubiquinol oxidation, resulting in a transient increased reduction of cytochrome b. Antimycin blocks reoxidation of b_H, enhancing the oxidant-induced reduction (45). Therefore, in the presence of

ferricyanide, not only cytochrome c_1 becomes oxidized as expected but cytochrome *b* is reduced (46).

b) There are two groups of inhibitors that bind to Qi and Qo sites. Qo site inhibitors block the oxidation of ubiquinol, whereas the Qi site inhibitors block the electron transfer from heme b_H to quinone or semiquinone (4, 7, 47-49). Class I inhibitors are further divided into three sub-classes (Ia, Ib, and Ic) based on chemical characteristics of the inhibitors, and on spectroscopic and biophysical effects of the b_L heme and the iron-sulfur cluster of ISP upon binding of the inhibitors. Class Ia inhibitors typically contain a β-methoxyacrylate (MOA) group (or a close chemical analogue) as a characteristic structural element and are referred to as the MOA inhibitors; they presumably block the electron transfer from quinol to the ISP, accompanying a red shift in the α and β-bands of the reduced heme b_L spectrum. Examples of the class Ia inhibitors are MOAS and myxothiazol. Class Ib inhibitors possess a chromone ring system and are believed to inhibit electron transfer from ISP to cyt c_1; they generate a pronounced increase in redox potential of the ISP and, like class Ia inhibitors, also cause a red shift of the reduced heme b_L spectrum. Stigmatellin is a representative of class Ib inhibitors. Class Ic inhibitors are 2-hydroxy quinone analogues such as 5-undecyl-6-hydroxy-4,7-dioxobenzothiazole (UHDBT); they block the electron transfer in a similar way to the chromone inhibitors, but cause a smaller positive redox potential shift of the ISP and have no effect on the spectrum of the b_L heme. Azoxystrobin (56) and famoxadone (51) also belong to Class I inhibitors. Antimycin belongs to class II inhibitors. NQNO is a dual site inhibitor (51,52) (Fig.6.).

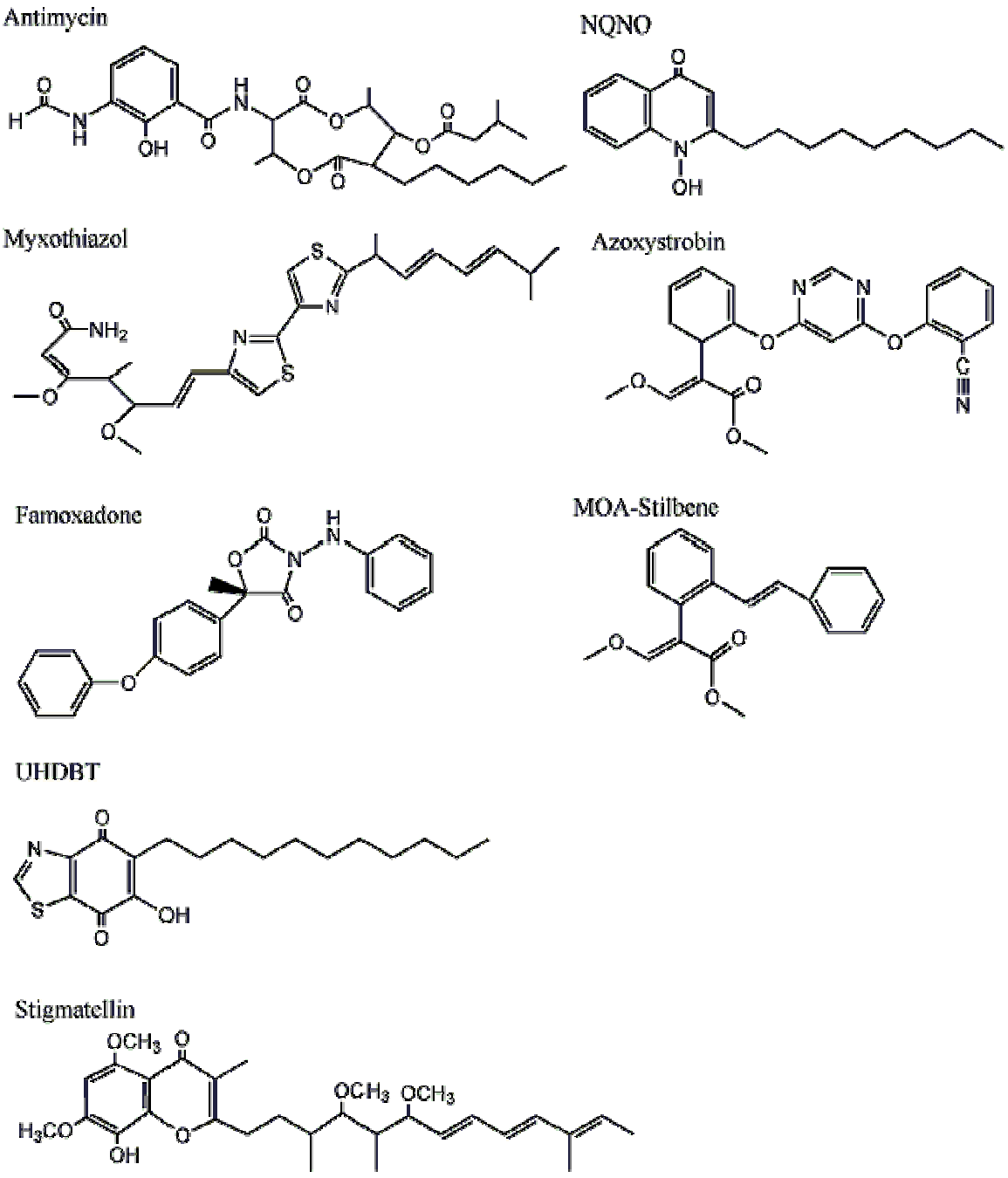

Fig.6. Chemical structures of bc_1 inhibitors.

c) Two protons being translocated across the membrane per one electron was observed during bc_1 complex catalysis (53).

d) A stable ubisemiquinone radical was detected in isolated mitochondrial bc_1 complex and the EPR signal from this semiquinone was eliminated upon addition of antimycin A (54), an inhibitor with higher affinity for Qi site than ubiquinone or ubisemiquinone.

Three-Dimensional Crystal Structure of Cytochrome bc_1 Complex

On the basis of x-ray diffraction data to a resolution of 2.9Å, atomic model of the bc_1 complex from bovine heart mitochondria was first built by Chang-an Yu's group in collaboration with Deisenhofer's group in 1997 (55). Crystallographic structures of mitochondrial bc_1 complex from other sources such as chicken and yeast were available from other groups (56-58), and later the resolutions were improved to 2.4Å in the bovine bc_1 complex structure (52).

a) Structure overview:

An overall view of the cytochrome bc_1 complex viewed parallel to the membrane is presented in Fig.7. Two bc_1 complex monomers interact in the crystal to form a dimer around a crystallographic twofold symmetry axis. The dimeric bc_1 complex is pear-shaped with a maximal diameter of 130 Å and a height of 155 Å (55). The cytochrome bc_1 complex can be divided into three regions, the intermembrane space region, the trans-membrane helix region and the matrix region. The intermembrane space region is composed of the functional domain of cytochrome c_1, ISP and subunit 8

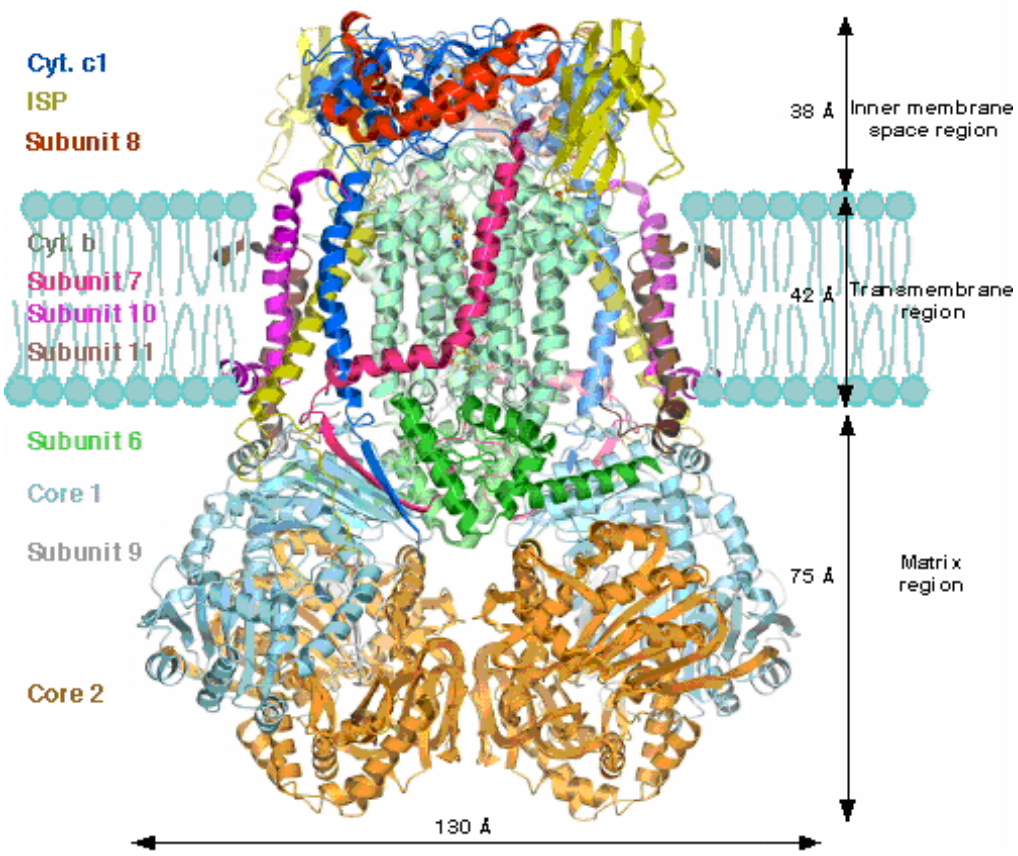

Fig.7. Ribbon model of the bovine dimeric cytochrome bc_1 complex (59) from bovine heat mitochondria. The molecule can be divided into three regions from the top to bottom: the intermembrane space region, membrane-spanning region and the matrix region. The dimensions for each region of the molecule and the color code for each subunit are indicated.

extending 38Å into the cytoplasm from the membrane surface. The transmembrane helix region is about 42Å thick with thirteen transmembrane helices in each monomer. Most parts of cytochrome *b* are located within the membrane. It has eight transmembrane helices, and the transmembrane region of cytochrome *b* houses heme b_L, b_H, and Qo, Qi pocket. Subunit 7, 10, and 11 each has a transmembrane helix. ISP and cytochrome c_1 each has a transmembrane anchor in their N-terminal and C-terminal, respectively. Two symmetry related large cavities are found in the membrane spanning region, which are made of the transmembrane helices D, C, F and H in one monomer and helices D' and E' from the other monomer of cytochrome *b*, and the transmembrane helices of cytochrome c_1, ISP subunit 10 and 11 (Fig.14A). More than half of the molecular mass is located in the matrix region of the molecule, extending from the trans-membrane helix region by 75Å, which consists of core 1, core 2, subunit 6, and part of subunit 7 and subunit 9. Subunit core II and cytochrome *b* contribute major dimer interactions across the two-fold symmetry axis.

b) Cytochrome *b* subunit:

The cytochrome *b* subunit of the bovine bc_1 complex has 379 amino acid residues and consists of eight membrane spanning helices named sequentially from A to H with both the N and C-terminal of cytochrome *b* subunit located in the mitochondrial matrix. The eight transmembrane helices of cytochrome *b* are arranged in two helical bundles: bundle I consists of the first five helices that incorporates two *b*-type hemes (b_L and b_H); bundle II is made of the rest of the helices. The two helical bundles contact each other at the matrix site of the membrane but separate from each other at the intermembrane space, thus creating the so-called Qo pocket between the two bundles near the intermembrane

space side. The CD loop contains two helices cd1 and cd2 of 15 and 9 residues, respectively, arranged in a hairpin, providing a "lid" for the Qo site and contributing residues to the docking site (the ISP crater) for interaction with ISP. The EF loop bridges between the two helical bundles as well as takes part in the formation of the ISP interaction site. Toward the end of the EF loop, there is a 12-residue helix, named ef, situated in a central position inside the Qo pocket. The PEWY motif, conserved in all organisms, is found at the beginning of the helix (50, 51) (Fig.8).

The Qi pocket (52) is located near the matrix side of the membrane with its entrance open to the center of the membrane bilayer. From the entrance, the cavity dives nearly vertically toward the matrix side of the membrane and is surrounded by residues from transmembrane helices A (Trp^{31}, Asn^{32}, Gly^{34}, Ser^{35}), D (Ala^{193}, Met^{194}, Leu^{197}, His^{201}), and E (Tyr^{224}, Lys^{227}, Asp^{228}); the amphipathic surface helix a (Phe^{18}); the A loop (Ile^{27}); the DE loop (Ser^{205}, Phe^{220}); and atoms from the high-potential heme b_H. These residues are identified by their interactions with the bound antimycin A (Fig.9A), NQNO (Fig.9B), and substrate ubiquinone (Fig.9C) in the cyt*b* subunit. Among these residues, Ser^{35}, His^{201}, Lys^{227}, Asp^{228}, and Ser^{205} are highly conserved (Fig.10) and located near the bottom of the pocket. The Qi pocket has a hydrophobic entrance but turns progressively hydrophilic inward; it has the dimensions of roughly 7 x 10 x 13Å and is potentially capable of accessing the mitochondrial matrix through the conserved residues His^{201} and Lys^{227}.

The Qo pocket of the native bc_1 complex (50) has the shape of a saddle. With a relatively wide opening at one end, it becomes increasingly narrower moving inwards; the pocket gets roomy again after the narrow, flat constriction and is sealed at the other

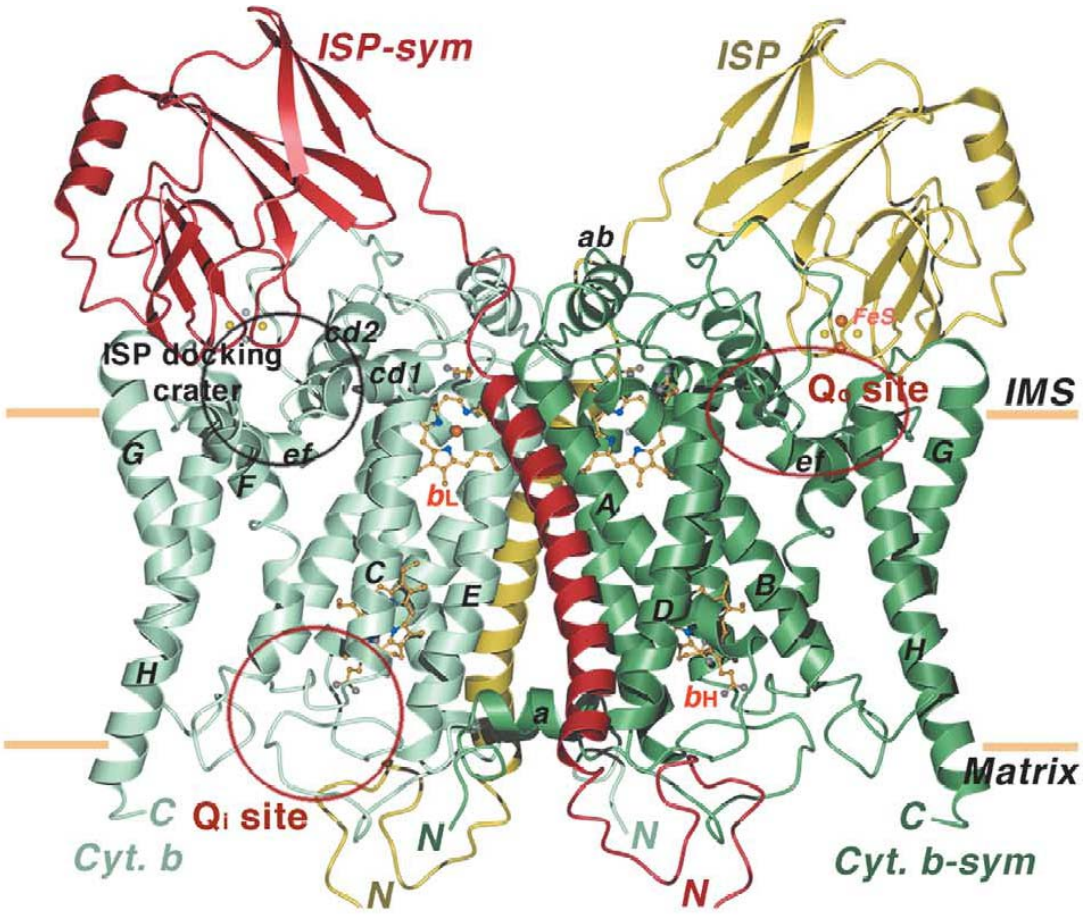

Fig.8. Ribbon diagram of the dimeric cyt*b* and ISP in the bc_1 complex. Two cyt*b* subunits (labeled cyt*b* in light blue and cyt*b*-sym in green, respectively) and two ISP subunits (labeled ISP in yellow and ISP-sym in red, respectively) related by a molecular 2-fold symmetry are shown. The eight transmembrane helices of cyt*b* are named sequentially from A to H. The two *b*-type hemes labeled b_L and b_H are shown as the ball-and-stick models. Two active sites in the cyt*b* are labeled: one is Qi site, the other is Qo site. The surface depression in cyt*b* on the inter-membrane space side is labeled as the ISP-docking crater for interacting with the ISP.

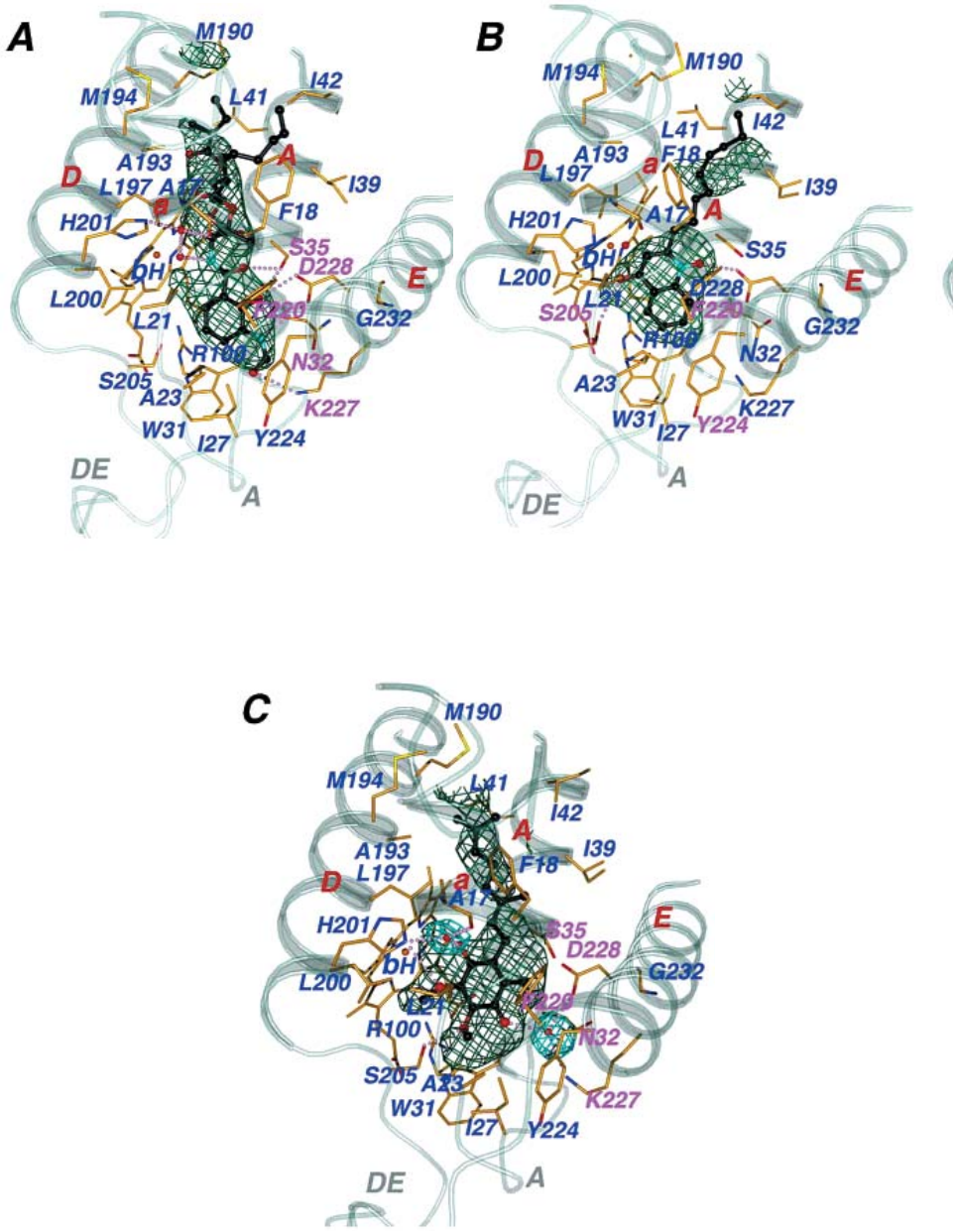

Fig.9. Interactions of the protein environment at the Qi site of the cyt*b* subunit with bound inhibitors and substrate. Secondary structure elements surrounding the Qi pocket, including portions of the N-terminal helix a, transmembrane helices A, D, and E, and extramembrane loops A and DE, are shown and labeled. Residues interacting with bound inhibitors or substrate and the b_H heme are drawn in stick models and are labeled with carbon atoms in yellow, nitrogen in blue, oxygen in red, and iron in orange. H-bonds are indicated with the pinkish dotted lines. Water molecules are shown as the isolated red balls. Inhibitors and the substrate ubiquinone are drawn as the ball-and-stick models with carbon atoms in black, nitrogen in light blue, and oxygen in red. (A) Qi pocket with the bound antimycin A, (B) Qi pocket with the bound NQNO, and (C) Qi pocket with the bound ubiquinone with two isoprenoid units visible in electron density.

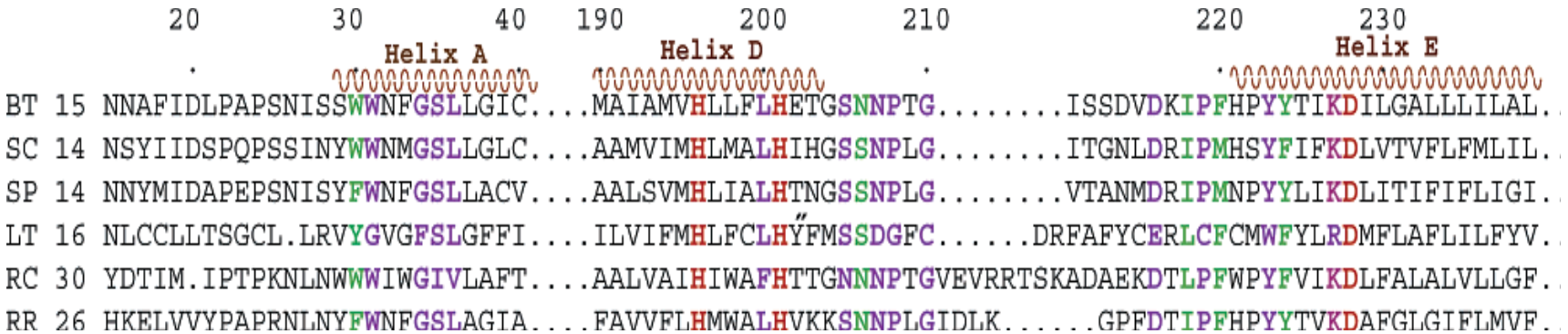

Fig.10. Sequence alignments of Qi pocket residues of cyt*b* subunits from different species: BT (*B. taurus*), SC (*S. cerevisiae*), SP (*S. pombe*), LT (*L. tarentolae*), RC (*R.capsulatus*), and RR (*R. rubrum*). The helical secondary structure elements are indicated with the sinuous curves in brown and as labeled. Amino acid positions in the bovine sequence are numbered above the sequences. Absolutely conserved residues in all sequences are colored red, those with a single conserved change are in magenta and those with two or more conserved changes are in green.

end (Fig.11). The Qo pocket is highly hydrophobic and lined with six prominent aromatic residues in addition to a number of aliphatic residues. The pocket is delimited against the membrane by three transmembrane helices (B, C and E) and by the buried ef helix, and capped by the cd1 and cd2 helices isolating the Qo site from the intermembrane space. Moreover, His161 of the ISP, ligand to one of the iron atoms in the 2Fe-2S cluster, may also contribute to the Qo site when the ISP is bound at the Qo site. The Qo pocket is exceptionally rich in highly conserved residues (Fig.12).

c) Iron-sulfur protein (ISP)

The structure of Rieske iron-sulfur protein (ISP) can be divided into three domains: the N-terminal domain, tail domain, (residues 1-62); the flexible linking domain, neck region, (residues 63-72); the soluble C-terminal domain, head domain, (residues 73-196), which is located in the intermembrane space region. The Rieske iron sulfur subunit is anchored to the membrane by the tail domain, and no ordered secondary structure was reported in the neck region (55, 56). In the bovine heart mitochondrial cytochrome bc_1 complex, the [2Fe-2S] cluster is coordinated by two cysteine and two histidine residues (Cys^{139} and His^{141}; Cys^{158} and His^{161}) (60) (Fig.12.) within a C-terminal water soluble domain which is bound to the rest of the bc_1 complex through this N-terminal membrane anchor (61, 62). In ISP, the [2Fe-2S] cluster is located at the tip of the head domain. Moreover, ISPs extend across the interface between the two monomers, with the transmembrane helix in one monomer and the head domain within the other, thus forming the intertwining dimer (59).

d) Cytochrome c_1 subunit.

Cytochrome c_1 both structurally and functionally links the cytochrome bc_1 complex

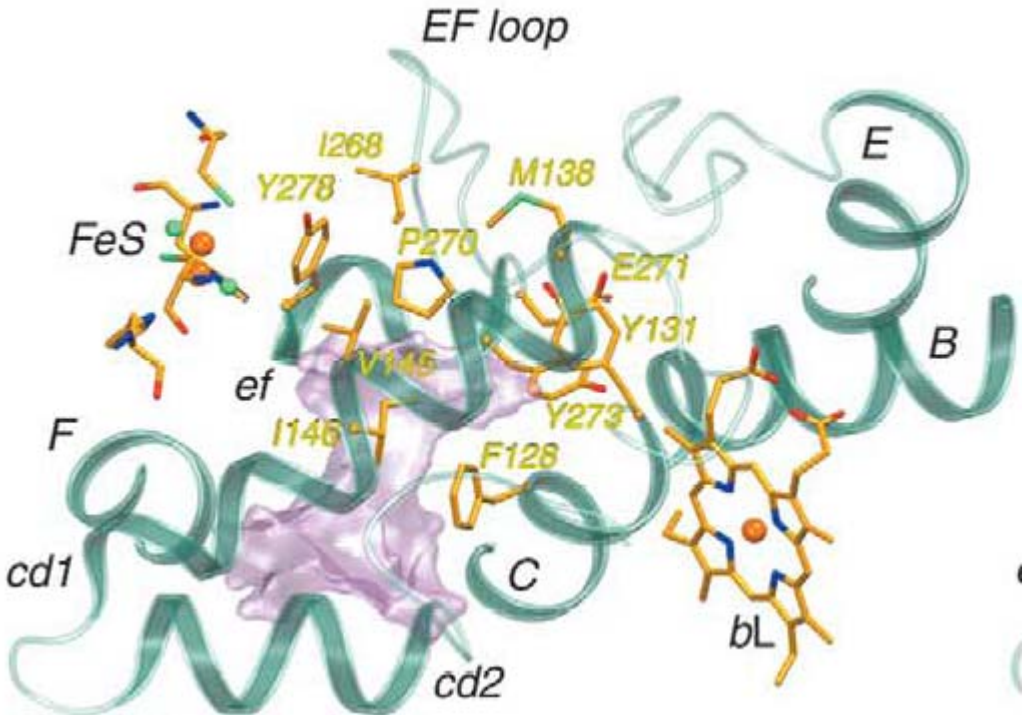

Fig.11. Structural environment of the native Qo site. The Qo pocket is depicted as a GRASP (63) surface with the surrounding secondary structure elements. Helices cd1, cd2 and ef as well as parts of B, C, E and F helices are shown and labeled. The heme b_L of cytb, 2Fe-2S cluster of the ISP, and the conserved residues are also shown in the ball-and-stick form. Carbon atoms are colored yellow, oxygen red, nitrogen blue and sulfur green.

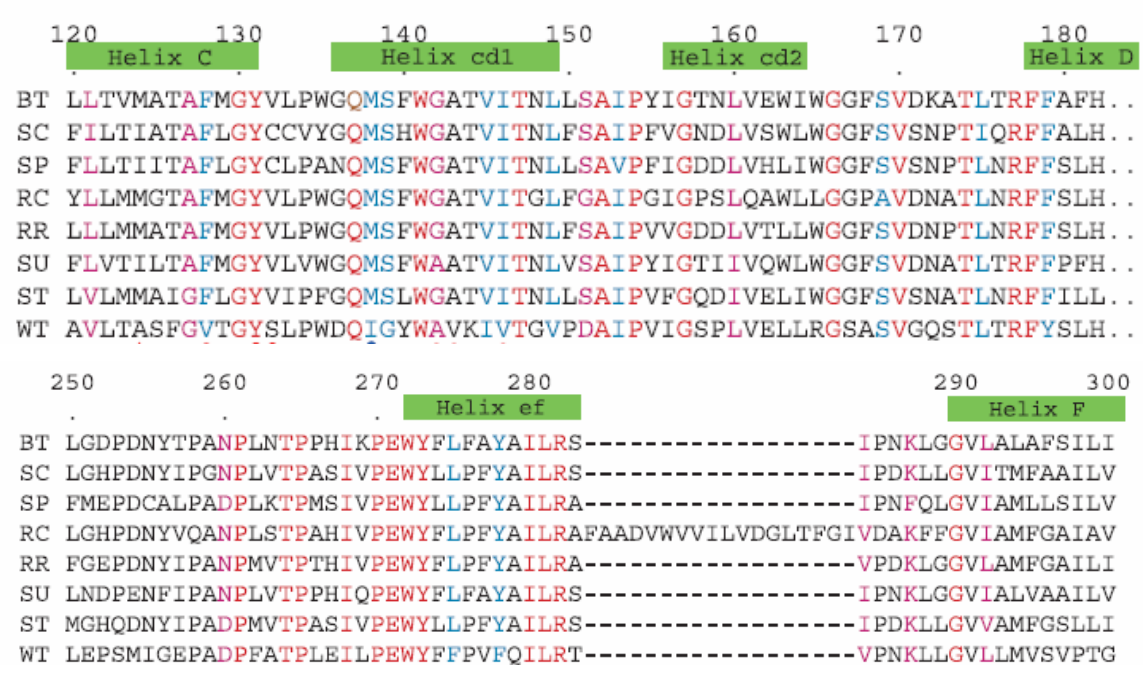

Fig.12. Sequence alignment of the Qo pocket residues. The Qo site is composed of residues from two sequence segments: one from residue 120 to 182 and another from residue 250 to 300. The sequence shown include BT (*B. Taurus*), SC (*S. cerevisiae*), SP (*S. pombe*), RC (*R. capsulatus*), RR (*R. rubrum*), SU (Sea Urchin, *S. purpuratus*), ST (*S. tenacellus*) and WT (wheat cytb_6, *T. aestivum*). Helical elements are indicated as green boxes and labeled. Absolutely conserved residues in all sequences are colored red; highly conserved residues with one conserved change are colored blue; highly conserved residues with more than one conserved change are colored magenta.

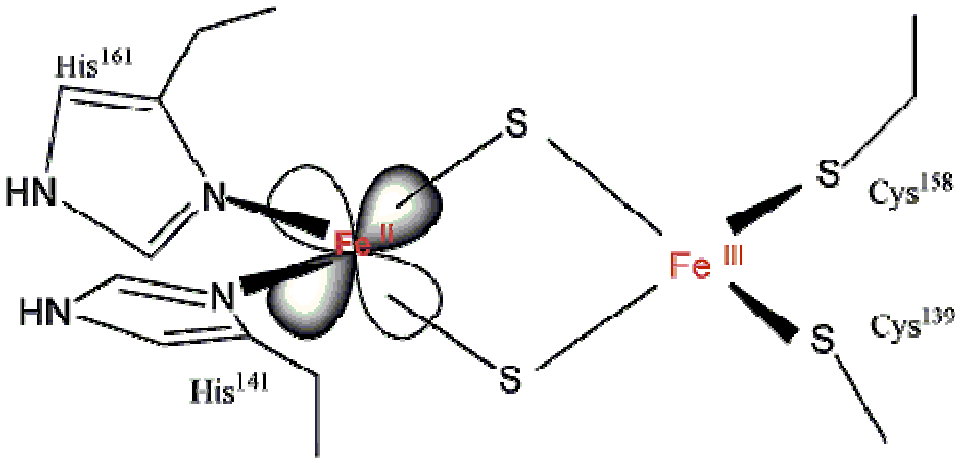

Fig.13. Structure of the “Rieske” [2Fe-2S] cluster.

with its physiological redox partners, soluble or membrane-attached cytochromes *c* or head domain of high-potential iron-sulfur proteins. Cytochrome c_1 provides a docking site for these proteins on its surface at the membrane-aqueous interface. Cytochrome c_1 is oxidized by cytochrome *c* (in bacteria, cytochrome c_2), in turn, the oxidized cytochrome c_1 acts to oxidize the [2Fe2S] cluster, which then moves to the Qo site. Cytochrome c_1 is attached to the membrane by a transmembrane helix located at the C-terminal end of the protein. The hydrophilic extramembrane domain including the heme is located in the intermembrane space region. The extrinsic domain of cytochrome c_1 contains the consensus heme-binding motif (CXXCH) located close to the N-terminus of the polypeptide that provides sites for covalent attachment of the heme group (cysteines) and fifth axial ligation to the heme iron (histidine). It also contains the invariant methionine residue present near the C-terminus that acts as the sixth axial ligand to the heme iron (56, 57, 64). The carboxy group of one of the propionates of the heme c_1 forms a salt bridge with Arg^{120}, while the other propionate of the heme c_1 extends toward the ISP. A methyl group on the porphyrin ring is solvent-exposed, likely near the binding site for cytochrome *c* (6). The x-ray crystal structures of beef and chicken cytochromes bc_1 have revealed that the exposed heme CD edge of cytochrome c_1 on the cytoplasmic surface of the membrane is surrounded by acidic residues that could form a docking site for cytochrome *c* (55-57). The acidic residues (Glu^{74}, Glu^{101}, Asp^{102}, Glu^{104}, Asp^{109}, Glu^{162}, Glu^{163}, and Glu^{168}) on the surface of cytochrome c_1 of *R. sphaeroides* cytochrome bc_1 complex are involved in binding positively charged cytochrome *c*. These acidic residues on opposite sides of the heme crevice of cytochrome c_1 direct the diffusion and binding of cytochrome *c* from the intramembrane space (65).

Functional Indication from Structural Analysis of Cytochrome bc_1 Complex

a) Head domain movement of ISP

Mobility of ISP head domain in the bc_1 crystal was first suggested by observation of a particularly low electron density of its extramembrane head domain (55). The mobility of the head domain of ISP was further substantiated by the anomalous light scattering signals of the [2Fe-2S] cluster observed in native and co-crystals with various Qo site inhibitors. In a native bovine heart mitochondrial bc_1 crystal, a much weaker anomalous light scattering signal was observed for the [2Fe-2S] cluster compared with that for the heme iron, b_H or b_L, despite the presence of two irons in the cluster. Furthermore, the electron density of the anomalous light scattering signal of [2Fe-2S] cluster was strongly enhanced in a co-crystal with stigmatellin or UHDBT, indicating that these inhibitors arrest the mobility of ISP in the fixed state position (66), and ISP head domain is on the surface of cytochrome *b* (*b* position). Conversely, the electron density of the anomalous scattering peak of [2Fe-2S] is abolished in a co-crystal with MOA-stilbene or myxothiazol, indicating that these inhibitors increase the mobility of ISP in the crystal and [2Fe-2S] has no predominant position, the ISP head domain is in a released state and found at the *c*-interface (c_1 position) (56, 67).

The hypothesis of the mobility of the ISP head domain not only provides an explanation for the unexpected findings in those crystal structures, but it also provides an explanation for the bifurcated reaction at the Qo site. The bifurcated quinol oxidation at the Qo site is the key step in the Q cycle mechanism as mentioned in the previous section. The major problem for the obligatory bifurcated reaction is that one of the two electrons

from quinol has to be transferred to the unfavorable low potential chain (cytochrome b_L and b_H). It's difficult to explain why both electrons are not moved to the thermodynamically favorable high potential chain (ISP and cytochrome c_1). On the other hand, in the bovine heart mitochondrial bc_1 crystal, the distances between heme b_L and the [2Fe-2S] cluster and between the [2Fe-2S] cluster and heme c_1, are 27 and 31 Å, respectively. Although the distance of 27 Å between heme b_L and the [2Fe-2S] cluster accommodates well the observed fast electron transfer between these two redox centers, the 31 Å distance between the [2Fe-2S] cluster and heme c_1 is difficult to understand in view of the rapid electron transfer rate observed for these two redox centers (32,68). Movement of the extramembrane domain of ISP offers an explanation for these paradoxes. The [2Fe-2S] cluster is reduced by the first electron of ubiquinol at a position 27 Å from heme b_L and 31 Å from cytochrome c_1. The reduced [2Fe-2S] cluster cannot donate an electron to cytochrome c_1 before the second electron of ubiquinol is transferred to heme b_L. It was speculated that the electron transfer from heme b_L to b_H causes a conformational change in cytochrome *b* that forces or allows reduced [2Fe-2S] to move close enough to heme c_1 for fast electron transfer (6, 56). This model also suggests that the re-oxidized ISP is unable to return to the *b*-position to be re-reduced, before the second electron is transferred to the low potential chain (40).

To study the movement of the head domain of ISP is required for bc_1 catalysis and the neck region of ISP confers the necessary mobility, molecular biology, biochemical and biophysical methods were used. Tian *et al*. (69) demonstrated that increasing the rigidity of the ISP neck region of the *R. sphaeroides* bc_1 complex by a double proline substitution at Ala^{46} and Ala^{48} or a triple proline substitution at residues

42-44 decreased the activity and increased the activation energy because the neck rigidity is increased in the mutant bc_1 complexes. In a continuous work, Tian *et al* (70) constructed mutants with cysteines pairs in the ISP neck region, Ala^{42} and Val^{44}; Pro^{40} and Ala^{42}. Oxidation of these two cystines pair to form a disulfide bond resulted in restricting the flexibility of the ISP neck region, in turn, decreased the mobility of the head domain, thus decreased activity of the bc_1 complex, however, the activity can be restored by reducing the disulfide bond with β-mercaptoethanol. The restored activity was diminished upon removal of β-mercaptoethanol but is retained if the β-mercaptoethanol-treated membrane was treated with the sulfhydryl reagent N-ethylmaleimide or p-chloromercuribenzoic acid. To further establish the essentiality of the movement of the head domain of ISP, *R. sphaeroides* bc_1 mutants with a pair of cysteines engineered on the interface between ISP and cytochrome *b*, $A^{185}C$ (cyt*b*)/$K^{70}C$ (ISP) was generated and characterized (71). Formation of the intersubunit disulfide bond in this cysteine pair mutant complex arrests the head domain of ISP in the "fixed state" position that is too far for electron transfer to heme c_1, resulting in the loss of the bc_1 activity, reduction of this disulfide bond by β-mercaptoethanol restores the activity.

b) The intertwined dimeric structure of cytochrome bc_1 complex

The dimeric association of cytochrome bc_1 complex has been reported extensively throughout the literature (72-74). Recently, three dimensional structures of mitochondrial cytochrome bc_1 complexes from beef (55, 57), chicken (56), and yeast (58) were determined. The structural information suggests the complex functioning as a dimer. The functional dimer hypothesis is supported by the following structural evidences:

(1) In the crystals of native oxidized bovine cytochrome bc_1 complex, the [2Fe-2S]

cluster in one monomer is 27 Å from heme b_L of the other monomer and 40 Å from the heme b_L of the same monomer (55). This structural arrangement suggests that mitochondrial bc_1 complex functions as a dimer, because the distance between the [2Fe-2S] cluster of ISP of one monomer and heme b_L of the other monomer is less than that between these groups in the same monomer. The shorter distance accommodates fast electron transfer from QH_2 to ISP and b_L. Xiao *et al* (59) demonstrated that the structure of the dimeric cytochrome bc_1 complex observed in the crystal also exists in solution. They constructed and characterized two pairs of cysteine substitutions, one in the interface between the head domain of ISP and cytochrome *b* and the other between the tail domain of ISP and cytochrome *b*. An adduct protein containing two cytochrome *b* and two ISP proteins is detected in the mutant complexes, confirming that the bc_1 complex exists as a dimer which the intertwining of ISP in one monomer is physically close to and interacting with the cytochrome *b* and cytochrome c_1 in the 2-fold symmetry-related to the other monomer (Fig.7).

(2) The presence of two apparently non-communicating cavities in the dimeric complex, each connecting the Qo pocket of one monomer to the Qi pocket of the other. Interestingly the two quinone binding sites from the same monomer do not connect each other. The membrane spanning cavity may help the transfer of quinone between Qo and Qi sites located on different monomers. As a result of that, quinone reduced at Qi site of one monomer can be oxidized at the nearby Qo site of the other monomer without leaving the bc_1 complex (Fig.14A).

(3) The distance between the Fe atoms of the two hemes b_L is only 21 Å, which is

(A)

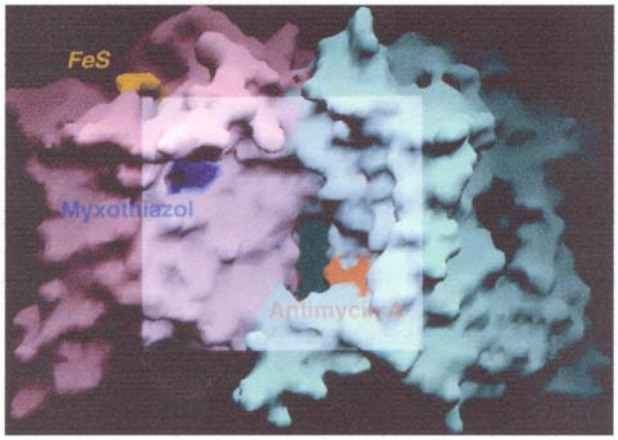

(B)

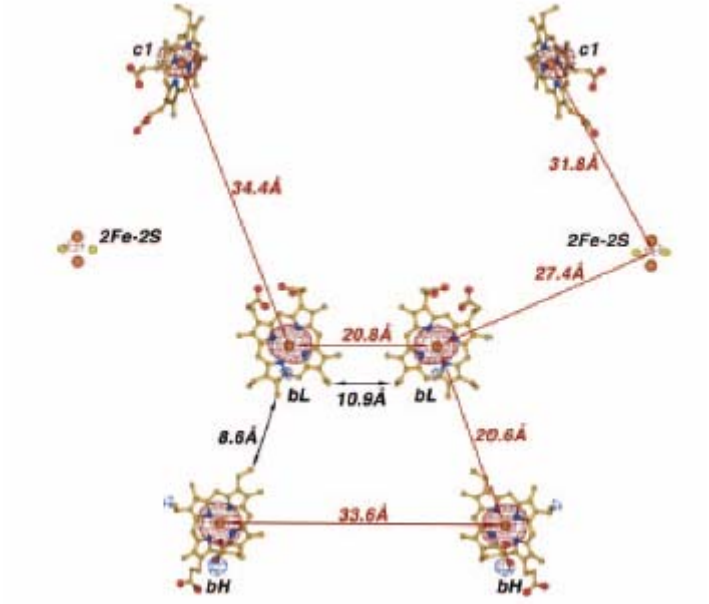

Fig.14. Cytochrome bc_1 exists as a functional and structural dimer. (A) Q binding cavity between cyt*b* dimer. (B) Distance between redox centers in bovine dimeric cytochrome bc_1 complex (75).

approximately the same as that between heme b_L and b_H in one monomer (Fig.14B). Because of the short distance between the two hemes b_L, the electron transfer or equilibrating between inter-monomer hemes b_L-b_L may occur during bc_1 catalysis (37,55,76), and such electron transfer may be facilitated by the aromatic pairs present between the two hemes b_L in the two symmetry-related monomers (Fig.15). To test this hypothesis, Gong *et al* (75) constructed and characterized *R. sphaeroides* mutants bc_1 complexes with mutations at three aromatic residues (Phe^{195}, Tyr^{199}, and Phe^{203}). Replacing only Phe^{195} to Ala decreases slightly the ubiquinol-cytochrome *c* reductase activity and increases the production of superoxide several fold, not only suggesting that this mutation interfered with electron transfer between two monomers, but also supporting the idea that the interruption of the electron transfer between the two b_L hemes enhance the electron leakage to oxygen and thus decreasing the activity. On the other hand, replacing the Phe^{195} with Tyr, His, or Trp results in mutant complexes having the same ubiquinol-cytochrome c reductase activity as the wild-type, indicating that the aromatic group at the position 195 is involved in electron transfer reaction.

Supernumerary Subunits of Cytochrome bc_1 Complex

There are two kinds of protein subunits in the cytochrome bc_1 complex, one are those contain a redox prosthetic group, such as heme b_L , b_H, c_1, and iron-sulfur cluster, called the core subunits, the other are those that do not, called the supernumerary subunits (77). All the bc_1 complexes contain three core subunits, cytochrome *b*, cytochrome c_1, and Rieske ISP, which are required for enzymatic activity of the complex

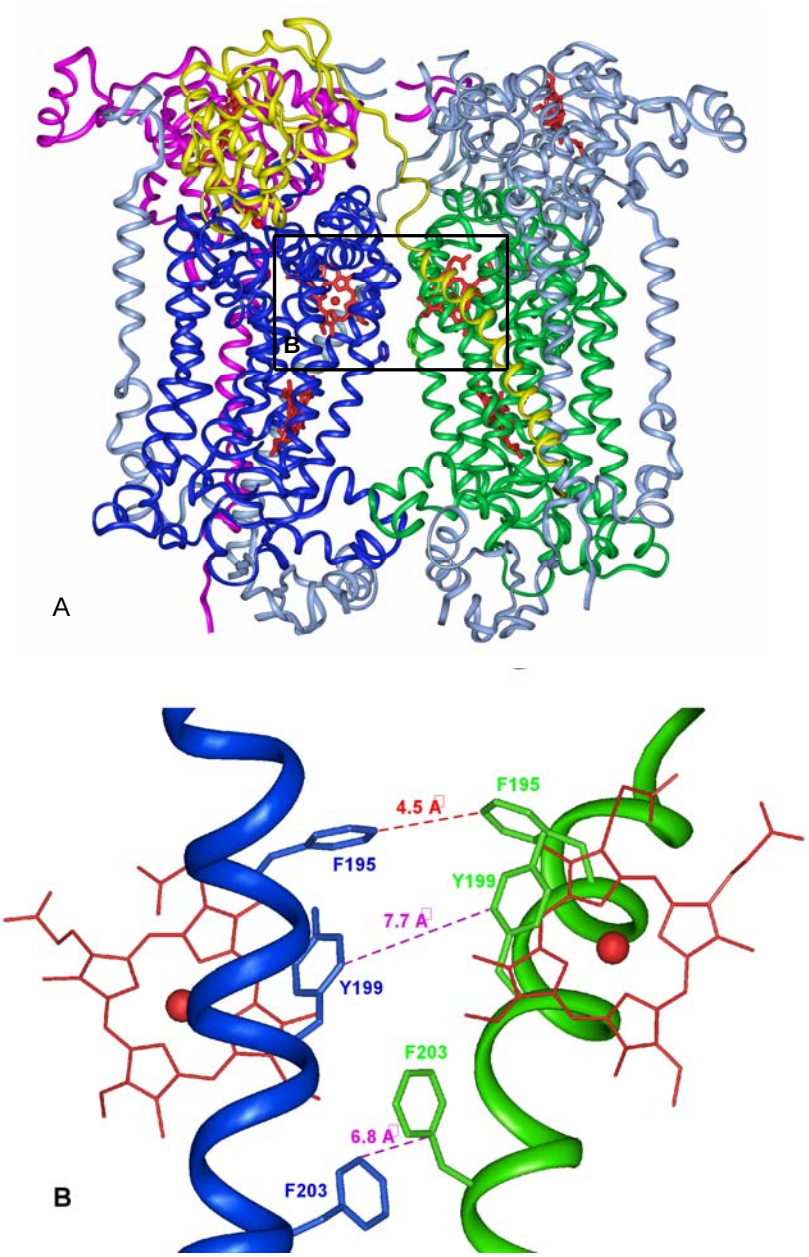

Fig.15. Location of aromatic residues in the structural model of the *R. sphaeroides* bc_1 complex. (A) cyt*b* is shown in blue ribbon in one monomer and green in the symmetric monomer, ISP (from the symmetric monomer) is in yellow, and the cytc_1 form the same monomer is in pink. Both subunit IVs, ISP (from one monomer) and cytc_1 (from the symmetric monomer) are shown in turquoise. All hemes are indicated by red sticks. (B) shows the aromatic residues located on the interface of two b_L hemes from different cyt*b*s. The nearest edge to edge distances between aromatic residues from different monomers are indicated. Some peptide sequences have been omitted for clarity (75).

(77). However, bc_1 complexes from different sources contain varied numbers of supernumerary subunits (4,77). Cytochrome bc_1 complexes from some bacteria contain only three core subunits, this is the case with the enzyme from *Paracoccus* (78), *Rhodospirillum rubrum* (85), and *Rhodobacter capsulatus* (79). Whereas the bc_1 complex from bovine heart mitochondria has eight supernumerary subunits (Fig.7) (81), that from yeast (82) has seven. *Rhodobacter sphaeroides* has only one, subunit IV (Fig.16A).

Although the function of supernumerary subunits are not fully understand, the complexes without supernumerary subunits are less stable and have lower activity than those with supernumerary subunits (82). It has been reported that the activation of cytochrome bc_1 complexes purified from the bovine mitochondria, yeast, and from the chromatophores of *R. sphaeroides* and *R. capsulatus*, by a single chromatographic procedure are: 1152, 219, 128, and $64s^{-1}$ (82). The increased activity in mitochondria complex may result from interactions of the core subunits with supernumerary subunits.

Some groups investigated the function of the supernumerary subunits of the mitochondrial cytochrome bc_1 complex. It's shown that subunit I and II of yeast bc_1 complex is essential for maintaining the proper conformation of apocytochrome *b* to aid in the addition of heme (83,84); subunit VI of yeast bc_1 complex is involved in manipulating dimmer/monomer transition (85,86); subunit VII and VIII of yeast bc_1 complex are essential for assembly of the complex (87); subunit IX of yeast bc_1 complex interacts with the iron-sulfur protein, cytochrome *b* and cytochrome c_1 (88); subunit I and II of plant or bovine bc_1 complex have the mitochondrial processing peptidase activity (89,90).

The gene of supernumerary subunit of *R. sphaeroides*, subunit IV (*fbc*Q), was cloned and sequenced (91). The molecular weight, deduced from the nucleotide sequence, is 14,348 Da (92). It is a relatively hydrophilic protein of 124 residues, with a transmembrane helix predicted at a hydrophobic stretch between residues 86 and 109 based on the hydropathy analysis (91), the C-terminal end on the periplasmic side and the N-terminal end on the cytoplasmic side (93). The interacting regions of subunit IV with cytochrome *b* in the core complex were identified as residues 41-53 and 77-85, which are on the cytoplasmic side of the chromatophore membrane and close to the DE loop and helix G of cytochrome *b*, respectively (94). Moreover, subunit IV is involved in the structural role of the complex indicated by mutational effects with a delay in photosynthetic growth and decreasing in the cytochrome bc_1 complex activity in chromatophores upon detergent treatment (95). The ubiquinone-binding functions of subunit IV is supported by photoaffinity labeling using azido-Q derivatives (92) and an increasing in the apparent Km for 2,3-dimethoxy-5-methyl-6-geranyl-1,4-benzoquinol (QH_2) of the complex. By using site-directed mutagenesis on the subunit IV gene followed by *in vitro* reconstitution, residues 6-11 are essential for structural function of subunit IV. Trp79 is essential for the structural and ubiquinone binding functions of subunit IV (95). Subunit IV was over-expressed in *E. coli* as a glutathione *S*-transferase fusion protein to solve the difficulty presented by mutagenesis studies by the *in vivo* reconstitution. Subunit IV can then be released from the fusion protein by proteolytic cleavage with thrombin. The recombinant subunit IV is functionally active and can be properly assembled into the active cytochrome bc_1 complex without subunit IV (96). By using site-directed mutagenesis coupled with *in vitro* reconstitution, it's possible to

further study the function of subunit IV.

Photosynthetic Bacteria: *Rhodobacter sphaeroides*

Our group uses *R. sphaeroides* bc_1 complex as a model system to study successfully the more elaborate mitochondrial cytochrome bc_1 complexes (6,59, 69-71, 75, 94, 96). *R. sphaeroides*, an anoxygenic, non-sulfur, purple facultative photosynthetic bacterium, belongs to gram-negative bacterium of the proteobacteria group. Unlike plants and algae, which carry out photosynthesis in an aerobic environment and produce oxygen as a product of the water splitting reaction, *R. sphaeroides* carries out photosynthesis in an anaerobic condition, and does not produce oxygen. Moreover, *Rhodobacter sphaeroides* is metabolically highly diverse. It can grow photosynthetically or heterotrophyically via aerobic or anaerobic respiration (97). It prefers to grow photoheterotrophically, under anaerobic conditions in light with various organic substrates. Therefore, the ecological niches of *R. sphaeroides* are anoxic parts of water and sediments, which receive light of sufficient quantity and quality to allow phototrophic development (98). Under aerobic conditions, it can grow well in the dark, as the synthesis of some photosynthetic pigments, for example, bacteriochlorophyll, in *R. sphaeroides* is repressed by oxygen (98), the culture becomes pink colored rather than brownish green as seen in photosynthetic cultures.

A very important feature of *R. sphaeroides* as a material for bc_1 complex study is that heterotrophic growth allows the isolation of mutants bc_1 complex impaired in

photosynthesis, since electron from quinol can be transferred to oxygen via a quinol oxidase as an alternative electron transfer pathway. Therefore, *R. sphaeroides* mutants with severely defective bc_1 complex are still able to grow in large quantities under aerobic conditions. The bacteria growing under "semi-aerobic dark" conditions develop intra-cytoplasmic membrane (ICM) that most of the photosynthetic machinery of *R. sphaeroides* is located (98-100), intra-cytoplasmic membrane with defective bc_1 complex can be prepared for biochemical and biophysical studies to assess the reasons of the defect.

In addition, the bc_1 complex from *R. sphaeroides* contains only four subunits (cytochrome *b*, cytochrome c_1, ISP and subunit IV) with the three catalytic subunits (cytochrome *b*, cytochrome c_1, ISP) homologous to their mitochondrial counterparts. It is much simpler than the mitochondrial complexes thus making it much easier for us to study structure-based functions of the bc_1 complex. Furthermore, efficient molecular engineering protocols for *R. sphaeroides* bc_1 complex are well established (6). $(His)_6$-tagged (69) on cytochrome c_1 of the cytochrome bc_1 complex is readily overexpressed in chromosomal deletion strain BC17 (lacking *fbc*FBC operon) by a plasmid carrying the genes complementing them *in trans,* which greatly facilitates the isolation of the bc_1 complex from cells using the nickel-nitrilotriacetic acid (Ni-NTA) agarose column. The purity, activity and cytochrome content of these histidine-tagged bc_1 complexes are similar to those of the un-tagged ones. Such genetic system has been used extensively to study site-directed mutants and proven to be extremely valuable for our knowledge of the cytochrome bc_1 complexes (6, 59, 65, 69-71, 75, 101-107).

Homology Structural Modeling and Extra Fragments of *Rhodobacter sphaeroides* bc_1 Complex

The *R. sphaeroides* bc_1 complex is functionally homologous to the mitochondrial complex. However, since the *R. sphaeroides* bc_1 complex contains only one supernumerary subunit, it's unlikely that the structures of the core subunits in the complex is stabilized through interactions between core subunits and their neighboring supernumerary subunits, as suggested for the mitochondrial complex (108). It's possible that interactions between part of a core subunit and another part of the same subunit or another core subunit contribute to the stability of a core subunit in *R. sphaeroides* bc_1 complex. This hypothesis finds some support from the fact that core subunits in *R. sphaeroides* bc_1 complex are generally bigger than their counterparts in the mitochondrial complex due to specific insertions that are uniquely present in the core subunits.

Since the crystal structure of *R. sphaeroides* bc_1 is unavailable at this time, the homology modeling is a practical way to predict its three dimensional structure based on the assumption that sequence conservation is directly proportional to structural conservation, a structure model of the *R. sphaeroides* bc_1 complex was constructed using coordinates of subunits from bovine complex (6) (Fig.16A.). Amino acid sequence alignment of *R. sphaeroides* cytochrome *b*, cytochrome c_1, and ISP with their counterparts in the bovine mitochondrial bc_1 complex reveals high sequence homology, except for several extra fragments in *R. sphaeroides* bc_1 complex. There are one extra fragment in ISP, two in cytochrome c_1, four in cytochrome *b*. By swapping coordinates from template to model in all regions where there is a corresponding match in the

sequence alignment, the majority of cytochrome *b*, cytochrome c_1, and ISP were modeled. Subunit IV and the extra fragments of cytochrome *b*, cytochrome c_1, and ISP were modeled with the coordinates from the corresponding supernumerary subunits in the bovine bc_1 complex. In the structure model of *R. sphaeroides* bc_1 complex (6), the four extra fragments of cytochrome *b* are located at the N terminus (residues 2-12), the connecting loop between helices D and E (residues 232-239), the connecting loop between helices E and F (residues 309-326), and the C-terminus (residues 421-445); the two extra fragment of cytochrome c_1 are located between helix α2 and helix α3 (residues 109-125), and between helix α4 and helix α5 (residues 161-179), respectively; the one extra fragment of ISP (residues 96-107) is located near the middle portion of the ISP. The first two extra fragments of cytochrome *b* (residues 2-12, 232-239) are located on the cytoplasmic side of the chromatophore membrane; the third one (residues 309-326) is located near to heme b_L, iron-sulfur cluster, and the Qo site; the forth one (residues 421-445) is in close proximity to subunit IV and ISP, and also located on the cytoplasmic side of the chromatophore membrane (106). The extra fragment of ISP shows an α-helical structure in the structure model (105) (Fig.16B.). It was shown that the first two extra fragments of cytochrome *b* (residues 2-12, 232-239) contribute little effect on structural integrity of the bc_1 complex. Chapter III and IV of this thesis will present evidence for the essentiality of the extra fragments of *R. sphaeroides* cytochrome *b* (residues 421-445) and ISP (residues 96-107) for maintaining structural integrity of the bc_1 complex. These findings support the idea that the extra fragments possess the supernumerary subunit function in stabilizing the structure of the bacterial complex. The studies of other extra fragments from *R. sphaeroides* bc_1 complex are the ongoing projects in our lab.

(A)

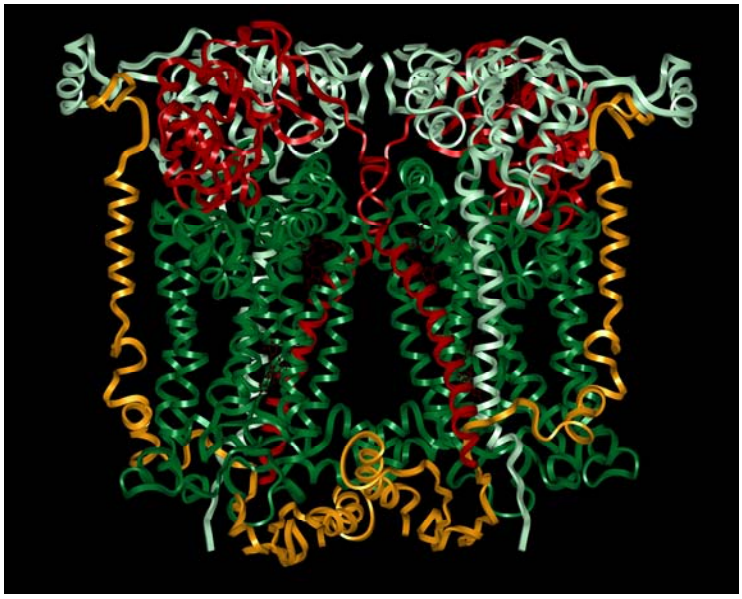

(B)

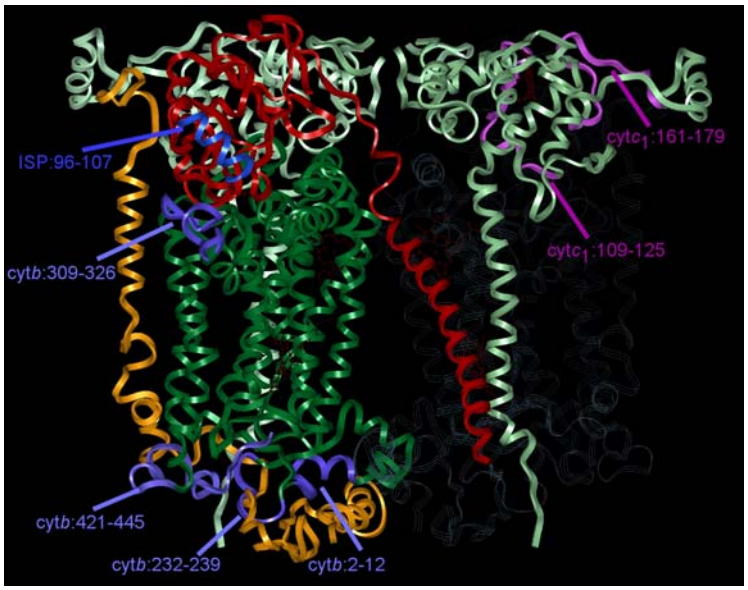

Fig.16. (A) Theoretical ribbon model of the *R. sphaeroides* dimeric cytochrome bc_1 complex. ISP is *red*, cyt*b* is *green*, cytc_1 is *silver*, subunit IV is *rust*. (B) Location of the extra fragments of ISP, cytochrome *b*, and cytochrome c_1 in the proposed structural model of *R. sphaeroides* cytochrome bc_1 complex. Cytc_1 is shown in both monomers, other subunits of the right monomer is grey for clarity, the extra fragments are labeled on the figure.

Cytochrome *c* oxidase and ATP-synthase

Cytochrome *c* oxidase

Cytochrome *c* oxidase (or Complex IV) is the terminal oxidase of cell respiration, reducing molecular oxygen (O_2) to water via a mechanism coupled with a proton pumping process. The proton motive force produced by the proton pumping process and O_2 reduction is energetically harnessed for production of ATP by ATP synthase (109). The mammalian cytochrome *c* oxidase enzyme is a large multicomponent membrane protein comprising 13 different subunits, four redox-active metal sites (hemes *a* and a_3, Cu_A and Cu_B), three redox-inactive metal sites (Mg^{2+}, Zn^{2+} and Na^{+}) and several different classes of phospholipids(110). Except for the redox-active metal sites, the roles of these components are essentially unknown. The O_2 reduction site comprises heme a_3 (in high-spin state in the oxidized state) and Cu_B (109). Electrons from cytochrome *c* are accepted by Cu_A and transferred to the O_2 reduction site via heme *a* (in six-coordinated low-spin state in both oxidation states (111)). Although cytochrome *c* oxidases of bacteria are less complex, they do include the three largest subunits (subunits I, II, and III) that are common to those of the mammalian enzymes. X-ray structures of bovine and bacterial enzymes indicate strong homology among the three-dimensional structures of these redox-active metal sites, providing convincing evidence for the existence of a conserved reaction mechanism (112).

It is believed that the protons are transferred through the D- and K-pathways in cytochrome *c* oxidase (113). No amino acid residues in the pathway are completely conserved. It has been claimed that completely different sets of amino acid residues

could function in a physiologically identical process (113). At present, X-ray structures of three bacterial oxidases have been solved at resolutions better than 2.8 Å (114-116). Two bacterial aa_3-type cytochrome *c* oxidases have a glycine at the point corresponding to the site of Asp51 in bovine cytochrome *c* oxidase (114,116). A small cavity capable of trapping a water molecule is located between the glycine and the peptide bond in the hydrogen-bond network. The glycine–water combination is expected to be capable of transferring protons from the hydrogen-bond network to the periplasmic phase with a conformational change controlling the accessibility of the water molecule to the aqueous phase. On the other hand, the ba_3-type cytochrome oxidase of an extreme thermophilic bacterium does not have a pathway homologous to the H pathway, but it does contain another hydrogen-bond network which extends across the enzyme molecule (116). These X-ray structural results also suggest variety in the structure of proton transfer pathways.

ATP-synthase

Mitochondrial ATP synthase is the terminal enzyme in oxidative phosphorylation and produces the energy ATP for the cell. It consists of two major units, F_1 in the matrix, which binds ADP/ATP and catalyzes ATP synthesis and hydrolysis, and F_0, which spans the inner mitochondrial membrane and directs protons to the F_1 moiety. As a result of this composition this enzyme is often referred to as F_1F_0 ATP synthase. F_1 is made up of the three α subunits, three β subunits, and one subunit each of γ, δ, and ε. F_0 also contains multiple subunits including an oligomycin sensitivity conferring protein (OSCP), 10-12 *c* subunits involved in gating of the proton channel, an α subunit that facilitates transfer of protons from the inter membrane space to the *c* subunits, two *b* subunits that are thought

to function as stators between F_1 and F_0 and two F_6 subunits that also mediate sensitivity to oligomycin (117). Also present in F_0 are *d*, *e*, *f*, and *g* subunits that are found in close association with the OSCP subunit (118).

F_1F_0 ATPase is able to catalyze both ATP synthesis and hydrolysis. The switch between these two activities is dependent on the proton gradient between the matrix and the inter membrane space. ATPase can use the energy from ATP hydrolysis to pump proton into the intermembrane space or if a large enough proton gradient exists, use the proton flow through the complex (from inter membrane space to matrix) to drive ATP synthesis.

The 10-12 *c* subunits form a ring at the base of the γ subunit and the pumping of protons by the *a* subunit to the *c* ring and is thought to result in the turning of both the *c* ring and the entire F_1 complex. This rotation is believed to provide the energy for the synthesis of ATP by the F_1 complex. Tsunoda *et al.* showed that the ε subunit can exist in two conformations in the F_1 complex (119). When the ε subunit is perpendicular to the inner membrane, ATP hydrolysis is inhibited, proton pumping is inhibited, but ATP synthesis is not. On the other hand, when the ε subunit is parallel to the inner membrane, ATP hydrolysis is activated and proton pumping functions normally, but there is no effect on ATP synthesis. This data indicates that the ε subunit may be important in the regulation of switching between ATP synthesis and ATP hydrolysis.

Oligomycin is a specific inhibitor of ATP synthase. It binds to the membrane portion of the F_0 complex of the enzyme and inhibits proton translocation. Sensitivity of ATP synthase to oligomycin appears to be mediated not only by the OSCP but also by the F_6 subunit and the *b* subunits. OSCP is found in close association with the α and β

subunits of F_1, with which it cross-links, and is nearby some F_0 components of the stalk (120).

References

1. Hauska, G., Hurt, E., Gabellini, N., and Lockau, W. (1983) *Biochim Biophys Acta* 726(2), 97-133
2. Hatefi, Y. (1985) *Annu Rev Biochem* 54, 1015-1069
3. Trumpower, B. L. (1990) *Microbiol Rev* 54(2), 101-129
4. Trumpower, B. L., and Gennis, R. B. (1994) *Annu Rev Biochem* 63, 675-716
5. Berry, E. A., Guergova-Kuras, M., Huang, L. S., and Crofts, A. R. (2000) *Annu Rev Biochem* 69, 1005-1075
6. Yun, C. H., Beci, R., Crofts, A. R., Kaplan, S., and Gennis, R. B. (1990) *Eur J Biochem* 194(2), 399-411
7. Trumpower, B. L. (1990) *J Biol Chem* 265(20), 11409-11412
8. Crofts, A. R. W., C.A. (1983) *Biochim. Biophys. Acta* 726, 149-185
9. ALberts, B. J., A.; et al., . (2002) *Molecular biology of the cell, 4th ed, Garland Science, p773*
10. Nitschke, W. D., S.M. . (1995) *Reaction center associated cytochromes. In Anoxygenic Photosynthetic Bacteria (Blankenship,R.E., Madigan, M.T. & Bauer, C.E., eds)* , pp. 775-805. Kluwer Academic, Dordrecht, Netherlands.
11. Stroebel, D., Choquet, Y., Popot, J. L., and Picot, D. (2003) *Nature* 426(6965), 413-418
12. Kurisu, G., Zhang, H., Smith, J. L., and Cramer, W. A. (2003) *Science* 302(5647), 1009-1014
13. Mitchell, P. (1975) *FEBS Lett* 59(2), 137-139
14. Rich, P. R., and Bendall, D. S. (1980) *Biochim Biophys Acta* 591(1), 153-161
15. Kallas, T., and Malkin, R. (1988) *Methods Enzymol* 167, 779-794
16. Kallas, T. (1994) *in The Molecular Biology of Cyanobacteria (Bryant, D. A., Ed.) pp 259-317, Kluwer Academic Publishers, Dordrecht, The Netherland*

17. Cramer, W. A., Soriano, G. M., Ponomarev, M., Huang, D., Zhang, H., Martinez, S. E., and Smith, J. L. (1996) *Annu Rev Plant Physiol Plant Mol Biol* 47, 477-508
18. Hauska, G., Schu¨tz, M., and Bu¨ttner, M. . (1996) in Oxygenic photosynthesis: The light reactions (Ort, D. R., and Yocum, C. F., Eds.) Kluwer Academic Publishers, Amsterdam.
19. Donald voet, J. G. V. (2004) Biochemistry, Third edition, Wiley John Wiley & Sons, Inc. PP883
20. Whitelegge, J. P., Zhang, H., Aguilera, R., Taylor, R. M., and Cramer, W. A. (2002) *Mol Cell Proteomics* 1(10), 816-827
21. Hauska, G., Nitschke, W., and Herrmann, R. G. (1988) *J Bioenerg Biomembr* 20(2), 211-228
22. Cramer, W. A., Black, M. T., Widger, W. R., and Girvin, M.E. . (1987) *in The Light Reaction (Parker, J., ed), pp.447-493*
23. Bertsch, J., and Malkin, R. (1991) *Plant Mol Biol* 17(1), 131-133
24. de Vitry, C., Breyton, C., Pierre, Y., and Popot, J. L. (1996) *J Biol Chem* 271(18), 10667-10671
25. Ketchner, S. L., and Malkin, R. (1996) *Biochim Biophys Acta* 1273(3), 195-197
26. Takahashi, Y., Rahire, M., Breyton, C., Popot, J. L., Joliot, P., and Rochaix, J. D. (1996) *Embo J* 15(14), 3498-3506
27. Mitchell, P. (1976) *J Theor Biol* 62(2), 327-367
28. Crofts, A. R., Meinhardt, S.W., Jones, K.R., and Snozzi, M. (1983) *Biochim. Biophys. Acta* 723, 202-218
29. Trumpower, B. L. (1976) *Biochem Biophys Res Commun* 70(1), 73-80
30. Trumpower, B. L., and Edwards, C. A. (1979) *J Biol Chem* 254(17), 8697-8706
31. Rich, P. R. (1986) *J Bioenerg Biomembr* 18(3), 145-156
32. Crofts, A. R., and Meinhardt, S. W. (1982) *Biochem Soc Trans* 10(4), 201-203
33. Brandt, U., and Trumpower, B. (1994) *Crit Rev Biochem Mol Biol* 29(3), 165-197
34. Link, T. A. (1997) *FEBS Lett* 412(2), 257-264
35. Junemann, S., Heathcote, P., and Rich, P. R. (1998) *J Biol Chem* 273(34), 21603-21607

36. Zhang, L., Snyder, C., Trumpower, B. L., Yu, L., and Yu, C. A. (1999) *FEBS Lett* 460(2), 349-352
37. Osyczka, A., Moser, C. C., Daldal, F., and Dutton, P. L. (2004) *Nature* 427(6975), 607-612
38. de Vries, S., Albracht, S. P., Berden, J. A., and Slater, E. C. (1981) *J Biol Chem* 256(23), 11996-11998
39. Orii, Y., and Miki, T. (1997) *J Biol Chem* 272(28), 17594-17604
40. Brandt, U. (1998) *Biochim Biophys Acta* 1365(1-2), 261-268
41. Crofts, A. R. (2004) *biochim. Biophys. Acta.* 1665, 77-92
42. Crofts, A. R., Guergova-Kuras, M., Kuras, R., Ugulava, N., Li, J., and Hong, S. (2000) *Biochim Biophys Acta* 1459(2-3), 456-466
43. Crofts, A. R., and Wang, Z. G. (1989) *Photosynthesis research* 22, 69-87
44. Donald voet, J. G. V. (2004) *Biochemistry, Third edition, Wiley John Wiley & Sons, Inc. PP887*
45. Slater, E. C. (1973) *Biochim Biophys Acta* 301(2), 129-154
46. Rieske, J. S. (1971) *Arch Biochem Biophys* 145(1), 179-193
47. Link, T. A., Haase, U., Brandt, U., and von Jagow, G. (1993) *J Bioenerg Biomembr* 25(3), 221-232
48. von Jagow, G., and Link, T. A. (1986) *Methods Enzymol* 126, 253-271
49. Geier, B. M., Haase, U., and von Jagow, G. (1994) *Biochem Soc Trans* 22(1), 203-209
50. Esser, L., Quinn, B., Li, Y. F., Zhang, M., Elberry, M., Yu, L., Yu, C. A., and Xia, D. (2004) *J Mol Biol* 341(1), 281-302
51. Gao, X., Wen, X., Yu, C., Esser, L., Tsao, S., Quinn, B., Zhang, L., Yu, L., and Xia, D. (2002) *Biochemistry* 41(39), 11692-11702
52. Gao, X., Wen, X., Esser, L., Quinn, B., Yu, L., Yu, C. A., and Xia, D. (2003) *Biochemistry* 42(30), 9067-9080
53. Brand, M. D., Reynafarje, B., and Lehninger, A. L. (1976) *J Biol Chem* 251(18), 5670-5679
54. Yu, C. A., Nagaoka, S., Yu, L., and King, T. E. (1978) *Biochem Biophys Res Commun* 82(4), 1070-1078

55. Soriano, G. M., Ponamarev, M. V., Carrell, C. J., Xia, D., Smith, J. L., and Cramer, W. A. (1999) *J Bioenerg Biomembr* 31(3), 201-213
56. Zhang, Z., Huang, L., Shulmeister, V. M., Chi, Y. I., Kim, K. K., Hung, L. W., Crofts, A. R., Berry, E. A., and Kim, S. H. (1998) *Nature* 392(6677), 677-684
57. Iwata, S., Lee, J. W., Okada, K., Lee, J. K., Iwata, M., Rasmussen, B., Link, T. A., Ramaswamy, S., and Jap, B. K. (1998) *Science* 281(5373), 64-71
58. Hunte, C., Koepke, J., Lange, C., Rossmanith, T., and Michel, H. (2000) *Structure Fold Des* 8(6), 669-684
59. Xia, D., Yu, C. A., Kim, H., Xia, J. Z., Kachurin, A. M., Zhang, L., Yu, L., Deisenhofer, J., (1997) *Science* 277(5322), 60-6
60. Link, T. A., and Iwata, S. (1996) *Biochim Biophys Acta* 1275(1-2), 54-60
61. Link, T. A., Saynovits, M., Assmann, C., Iwata, S., Ohnishi, T., and von Jagow, G. (1996) *Eur J Biochem* 237(1), 71-75
62. Iwata, S., Saynovits, M., Link, T. A., and Michel, H. (1996) *Structure* 4(5), 567-579
63. Nicholls, A., Sharp, K. A., and Honig, B. (1991) *Proteins* 11(4), 281-296
64. Osyczka, A., Dutton, P. L., Moser, C. C., Darrouzet, E., and Daldal, F. (2001) *Biochemistry* 40(48), 14547-14556
65. Tian, H., Sadoski, R., Zhang, L., Yu, C. A., Yu, L., Durham, B., and Millett, F. (2000) *J Biol Chem* 275(13), 9587-9595
66. Kim, H., Xia, D., Yu, C. A., Xia, J. Z., Kachurin, A. M., Zhang, L., Yu, L., and Deisenhofer, J. (1998) *Proc Natl Acad Sci U S A* 95(14), 8026-8033
67. Crofts, A. R. (2004) *Annu Rev Physiol* 66, 689-733
68. Tsai, A. L., Olson, J. S., and Palmer, G. (1987) *J Biol Chem* 262(18), 8677-8684
69. Tian, H., Yu, L., Mather, M. W., and Yu, C. A. (1998) *J Biol Chem* 273(43), 27953-27959
70. Tian, H., White, S., Yu, L., and Yu, C. A. (1999) *J Biol Chem* 274(11), 7146-7152
71. Xiao, K., Yu, L., and Yu, C. A. (2000) *J Biol Chem* 275(49), 38597-38604
72. Nieboer, P., and Berden, J. A. (1992) *Biochim Biophys Acta* 1101(1), 90-96
73. Musatov, A., and Robinson, N. C. (1994) *Biochemistry* 33(44), 13005-13012

74. Capaldi, R. A. (1982) *Biochim Biophys Acta* 694(3), 291-306
75. Gong, X., Yu, L., Xia, D., and Yu, C. A. (2005) *J Biol Chem* 280(10), 9251-9257
76. Covian, R., Gutierrez-Cirlos, E. B., and Trumpower, B. L. (2004) *J Biol Chem* 279(15), 15040-15049
77. Yang, X. H., and Trumpower, B. L. (1988) *J Biol Chem* 263(24), 11962-11970
78. Yang, X. H., and Trumpower, B. L. (1986) *J Biol Chem* 261(26), 12282-12289
79. Kriauciunas, A., Yu, L., Yu, C. A., Wynn, R. M., and Knaff, D. B. (1989) *Biochim Biophys Acta* 976(1), 70-76
80. Robertson, D. E., Ding, H., Chelminski, P. R., Slaughter, C., Hsu, J., Moomaw, C., Tokito, M., Daldal, F., and Dutton, P. L. (1993) *Biochemistry* 32(5), 1310-1317
81. Schagger, H., Brandt, U., Gencic, S., and von Jagow, G. (1995) *Methods Enzymol* 260, 82-96
82. Ljungdahl, P. O., Pennoyer, J. D., Robertson, D. E., and Trumpower, B. L. (1987) *Biochim Biophys Acta* 891(3), 227-241
83. Tzagoloff, A., Wu, M. A., and Crivellone, M. (1986) *J Biol Chem* 261(36), 17163-17169
84. Oudshoorn, P., Van Steeg, H., Swinkels, B. W., Schoppink, P., and Grivell, L. A. (1987) *Eur J Biochem* 163(1), 97-103
85. Schoppink, P. J., Hemrika, W., and Berden, J. A. (1989) *Biochim Biophys Acta* 974(2), 192-201
86. Schmitt, M. E., and Trumpower, B. L. (1990) *J Biol Chem* 265(28), 17005-17011
87. Maarse, A. C., De Haan, M., Schoppink, P. J., Berden, J. A., and Grivell, L. A. (1988) *Eur J Biochem* 172(1), 179-184
88. Phillips, J. D., Schmitt, M. E., Brown, T. A., Beckmann, J. D., and Trumpower, B. L. (1990) *J Biol Chem* 265(34), 20813-20821
89. Braun, H. P., and Schmitz, U. K. (1995) *Trends Biochem Sci* 20(5), 171-175
90. Deng, K., Zhang, L., Kachurin, A. M., Yu, L., Xia, D., Kim, H., Deisenhofer, J., and Yu, C. A. (1998) *J Biol Chem* 273(33), 20752-20757
91. Usui, S., and Yu, L. (1991) *J Biol Chem* 266(24), 15644-15649

92. Chen, Y. R., Usui, S., Yu, C. A., and Yu, L. (1994) *Biochemistry* 33(33), 10207-10214
93. Wu, J., and Niederman, R. A. (1995) *Biochem J* 305 (Pt 3), 823-828
94. Tso, S. C., Shenoy, S. K., Quinn, B. N., and Yu, L. (2000) *J Biol Chem* 275(20), 15287-15294
95. Chen, Y. R., Shenoy, S. K., Yu, C. A., and Yu, L. (1995) *J Biol Chem* 270(19), 11496-11501
96. Chen, Y. R., Yu, C. A., and Yu, L. (1996) *J Biol Chem* 271(4), 2057-2062
97. Hohmann, I., Bill, R. M., Kayingo, I., and Prior, B. A. (2000) *Trends Microbiol* 8(1), 33-38
98. Imhoff, J. F. (1992) *in Photosynthetic Prokaryotes (Carr, N. H. M. a. N. G., ed), pp. 53-92, Plenum Press, New York*
99. Hacker, B., Barquera, B., Crofts, A. R., and Gennis, R. B. (1993) *Biochemistry* 32(16), 4403-4410
100. Thony-Meyer, L. (1997) *Microbiol Mol Biol Rev* 61(3), 337-376
101. Sadoski, R. C., Engstrom, G., Tian, H., Zhang, L., Yu, C. A., Yu, L., Durham, B., and Millett, F. (2000) *Biochemistry* 39(15), 4231-4236
102. Engstrom, G., Xiao, K., Yu, C. A., Yu, L., Durham, B., and Millett, F. (2002) *J Biol Chem* 277(34), 31072-31078
103. Xiao, K., Engstrom, G., Rajagukguk, S., Yu, C. A., Yu, L., Durham, B., and Millett, F. (2003) *J Biol Chem* 278(13), 11419-11426
104. Engstrom, G., Rajagukguk, R., Saunders, A. J., Patel, C. N., Rajagukguk, S., Merbitz-Zahradnik, T., Xiao, K., Pielak, G. J., Trumpower, B., Yu, C. A., Yu, L., Durham, B., and Millett, F. (2003) *Biochemistry* 42(10), 2816-2824
105. Xiao, K., Liu, X., Yu, C. A., and Yu, L. (2004) *Biochemistry* 43(6), 1488-1495
106. Liu, X., Yu, C. A., and Yu, L. (2004) *J Biol Chem* 279(45), 47363-47371
107. Gurung, B., Yu, L., Xia, D., and Yu, C. A. (2005) *J Biol Chem*
108. Phillips, J. D., Graham, L. A., and Trumpower, B. L. (1993) *J Biol Chem* 268(16), 11727-11736
109. S. Ferguson-Miller and G.T. Babcock. *Chem. Rev.* 96 (1996), 2889–2907

110. T. Tsukihara, H. Aoyama, E. Yamashita, T. Tomizaki, H. Yamaguchi, K. Shinzawa-Itoh, R. Nakashima, R. Yaono and S. Yoshikawa. *Science* 272 (1996), 1136–1144.

111. B.C. Hill. *J. Biol. Chem.* 269 (1994), 2419–2425.

112. S. Iwata, C. Ostermeier, B. Ludwig and H. Michel. *Nature* 376 (1995), 660–669.

113. M.M. Pereira, M. Santana and M. Tiexiera. *Biochim. Biophys. Acta* 1505 (2001), 185–208.

114. C. Ostermeier, A. Harrenga, U. Ermler and H. Michel. *Proc. Natl. Acad. Sci. USA* 94 (1997), 10547–10553.

115. T. Soulimane, G. Buse, G.P. Bourenkov, H.D. Bartunik, R. Huber and M.E. Than. *EMBO J.* 19 (2000), 1766–1776.

116. M. Svensson-Ek, J. Abrzmson, G. Larsson, S. Törnroth, P. Brzezinski and S. Iwata. *J. Mol. Biol.* 321 (2002), 329–339.

117. M. Saraste. Science 283 (1999), 1488-1493.

118. G. Belogrudov, Y. Hatefi. *J. Biol. Chem.* 271 (1996) 20340-20345.

119. S. Tsunoda. *Proc. Natl. Acad. Sci. U.S.A.* 98 (2001) 6560-6564.

120. D. Medeiros, D. Jennings. *J. Bioenerg. Biomem.* 34 (2002) 389-395.

Chapter II

Material and Methods

Growth of Bacteria: *Rhodobacter sphaeroides* and *Escherichia coli*

Rhodobacter sphaeroides

R. sphaeroides cells, wild-type and mutant were grown photosynthetically at 30°C in an enriched Sistrom medium containing 0.2% casamino acids and 5 mM glutamate (1, 2), the pH of the medium was adjusted to 7.1 with the mixture of 6N NaOH and 2N KOH to increase the sodium and potassium ion content of the medium to a more optimal level (1). When the cells reached the end of log growth phase, i.e., the density OD_{600} of the cell culture reached about 2.0, cells were harvested by centrifugation at 3,300 x g for 45 minutes using Beckman J6-HC centrifuge and JS4.2 rotor. The cells were suspended with buffer containing 1mM EDTA, 20 mM Tris-succcinate, pH 7.5 at 4°C. The suspended cells were centrifuged at 22,000 x g for 25 using Beckman J2-HS centrifuge and JA14 rotor to wash off the medium. The supernatant was discarded and the celles were weighed, and stored at -20°C. About 5-6 grams of cells were routinely obtained from 1 liter of culture.

The concentrations and antibiotics used were: kanamycin sulfate, 30 μg/ml;

tetracycline, 1 μg/ml; and trimethoprim, 30 μg/ml.

Escherichia coli

The cells were grown aerobically at 37°C in LB medium. Antibiotics, when needed, were added at the following concentrations: ampicillin, 125 μg/ml; kanamycin sulfate, 30 μg/ml; tetracycline, 10 μg/ml; and trimethoprim, 100 μg/ml.

Construction of Expression Plasmid and Site-Directed Mutagenesis

Construction of an *R. sphaeroides* Strain Expressing the His_6-Tagged Cytochrome bc_1 Complex

The expression vector for His-tagged four-subunit cytochrome bc_1 complex (pRKD418*fbc*$FB_{KmBP}C_{6H}Q$) was constructed.

(1) Construction of pRKD*fbc*$FB_{Km\mathit{BP}}CQ$ (pRKDNB35KmBP) (2).

The gene encoding a trimethoprim-resistant dihydrofolate reductase from R388 (3) (excised from pSup5Tp) and the engineered *fbc*-containing insert from pSELNB3503 (2) were combined into the multiple cloning site polylinker of pSL1180 by a series of in vitro manipulations. The resulting 4,400-base pair fragment containing the dihydrofolate reductase gene and the *R. sphaeroides fbc* operon were subcloned together into the *Hin*dIII and *Eco*RI sites of the vector pRK415 (4), producing pRKDNB3503. For the purpose of subcloning the 200-base pair *Bst*EII-*Pin*AI fragments from pSELNB3503

following mutagenesis, pRKDNB35KmBP was constructed by inserting the kanamycin resistance cassette from pUC4K between the *Bst*EII and *Pin*AI sites of pRKDNB3503. Using pRKDNB3503KmBP to receive the mutated *Bst*EII-*Pin*AI fragments eliminates the possibility of retaining or recloning the wild-type fragment when attempting to subclone the mutated fragments into the expression vector (5). Loss of kanamycin resistance was then used to screen for recombinant plasmids.

(2) Construction of pRKD*fbc*FBC$_{6H}$Q (6).

A 1,200-base pair *Xba*I-*Hin*dIII fragment containing the *fbc*C and *fbc*Q genes from pRKD*fbc*FBCQ (2), containing *fbc*F, *fbc*B, *fbc*C, and *fbc*Q, was inserted into a modified pSELECT-1 vector in which the unique *Acc*65I site was eliminated. The resulting pSEL*fbc*CQ was used as template for site-directed mutagenesis to introduce an *Acc*65I recognition site right before the stop codon of the *fbc*C gene. Two complementary oligonucleotides with His$_6$ tag coding sequence and the *Acc*65I overhang attached at the 5'-ends (5'-GTACGGGC CAT CAC CAC CAC CAT CAC TAA-3' and 3'-CCCG GTA GTG GTG GTG GTA GTG ATTCATG-5') were synthesized, annealed together by heating up to 70°C and cooling slowly to room temperature, and ligated into the *Acc*65I site of pSEL*fbc*CQ to generate pSEL*fbc*C$_{6H}$Q. The 6-histidine insertion was confirmed by DNA sequencing. A 1,200-base pair *Xba*I-*Hin*dIII fragment containing *fbc*C$_{6H}$Q from pSEL*fbc*C$_{6H}$Q was subcloned into an expression vector (pRKDNB3503) containing the *fbc*FBCQ genes to generate pRKD*fbc*FBC$_{6H}$Q. pRKD*fbc*FBC$_{6H}$Q was transformed into *E. coli* S-17, and then mobilized into *R. sphaeroides* BC17 by using a plate-mating procedure (2). *R. sphaeroides* BC17 is a strain from which most of the *fbc*FBC operon has been deleted (7).

(3) Construction of pRKD418*fbc*FB$_{KmBP}$C$_{6H}$Q.

A 4,887 base pair *Eco*RI-*Hin*dIII fragment containing *fbc*F, *fbc*B, *fbc*C, and *fbc*Q, was inserted into pRKD418 vector which contains an additional resistance gene and an enlarged multiple cloning site region (8). The resulting 16,587 base pair pRKD418 *fbc*FBC$_{6H}$Q plasmid was digested by *Eco*RI and *Xba*I to get 13,207 base pair fragment containing *fbc*C with 6-Histidine at the C-terminal and *fbc*Q. The plasmid pRKD*fbc*FB$_{KmBP}$CQ was also digested with *Eco*RI and *Xba*I to get the 4,632 base pair fragment containing *fbc*F, *fbc*B with kanamycin resistance cassette inserted between the *Bst*EII and *Pin*AI sites. Then a 13,207 base pair fragment was ligated with a 4,632 base pair fragment to get pRKD418*fbc*FB$_{KmBP}$C$_{6H}$Q plasmid. Loss of kanamycin resistance was then used to screen for recombinant plasmids containing the mutant cytochrome *b* gene.

Site-Directed Mutagenesis on Cytochrome *b* with QuickChange

A 3,380 base pair *Eco*RI-*Xba*I fragment containing the *fbc*F and *fbc*B genes from pRKD*fbc*FBCQ, containing *fbc*F, *fbc*B, *fbc*C, and *fbc*Q, was inserted into a pGEM7Zf(+) vector from Promega. The resulting pGEM7Zf(+)*fbc*FB was used as the template and two synthetic oligonucleotides containing desired mutation were used as primers for site-directed mutagenesis. All template and primers are listed in Table 1.

The mutagenic oligonucleotides primers used with QuickChange system must be designed to meet the following considerations (9):

Table 1. Mutations of Cytochrome *b*

Mutamts	Mutagenesis method	Template	primer
cyt*b*Δ(421–445)	QuickChange	pGEM[a]	f[b]:CGAGAAGCCGGTGGCTCCG**TA** **A**GCGACCATCGAAGAAG[c] r[d]: CTTCTTCGATGGTCGC**TTA**CG GAGCCACCGGCTTCTCG
cyt*b*Δ(425–445)	QuickChange	pGEM	f:CCGCCCGCGACCATC**TAA** GAAGACTTCAAC r:GTTGAAGTCTTC**TTA**GAT GGTCGCGGGCGG
cyt*b*Δ(427–445)	QuickChange	pGEM	f:CCCGCGACCATCGAAGAA**TAA** TTCAACGCCCACTACTCG r:CGAGTAGTGGGCGTTGAA**TTA**T TCTTCGATGGTCGCGGG
cyt*b*Δ(433–445)	QuickChange	pGEM	f:CAACGCCCACTAC**TAA** CCGGCGACCGGCGG r:CCGCCGGTCGCCGG**TTA** GTAGTGGGCGTTG

a, pGEM7Z(+)*fbc*FB
b, forward primer
c, all primers are listed from 5' end to 3' end
d, reverse primer

1. Both mutagenic primers must contain the desired mutation and anneal to the same sequence on opposite strands of the plasmid.
2. Primers should be between 25 and 45 bases in length, and the melting temperature (Tm) of the primers should be greater than or equal to 78°C. The following formula is commonly used for estimating the Tm of primers:

   Tm = 81.5 + 0.41 x (%GC) - 675/N - %mismatch (N is the primer length in bases).
3. The desired mutation should be in the middle of the primer with ~10-15 bases of correct sequence on both sides.
4. The primers optimally should have a minimum GC content of 40% and should terminate in one or more C or G bases.

The sample reactions were prepared as indicated below:

5 µl of 10 x reaction buffer

20 ng of double strand DNA template

125 ng of oligonucleotide primer #1

125 ng of oligonucleotide primer #2

1 µl of dNTP mix (10mM, from Promega)

ddH_2O to a final volume of 50 µl

Then add 1 µl of *PfuTurbo* DNA polymerase (2.5 U/µl, from Stratagene®)

Then overlay each reaction with ~30 µl of mineral oil.

The thermal cycle was set up in a MiniCycler™ from M. J. Research as follows:

Step 1: 95°C 2 minutes for initiation;

Step 2: 95°C 50 seconds for denaturation;

Step 3: 63°C 1 minute for annealing reaction;

Step 4: 72°C 7 minutes for extension reaction;

Step 5: Step 2 to Step 4 were repeated 18 times

Step 6: 72°C 7 minutes

The amplification can be checked by electrophoresis of 10 μl of the product on a 1% agarose gel. A ~6,000 base pair band should be clearly visualized at this stage.

Following the thermal cycle, the amplification product was treated with the restriction enzyme *Dpn*I (from Promega, 1 μl each time, two times). The *Dpn*I endonuclease is specific for hemimethylated and methylated DNA, therefore, this digestion is used to select mutation-containing synthesized DNA, since DNA isolated from most of *E.coli* stains are *dam* methylated at adenine residues in the sequence 5'…G^{m}ATC…3' and susceptible to *Dpn*I digestion, while the in vitro synthesized DNA is not. The *Dpn*I treated product was then transformed into XL1-Blue competent cells. Plasmid purified from a single XL1-Blue colony was digested with *Eco*RI and *Xba*I, ran the 1% agarose gel to check the size, if the size of the plasmid was correct, this plasmid was sequenced to confirm the mutation.

The pGEM7Z(+)*fbc*FB plasmid with the mutation (pGEM7Z(+)*fbc*FBm) was digested with *Bst*EII and *Xba*I (*Bst*EII /*Xba*I) or *Eco*RI and *Xba*I (*Eco*RI /*Xba*I) to get 961bp or 3379bp insert, respectively. The pRKD418*fbc*FB$_{KmBP}$C$_{6H}$Q plasmid also digested with *Bst*EII and *Xba*I (*Bst*EII /*Xba*I) or *Eco*RI and *Xba*I (*Eco*RI /*Xba*I) to get 15,626 base pair or 13,208 base pair vector. Then the insert was ligated into the respective vector to get the pRKD418/*fbc*FBmC$_{6H}$Q plasmid. Loss of kanamycin resistance was used to screen for recombinant plasmids containing the mutant cytochrome *b* gene.

The pRKD418/*fbc*FBmCHQ plasmid in *E. coli* S17-1 cells was mobilized into *R. sphaeroides* BC-17 cells by a plate-mating procedure (2). The presence of engineered mutations was confirmed twice by DNA sequencing of the 962 base pair *Bst*EII-*Xba*I fragment before and after photosynthetic growth.

Protein Purification of Histidine-Tagged Cytochrome bc_1 Complex

Frozen *R. sphaeroides* cell (wild-type or mutated) was suspended in 20 mM Tris-succinate, 1 mM EDTA (3 ml/g of cells) and passed through French Press with at about 1000 psig with 1'' diameter piston to break the cell. Protease inhibitor phenylmethanesulfonyl fluoride (PMSF)**,** which was prepared routinely as 1 M in dimethyl sulfoxide (DMSO), was added to the cell suspension to a final concentration of 1mM before passing through the French Press, and was added to the same concentration one more time after the first time passage through the French Press.

The broken cells were centrifuged at 40,000 x g (19,000 rpm) with the Beckman J2-HS centrifuge and JA20 rotor for 20 minutes to get rid of the unbroken cell and cell debris. The supernatant was then subjected to centrifugation at 220,000 x g (54,500 rpm with Ti70 rotor) for 150 minutes to separate the chromatophore fraction from the soluble protein fraction. The precipitate obtained was suspended with 50 mM Tris-Cl, pH 7.5 (room temperature), 1 mM $MgSO_4$ containing 1 mM PMSF, and then homogenized. The homogenate was then subjected to centrifugation at 220,000 x g (54,500 rpm with Ti70 rotor) for 90 minutes to recover chromatophore in precipitate. The resulting chromatophore was suspended in 50 mM Tris-Cl, pH 7.5 (room temperature), 1 mM

$MgSO_4$, 20% glycerol with final volume about 1 ml per 1g cell, and stored at -80°C.

To purify the His-tagged cytochrome bc_1 complex, the frozen chromatophore was thawed and adjusted to a cytochrome *b* concentration of 25 μM with 50 mM Tris-Cl, pH 7.5 (room temperature), 1 mM $MgSO_4$. 10% of dodecylmaltoside (DM) solution (w/v) was added drop by drop to the chromatophore suspension to 0.56 mg/nmol of cytochrome *b*, 4 M NaCl was also added to the final concentration of 100 mM. Then the mixture was stirred at 4°C for 1 hour and then centrifuged at 220,000 x g (54,500 rpm with Ti70 rotor) for 90 minutes. The supernatant was collected and passed through a Ni-NTA agarose column (about 1ml bed volume for every 100nmol of cytochrome *b* in the chromatophore suspensinon), equilibrated with 50 mM Tris-Cl, pH7.5 (room temperature) containing 1 mM $MgSO_4$. The column, absorbed with bc_1 complexes, was then subjected to a sequence of washing with (1) 4 volume of 50 mM Tris-Cl pH8.0 (4°C), 200 mM NaCl, 0.01%DM; (2) 4 volume of 50 mM Tris-Cl pH8.0 (4°C), 200mM NaCl, 5mM Histidine, 0.01%DM; (3) 2 volume of 50mM Tris-Cl pH8.0 (4°C), 200mM NaCl, 0.5% octyl glucoside (OG). The pure cytochrome bc_1 complex was eluted with 50 mM Tris-Cl pH8.0 (4°C), 200 mM NaCl, 200 mM Histidine, 0.5% OG, and concentrated to a final concentration of 300 μM or higher by using a Centriprep concentrator with a 30 KDa or 50 kDa cut-off. The purified complex was stored at -80°C in the presence of 20% glycerol.

Determination of Cytochrome Content

Absorption spectra were recorded at room temperature in a Shimadzu UV2101 PC spectrophotometer at 23 °. Samples were fully oxidized by the addition of aliquots of

10 mM potassium ferricyanide. The cytochrome c_1 was reduced by adding a few crystals of sodium ascorbate, and the content of cytochrome c_1 was determined from the sodium ascorbate reduced minus potassium ferricyanide difference spectrum using the extinction coefficient of 17.5 $cm^{-1}mM^{-1}$ for wavelength pair 552 and 540 nm (10). The cytochrome *b* was reduced by adding a few crystals of sodium dithionite. The content of cytochrome *b* was determined from the sodium dithionite reduced minus potassium ferricyanide difference spectrum using the extinction coefficient of 28.5 $cm^{-1}mM^{-1}$ for wavelength pair 560 and 576 nm (11).

Enzymatic Activity Assay

Chromatophores or purified cytochrome bc_1 complexes were diluted with 50 mM Tris-Cl, pH 8.0 (4°C), containing 200 mM NaCl and 0.01% dodecyl-maltoside to a final concentration of cytochrome *b* of 3 μM. Appropriate amounts of the diluted samples were added to 1 ml of assay mixture containing 100 mM Na^+/K^+ phosphate buffer, pH 7.4, 1 mM EDTA, 100 μM cytochrome *c* (from horse heart, Sigma), and 25 μM $Q_0C_{10}BrH_2$. Ubiquinol cytochrome *c* reductase activity of *R. sphaeroides* bc_1 complex was determined by measuring the reduction of cytochrome *c* by following the increase of absorbance at 550 nm in a Shimadzu UV 2101 PC spectrophotometer at 23 °C, using a millimolar extinction coefficient of 18.5 cm^{-1} for calculation. The nonenzymatic oxidation of $Q_0C_{10}BrH_2$, determined under the same conditions, in the absence of enzyme, was subtracted. Although the chemical properties of $Q_0C_{10}BrH_2$ are comparable with those of $Q_0C_{10}H_2$, it is a better substrate for the cytochrome bc_1 complex (12). To

measure bc_1 activity in chromatophore, 30 μM potassium cyanide was added to the assay mixture to inhibit the cytochrome *c* oxidase activity.

Detergent Titration

Different amounts of dodecyl maltoside were added into 1 ml aliquots of chromatophore prepared from wild type and mutants cells containing 50 μM cytochrome *b* in 50 mM Tris-Cl, pH8.0 (4°C), 1 mM $MgSO_4$. After incubating at 0 °C for 1 h, appropriate aliquots were withdrawn from each sample and assayed for ubiquinol-cytochrome *c* reductase activity using a 3 ml assay mixture containing100 mM Na^+/ K^+ phosphate buffer, pH 7.4, 1 mM EDTA, 100 μM cytochrome *c* (from horse heart, Sigma), and 25 μM $Q_0C_{10}BrH_2$. The assay method is the same as the one described in Enzymatic Activity Assay section. The rest of the samples were subjected to centrifugation at 20,000 x *g* (75,000 rpm) in Beckman Optima™ TL-100 Ultracentrifuge with TLA 100.4 rotor for 90 min. The cytochrome *b* content in supernatant fractions was determined as mentioned above. The 100% cytochrome *b* content refers to that in the dodecyl maltoside-treated sample before centrifugation. The unit of specific activity is μmol of cytochrome *c* reduced/min/nmol of cytochrome *b*.

SDS-Polyacrylamide Gel Electrophoresis

Analytical SDS-polyacrylamide gel electrophoresis was performed using a Bio-Rad Mini-Protean® 3 Cell using Laemmli system (13). Gel preparation was according to

Table 2. Purified wild type and mutants bc_1 complex (50 pmol of cytochrome c_1) were digested in the sample buffer (0.0635 M Tris-CL, pH6.8, 2% SDS, 5% β-mercaptoethanol, 0.002% Bromophenol Blue and 10% glycerol) at 37°C for 30 minutes. Then the samples were subjected to SDS-PAGE under different conditions (Table 2).

Western blot

After SDS-PAGE was done, the gel was equilibrated with transfer buffer (25 mM Tris, 192 mM glycine, 20% v/v methanol) at room temperature for 20 min with gentle shaking. This procedure was repeated three times. The polypeptides separated in the SDS-PAGE gel were transferred to a 0.22 μm nitrocellulose membrane by using Trans-Blot®SD Semi-Dry Transfer cell from BIO-RAD for 30 minutes, and the voltage used was 15V. The membrane was now ready for the immunoblotting assay.

The procedure of immunoblotting assay was as the following:

1) After electophoretic blotting was done, the membrane was immersed in TBS buffer (20 mM Tris, 500 mM NaCl, pH7.5) for 10 minutes, face up;
2) The TBS solution was discarded and replaced with blocking solution (3% gelatin, 20 mM Tris, 500 mM NaCl, pH7.5), and gently agitated for one hour at room temperature;
3) The blocking solution was discarded and replaced with TTBS buffer (0.05% Tween-20, 20 mM Tris, 500 mM NaCl), and gently agitated at room temperature for 5 minutes. The membrane was washed using TTBS buffer one more time;

4) The TTBS solution was discarded and replaced with the first antibody solution (1% gelatin, 20 mM Tris, 500 mM NaCl, pH7.5, and the diluted rabbit polyclonal antibodies raised against purified ISP and subunit IV), and gently agitated overnight at room temperature.
5) The first antibody solution was discarded and replaced with TTBS, and gently agitated for 5 minutes at room temperature. The membrane was washed using TTBS buffer one more time;
6) The TTBS solution was discarded and replaced with Protein A horseradish peroxidase conjugate from Bio-rad (second antibody), and gently agitated for one hour at room temperature;
7) The second antibody solution was discarded and replaced with TTBS, and gently agitated for 5 minutes. The membrane was washed using TTBS buffer one more time;
8) The TTBS solution was discarded and replaced with TBS solution, gently agitated for 5 minutes at room temperature. The membrane was washed using TBS buffer one more time;
9) The TBS solution was discarded and added HRP color development solution prepared freshly ([a]. Dissolve 30 mg HRP Color Development Reagent from Bio-rad in 10 ml ice cold methanol, [b]. Immediately prior to use, add 30 μl of ice cold 30% H_2O_2 to 50 ml room temperature TBS, [c]. Mix [a] with [b] right before use.). During color development, the chamber which the membrane was soaked in the solution should be wrapped with aluminum foil. Gently agitate until color shows;

Table 2. SDS-PAGE gel preparation and running condition

			Staking gel	Separating gel	Running conditions
Regular	T=12.5% C=3%	1.5M Tris-Cl, pH 8.0	1 ml	2.5 ml	Running buffer: 3.028% (w/v) Tris, 14.412% (w/v) glycine, 1% (w/v) SDS; 200V for 45 minutes
		deionized H_2O	2.3 ml	3.2 ml	
		30% acrylamide:Bis	0.63 ml	4.17 ml	
		10% SDS	40 µl	0.1 ml	
		10% APS	50 µl	50 µl	
		TEMED	5 µl	5 µl	
High Resolution	T=16.5% C=4%	Acrylamide	0.24 g	1.6 g	Running buffer: anode buffer: 0.2 M Tris, pH 8.9; cathode buffer: 0.1 M Tris, 0.1M Tricine, 0.1% SDS; 20V for 2 hours 30V overnight
		Bis-acrylamide	0.0075 g	0.07 g	
		Gel buffer	1.5 ml	3.34 ml	
		Urea	0	4.2 g	
		Total volume	3 ml	10 ml	
		10% APS	50 µl	50 µl	
		TEMED	5 µl	5 µl	

APS: Ammonium persulfate;
Gel buffer: 3 M Tris, 1 M HCl, 0.3 % SDS;
T: the total concentration of acrylamide and bisacrylamide;
C: cross-linker concentration

10) The HRP color development solution was discarded and replace with distilled water, gently agitated for 10 minutes and changed to the deionized water at least once.

11) The membrane was stored at dark.

Potentiometric Titration

Redox titrations of cytochromes *b* and c_1 in complement and mutant bc_1 complexes were essentially according to the previously published method (14,15). 3 ml of aliquots of the bc_1 complex (2 μM cytochrome *b* or 2 μM cytochrome c_1) in 0.1 M Na^+/K^+ phosphate buffer, pH 7.0, containing 20 μM phenazine methosulfate (midpoint redox potential (*Em* +80 mV), 20 μM phenazine ethosulfate (*Em* +55 mV), 20 μM phenazine (*Em* -120 mV), 20 μM pyocyanine (*Em* -34 mV), 25 μM 1,4-benzoquinone (*Em* +293 mV), 25 μM 1,2-naphthoquinone (*Em* +143 mV), 25 μM 1,4-naphthoquinone (*Em* +36 mV), 50 μM duroquineone (*Em* +5 mV), 70 μM 2,3,5,6-tetramethyl-*p*-phenylenediamine (*Em* +260 mV), and 15 μM 2-hydroxy-1,4-naphthoquinone (*Em* -145 mV), were used. Reductive titrations were carried out by addition of sodium dithionite solution to the ferricyanide-oxidized sample; oxidative titrations were carried out by addition of ferricyanide solution to the dithionite-reduced sample. At indicated E_h values during the redox titration, absorption spectra from 600 to 500 nm were taken with a Shimadzu model UV-2100 spectrophotometer. The absorbance at 562 nm, minus that at 575 nm, is used for cytochrome *b* and that at 552 minus 540 nm for cytochrome c_1. The

midpoint potentials of cytochrome b_L and b_H were calculated by fitting the redox titration data, obtained for cytochrome *b*, the Nernst equation for a one-electron carrier (n =1) with two components using the KaleidaGraph 3.5 program, and that of cytochrome c_1 was fitted for a one-electron carrier with one component.

Electron Paramagnetic Resonance Spectrometry

EPR spectra were recorded with a Bruker EMX spectrometer, equipped with a liquid helium flow cryostat, at 7 K. Purified wild-type and mutant bc_1 complexes (230 μM cytochrome *b*) were treated with a small excess of ascorbate solution to fully reduce cytochrome c_1 and frozen in liquid nitrogen immediately. EPR spectra of the [2Fe-2S] cluster of the Rieske iron-sulfur protein were obtained from samples scanning once from 3200 to 4000 G magnetic field. In order to get the *gy* signal amplitude in mutant complexes about the same as that in the wild type complex, different scanning times were applied. EPR spectra were recorded with the following instrument settings: microwave frequency, 9.3 GHz; microwave power, 2.2 milliwatts; modulation amplitudes, 6.3 G; modulation frequency, 100 kHz; time constant, 665.4 ms; sweep time: 167.8 s; conversion time, 163.8 ms. Sample preparation and instrument settings of EPR spectra of cytochrome b_L and b_H were the same as those for the [2Fe-2S] cluster of the Rieske iron-sulfur protein, except that the microwave power used was 108.1 milliwatts and modulation amplitude was 20 G.

Saturation Transfer EPR (ST EPR) Measurement

EPR measurements were made with a Bruker EMX EPR spectrometer, using an aqueous quartz flat cell. The temperature of the microwave cavity was controlled by circulation of cooled nitrogen gas from a modified variable temperature housing assembly equipped with an electric temperature sensor. The instrument settings were as follows: field modulation frequency, 100kHz; microwave power, 107.8 mW; time constant, 1310.72 ms, modulation amplitute, 8 G; microwave frequency, 9.757 GHz, which were employed with phase-sensitive detection at 100 Hz (second harmonic) 90^0 out of phase. The phase was adjusted to minimize the second harmonic signal. Approximate rotational correlation time (τ_2) was obtained from the ratio of the two field lines (L"/L).

Mass Spectrometry Determination

The mass spectrometry determination of molecular weights of cytochrome *b* in the wild type and mutant bc_1 complexes was performed with an Applied Biosystems DE-PRO MALDI-TOF mass spectrometer operated in delayed-extraction positive-ion liner mode according to the method of Ghaim *et al.* (16) with modifications. Samples (~30 μl) were mixed with 6 volumes of 10% trichloroacetic acid, chilled for 5 min on ice, centrifuged, and the precipitate was rinsed briefly with 95% ethanol to remove salts. The resulting pellet was redissolved in 30 μl of 99% formic acid and a 1:1 dilution with 99%

formic acid to a final volume of 60 µl, which gave the best crystals and signal. As matrix for MALDITOF analyses, 1% of 2,5-dihydroxybenzoic acid in 30% acetonitrile, 0.1% trifluoroacetic acid and 1% 5-methoxysalicilic acid in 30% acetonitrile, 0.1% trifluoroacetic acid were mixed 9:1 (v/v). This matrix solution was mixed 1:1 (v/v) with protein samples. Matrix and sample were spotted onto the sample plate, and were cocrystallized by evaporation in a covered Petri dish under ambient temperature and pressure (16).

Differential Scanning Calorimetry (DSC)

Differential scanning calorimetric measurements were performed with a CSC 6100 NanoII DSC instrument. The bc_1 sample was diluted in phosphate buffer (Na/K Pi 100mM, pH 7.4) instead of Tris buffer to avoid the large pH change during the heating. Prior to being loaded in the "sample cell" of the machine. 0.50 ml sample of bc_1 solution, 2 mg/ml, in 50 mM K^+/Na^+ phosphate buffer, pH7.4, containing 100mM KCl and 0.5% octyl glucoside was degassed for 5 min to remove dissolved air, which may interfere with the DSC data during the heating process. The same volume of buffer was loaded into the "reference cell" of the instrument, after being degassed. During the scanning, both the sample and the buffer were heated from 10°C to 90°C, cooled back to 10°C and heated again to 90°C, with the scanning rate of 1°C/min for both heating and cooling. The cells were equilibrated at 10°C and 90°C for 10 min before heating and cooling. The difference of power input between the "sample cell" and the "reference cell" was recorded in µW, with one data point taken every 10 seconds, as heating and cooling of the

cells were done at a steady rate of 1°C per minute. The second heating scan was used as the baseline. Melting temperature (Tm) and enthalpy change (ΔH) of the sample were calculated by using the program known as "CpCalc" from the Nano DSC program group.

References

1. Sistrom, W. R. (1960) *J Gen Microbiol* **22**, 778-785
2. Mather, M. W., Yu, L., and Yu, C. A. (1995) *J Biol Chem* **270**(48), 28668-28675
3. Ward, J. M., and Grinsted, J. (1982) *Plasmid* **7**(3), 239-250
4. Ditta, G., Schmidhauser, T., Yakobson, E., Lu, P., Liang, X. W., Finlay, D. R., Guiney, D., and Helinski, D. R. (1985) *Plasmid* **13**(2), 149-153
5. Hacker, B., Barquera, B., Crofts, A. R., and Gennis, R. B. (1993) *Biochemistry* **32**(16), 4403-4410
6. Tian, H., Yu, L., Mather, M. W., and Yu, C. A. (1998) *J Biol Chem* **273**(43), 27953-27959
7. Yun, C. H., Beci, R., Crofts, A. R., Kaplan, S., and Gennis, R. B. (1990) *Eur J Biochem* **194**(2), 399-411
8. Mather, M. W., McReynolds, L. M., and Yu, C. A. (1995) *Gene* **156**(1), 85-88
9. QuikChangeTM XL Site-directed Mutagenesis Kit, I. M. (2001) pp. 5, 8
10. Yu, L., Dong, J. H., and Yu, C. A. (1986) *Biochim Biophys Acta* **852**(2-3), 203-211
11. Berden, J. A., and Slater, E. C. (1970) *Biochim Biophys Acta* **216**(2), 237-249
12. Yu, C. A., and Yu, L. (1982) *Biochemistry* **21**(17), 4096-4101
13. Laemmli, U. K. (1970) *Nature* **227**(5259), 680-685
14. Dutton, P. L. (1978) *Methods Enzymol* **54**, 411-435
15. Guner, S., Robertson, D. E., Yu, L., Qiu, Z. H., Yu, C. A., and Knaff, D. B. (1991) *Biochim Biophys Acta* **1058**(2), 269-279
16. Ghaim, J. B., Tsatsos, P. H., Katsonouri, A., Mitchell, D. M., Salcedo-Hernandez,

R., and Gennis, R. B. (1997) *Biochim Biophys Acta* **1330**(2), 113-120

Chapter III

The Role of Extra Fragment at the C-terminal of Cytochrome *b* (Residues 421–445) in the Cytochrome bc_1 Complex from *Rhodobacter sphaeroides*

Introduction

The cytochrome bc_1 complex is an essential energy transduction electron transfer complex in mitochondria and many aerobic and photosynthetic bacteria (1). The complex catalyzes electron transfer from ubiquinol to cytochrome c_1 with concomitant translocation of protons across the membrane to generate a membrane potential and proton gradient for ATP synthesis. All the cytochrome bc_1 complexes contain three core subunits, cytochrome *b*, cytochrome c_1, and Rieske iron-sulfur protein (ISP), which house two *b*-type hemes (b_L and b_H), one *c*-type heme (heme c_1), and a high potential [2Fe-2S] cluster, respectively. In addition to these three core subunits, the cytochrome bc_1 complex also contains varying numbers (one to eight) of non-redox containing subunits, known as supernumerary subunits (2,3).

Because the bacterial complexes contain no (or one) supernumerary subunit, it is unlikely that the structures of the core subunits in these complexes are, as suggested for the mitochondrial complex (4), stabilized through interactions between core subunits and their neighboring supernumerary subunits. Perhaps interactions between a part of a core

subunit and another part of the same subunit or another core subunit contribute to the stability of a core subunit in the bacterial complex. This speculation finds some support from the fact that core subunits in bacterial complexes are generally bigger than their counterparts in the mitochondrial complex.

Sequence alignment of cytochrome *b*, cytochrome c_1, and ISP in bacterial complexes with their counterparts in mitochondrial complexes reveals four extra fragments in bacterial cytochrome *b* and one each in bacterial cytochrome c_1 and ISP (5). These extra fragments are modeled into the structure of the *Rhodobacter sphaeroides* bc_1 complex by using coordinates of mitochondrial supernumerary subunits (5). These findings encouraged us to suggest that these extra fragments may possess mitochondrial supernumerary subunit function in stabilizing the structure of the core subunits in the bacterial complex. This suggestion is further supported by the recent finding that ISP is lost from the *R. sphaeroides* bc_1 complex if the extra fragment of ISP is deleted or substituted with alanine (6). Of course, confirmation of this suggestion will have to wait until the function of extra fragments in cytochrome *b* and c_1 are established.

Cytochrome *b* holds a central role in the cytochrome bc_1 complex because it houses two ubiquinone binding sites, Qo and Qi, and two redox centers, heme b_L and heme b_H. According to the Q-cycle mechanism (7), electrons from ubiquinol are bifurcated at the Qo site. The first electron of ubiquinol is transferred through the so-called "high potential" chain consisting of [2Fe-2S] and heme c_1. The second electron of ubiquinol is passed through the "low potential" chain consisting of hemes b_L and b_H. Thus, maintaining the structural stability of cytochrome *b* in the bc_1 complex is crucial for the electron and proton transfer functions of this complex.

In the structure model of *R. sphaeroides* cytochrome bc_1 complex (5), the four extra fragments of cytochrome *b* are located at the N terminus (residues 2 to 12), the connecting loop between helices D and E (residues 232 to 239), the connecting loop between helices E and F (residues 309 to 326), and the C terminus (residues 421–445) (see Fig. 1). We started functional studies of these cytochrome *b* extra fragments with the one at the C terminus because this extra fragment is in close proximity to subunit IV and ISP. Herein we report generation of *R. sphaeroides* mutants expressing His-tagged cytochrome bc_1 complexes with progressive deletion of the C-terminal extra fragment of cytochrome *b*. The photosynthetic growth behavior, the bc_1 activity, and the amount of cytochrome *b*, cytochrome c_1, ISP, and subunit IV, in the chromatophore membrane and the purified state, of the complement and mutants, were determined and compared. The lability of mutant bc_1 complex, in the chromatophore membranes, toward dodecylmaltoside treatment, was investigated. The effect of mutations on EPR spectra of the cytochromes *b* and ISP and on redox potentials of the cytochromes *b* and c_1, in complement and mutant complexes, is also reported.

Results and Discussion

Comparison of Electron Transfer Activity, Subunit Composition, and Detergent Lability of Cytochrome bc_1 Complexes in Chromatophore Membranes from Complement and C-terminal Truncated Cytochrome *b* Mutants

The C-terminal extra fragment of *R. sphaeroides* cytochrome *b* corresponds to residues 421–445 with a sequence of PATIEEDFNAHYSPATGGTKTVVAE (see Fig.

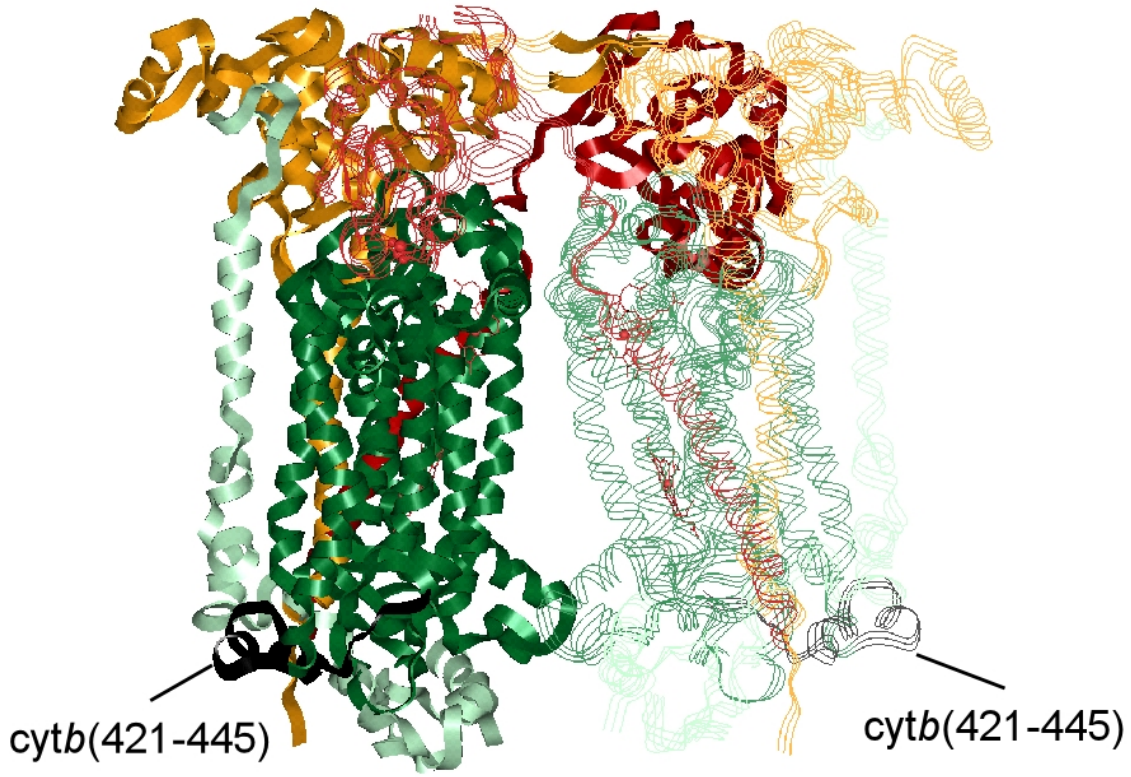

Fig.17. **Location of the C-terminal extra fragment of cytochrome *b* in the proposed structural model of *R. sphaeroides* cytochrome bc_1 complex.** One monomer (*left*) is displayed in *solid ribbons*, and the symmetric monomer (*right*) is displayed in *three-treadline ribbons*. Cytochrome c_1 is *rust*; ISP is *brown*; subunit IV is *silver*; cytochrome *b* is *green*; and the C-terminal extra fragment is *black*.

Fig.18. Partial sequence comparison in the C-terminal extra fragment of various cytochrome *b***.** The abbreviations used are: *Rs*, *R. sphaeroides*; *Rc*, *R. capsulatus*; *Pd*, *P. denitrificans*; *Bf*, bovine; *Yt*, *S. cerevisiae*; *Ck*, chicken.

18). To probe the role of this fragment, *R. sphaeroides* mutants with progressive deletion of amino acid residues from the C terminus of cytochrome *b* were generated and characterized. These are: cyt*b*Δ(433–445), cyt*b*Δ(427–445), cyt*b*Δ(425–445), and cyt*b*Δ(421–445) with deletion of 13, 19, 21, and all residues from this C-terminal extra fragment of cytochrome *b*, respectively.

When these four C-terminal-truncated cytochrome *b* mutants were subjected to anaerobic photosynthetic growth conditions, all of them grew at a rate comparable with that of the complement cells. Chromatophores prepared from these mutant cells have the content and absorption spectral properties of cytochrome *b* and cytochrome $c_1 + c_2$ similar to those in the complement chromatophores (data not shown). The amounts of ISP and subunit IV in these mutant chromatophores, determined by Western blotting using antibodies against *R. sphaeroides* ISP and subunit IV, respectively, are also comparable with those in complement chromatophores. These results indicate that the C-terminal extra fragment of cytochrome *b* is not required for assembly of the cytochrome bc_1 complex protein subunits (cytochromes *b* and c_1, ISP, and subunit IV) into the chromatophore membrane.

Fig. 19*A* shows the effect of DM concentration on bc_1 activity in the complement and four mutant chromatophores. When chromatophores from the complement and four mutants, at a cytochrome *b* concentration of 25 μM, were treated with varying concentrations of DM (up to 0.64 mg of DM per nmol of cytochrome *b*), bc_1 activities in all preparations increase at lower and decrease at higher detergent concentrations. However, the detergent concentrations required for maximum activity increasing and decreasing differ significantly. Also, the activity increase or decrease in a given

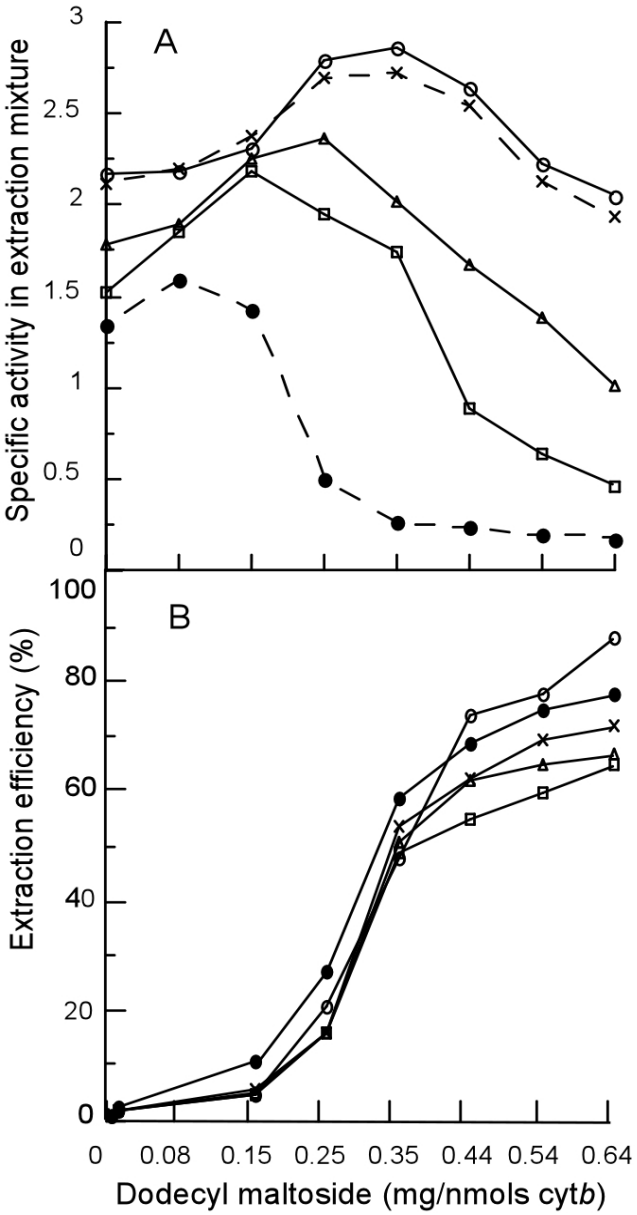

Fig.19. Effect of DM concentration on bc_1 activity and solubilization of cytochrome *b* from complement and mutant chromatophores. 1-ml aliquots of chromatophore preparations from complement (o), and mutants cyt*b*Δ-(433-445) (x), cyt*b*Δ-(427-445) (Δ), cyt*b*Δ-(425-445) (□), and cyt*b*Δ-(421-445) (•), containing 50 μM cytochrome *b*, were added at the indicated amounts of DM. After incubating at 0°C for 1 hr, appropriate aliquots were withdrawn from each sample and assayed for ubiquinol-cytochrome *c* reductase activity using a 3-ml assay mixture (A). The rest of samples were subjected to centrifugation at 100,000 x g for 90 min. The cytochrome *b* content in supernatant fractions was determined (B). The 100% cytochrome *b* content refers to that in the DM-treated sample before centrifugation. The unit of specific activity is μmol of cytochrome *c* reduced/min/nmol of cytochrome *b*.

detergent concentration varies greatly among these chromatophores.

Mutant chromatophores of cyt*b*Δ(433–445), cyt*b*Δ(427–445), cyt*b*Δ(425–445) and cyt*b*Δ(421–445), without DM treatment, have, respectively, 100, 82, 70, and 62% of the bc_1 activity found in untreated complement chromatophores. Maximum bc_1 activities are obtained for mutant chromatophores of cyt*b*Δ(433–445), cyt*b*Δ(427–445), cyt*b*Δ(425–445), and cyt*b*Δ(421–445) at DM concentrations of 0.35, 0.25, 0.15, and 0.08 mg/nmol of cytochrome *b,* respectively. These correspond, respectively, to 95, 83, 77, and 56% of maximum bc_1 activity of the complement chromatophores treated with 0.35 mg of DM per nmol of cytochrome *b* (see Fig. 19*A*). Thus the bc_1 complexes with decreasing lengths of the C-terminal extra fragment of cytochrome *b* require decreasing amounts of DM to obtain maximum activity. Furthermore, maximum bc_1 activity in the chromatophore membrane decreases as the C-terminal extra fragment of cytochrome *b* shortens.

Whereas the complement chromatophores treated with 0.35 mg of DM/nmol of cytochrome *b* shows maximum bc_1 activity, mutant chromatophores of cyt*b*Δ(433–445), cyt*b*Δ(427–445), cyt*b*Δ(425–445), and cyt*b*Δ(421–445) treated with the same concentration of DM lost, respectively, 0, 22, 35, and 81% of their maximum bc_1 activity, indicating that the lability of the bc_1 complex toward detergent treatment increases as the size of the C-terminal extra fragment decreases. The increase in lability of the bc_1 complex to detergent treatment should be indicative of a decrease in structural stability of the complex. Thus, the structural stability of the bc_1 complex decreases as the C-terminal extra fragment of cytochrome *b* decreases. Residues 433–445 make little contribution to the structural stability of the bc_1 complex, as the electron transfer activity and detergent

lability of the cyt*b*Δ(433–445) bc_1 are similar to those of the complement complex.

It should be noted that the effectiveness of DM in solubilizing the bc_1 complex from these deletion mutant chromatophores is comparable with that for the complement chromatophores (Fig.19*B*). When complement and mutant chromatophores of cyt*b*Δ(433–445), cyt*b*Δ(427–445), cyt*b*Δ(425–445), and cyt*b*Δ(421–445) treated with various concentrations of DM were centrifuged at 200,000 x *g* for 90 min, the contents of cytochrome *b*, determined spectrophotometrically (see Fig. 19*B*), ISP, and subunit IV determined by Western blotting (data not shown), in the supernatant fractions, at a given DM concentration, are about the same. This suggests that the loss of bc_1 activity in the cyt*b*Δ(421–445) mutant chromatophores treated with 0.35 mg of DM/nmol of cytochrome *b* is not because of a decrease of binding affinity of the bc_1 complex to the membrane, but to a lesser structural integrity of the mutant complex.

Effect of the C-terminal Extra Fragment of Cytochrome *b* on the Binding of Cytochrome *b*, ISP, and Subunit IV to Cytochrome c_1

To further confirm that the structural integrity of the bc_1 complex decreases as the C-terminal extra fragment of cytochrome *b* decreases, binding affinities of protein subunits in mutant complexes of cyt*b*Δ(433–445), cyt*b*Δ(427–445), cyt*b*Δ(425–445), and cyt*b*Δ(421–445) were determined and compared with those of the complement complex. Because the expressed *R. sphaeroides* bc_1 complex has a His_6 tag at the C terminus of cytochrome c_1, one can determine binding affinities of cytochrome *b*, ISP, and subunit IV

to cytochrome c_1 in complement and mutant complexes using a Ni-NTA column.

When various chromatophores were treated with 1.2% DM and centrifuged at 200,000 x *g* for 90 min, about 80% of cytochrome *b*, cytochrome c_1, ISP, and subunit IV in the complement and mutant chromatophores was recovered in the supernatant fractions. When these supernatant fractions were applied to Ni-NTA columns, most of cytochrome c_1 in all of these supernatant fractions as absorbed on the Ni-NTA gel, and as recovered in column eluates using an eluting buffer containing 200 mM histidine. This is as expected because the His_6 tag is placed at the C terminus of cytochrome c_1. The b/c_1 ratios in column eluates of the complement and mutants cyt*b*Δ(433–445), cyt*b*Δ(427–445), cyt*b*Δ(425–445), and cyt*b*Δ(421–445) are 1.51, 1.45, 0.81, 0.72, and 0.29, respectively (see Table 3), indicating that the binding affinity of cytochrome *b* to cytochrome c_1 decreases as the C-terminal extra fragment of cytochrome *b* shortens. The amount of mutant cytochrome *b* of cyt*b*Δ(433–445), cyt*b*Δ(427–445), cyt*b*Δ(425–445), and cyt*b*Δ(421–445) associated with cytochrome c_1, as compared with the amount of wild-type cytochrome *b* associated with cytochrome c_1, decreases by 4, 46, 52, and 80%, respectively.

Fig.20. shows Western blot analysis of ISP and subunit IV recovered in the Ni-NTA column eluate (purified bc_1 complex) and effluent fractions from DM-solubilized complement and mutant chromatophores. The purified cyt*b*Δ(421–445) mutant complex contains no detectable ISP or subunit IV, however, purified mutant complexes of cyt*b*Δ(425–445), cyt*b*Δ(427–445), and cyt*b*Δ(433–445) have 50, 80, and 100%, respectively, of the amount of ISP or subunit IV found in the complement complex (see

Table 3. Characterization of mutants having deletions on the C-terminal extra fragment of cytochrome *b*

		Cytochrome bc_1 complex					
		Chromatophore			Purified complex		
Strains	Ps[a]	specific activity[b]	cyt*b*/ cytc_1+c_2	subunit composition	specific activity[b]	cyt*b*/cytc_1	subunit composition
complement	+++[c]	2.24	1.26	FBCQ[d]	3.20	1.51	FBCQ
cyt*b*Δ(433-45)	+++	2.23	1.30	FBCQ	2.91	1.45	FBCQ
cyt*b*Δ(427-45)	+++	1.87	1.39	FBCQ	2.88	0.81	FBCQ
cyt*b*Δ(425-45)	+++	1.52	1.35	FBCQ	1.69	0.72	FBCQ
cyt*b*Δ(421-45)	+++	1.32	1.23	FBCQ	0	0.29	FB

[a]Ps: photosynthetic growth. [b]enzyme activity is expressed as μmol cytochrome *c* reduced/min/nmol cytochrome *b*. [c]+++ indicates the cells can grow photosynthetically and the growth rate was essentially the same as that of the complement cells. [d]FBCQ indicates gene products of the *fbc*F (ISP) (F), *fbc*B(cytochrome *b*) (B), *fbc*C (cytochrome c_1) (C), and *fbc*Q (subunit IV) (Q), respectively.

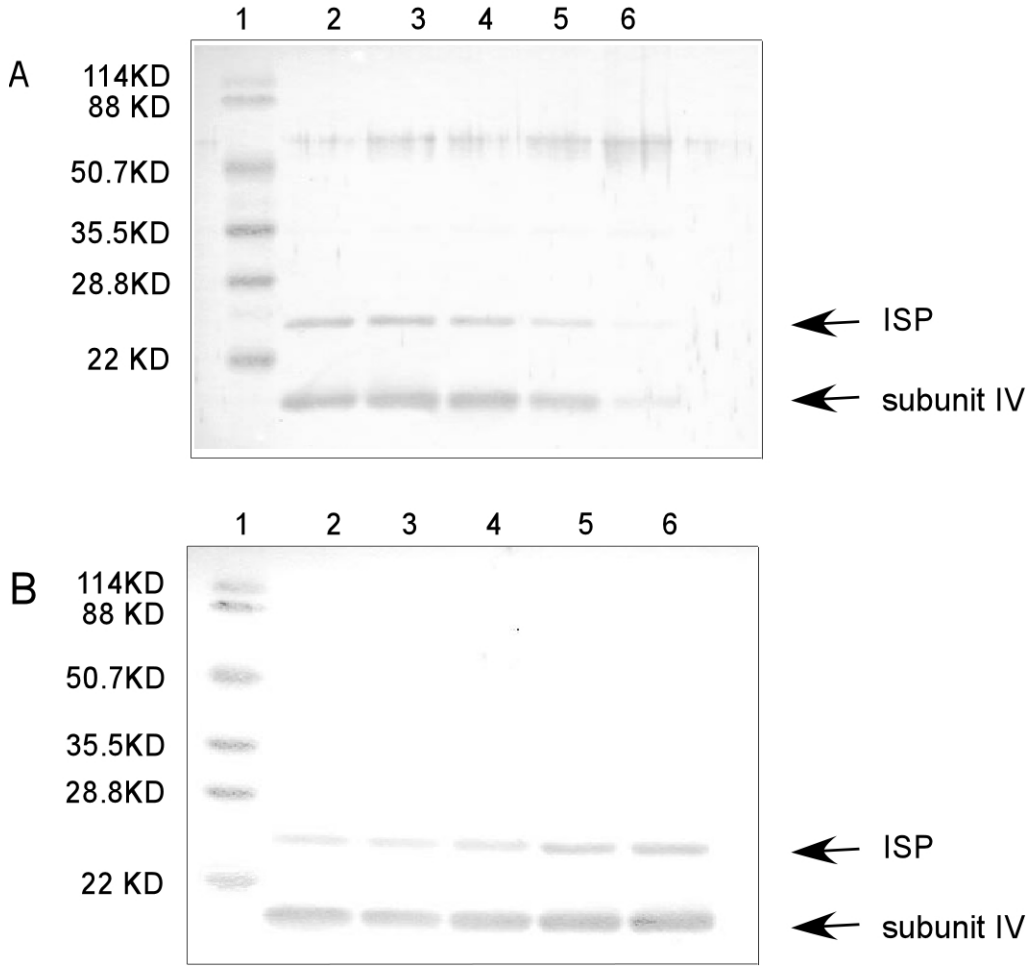

Fig.20. Western blot analysis of ISP and subunit IV in the Ni-NTA column effluent and eluate fractions from DM-solubilized complement and mutant chromatophores. 2-ml of DM-solubilized complement (*lane 2*) and mutant chromatophores of cyt*b*Δ(433–445) (*lane 3*), cyt*b*Δ(427–445) (*lane 4*), cyt*b*Δ(425–445) (*lane 5*), and cyt*b*Δ(421–445) (*lane 6*) were applied to Ni-NTA columns (500-µl bed volume) equilibrated with 50 mM Tris-Cl, pH 8.0, containing 1 mM $MgCl_2$. The column was washed with 1 ml of 50 mM Tris-Cl, pH 8.0, containing 200 mM NaCl and 0.01% DM, and then eluted with 1 ml of 50 mM Tris-Cl, pH 8.0, containing 200 mM NaCl, 200 mM histidine, and 0.5% octyl glucoside. The volume of column eluate was adjusted to that of the column effluent (unabsorbed plus wash). 2-µl aliquots were withdrawn from column elute (*A*) and column effluent (*B*) fractions and subjected to SDS-PAGE. Samples in the gel were transferred to a 22-µm nitrocellulose membrane and treated with antibodies against *R. sphaeroides* ISP and subunit IV. ProteinA-horseradish peroxide conjugate was used as a second antibody. *Lane 1* shows low range prestained standards.

Fig. 20*A*). These results are consistent with the presence of increasing amounts of ISP and subunit IV in the Ni-NTA column effluents of cyt*b*Δ(433–445), cyt*b*Δ(427–445), cyt*b*Δ(425–445), and cyt*b*Δ(421–445) (see Fig. 20*B*). It should be noted that subunit IV of the bc_1 complex produced by *R. sphaeroides* BC-17 cells carrying the pRKD418/*fbcFBCQ* plasmid includes chromosomal and plasmid copies, whereas cytochrome *b*, c_1, and ISP have only the plasmid copy. These results indicate that the binding affinities of ISP and subunit IV to the complex are affected by the first 12 residues (residues 421–432) at the N-terminal end of the C-terminal extra fragment of cytochrome *b*; binding affinity decreases as the fragment size decreases.

The finding that the binding of ISP and subunit IV to cytochrome c_1 are affected by the C-terminal extra fragment of cytochrome *b* is rather surprising, because they are not in the same subunit as cytochrome *b*. Perhaps interactions between the C-terminal extra fragment of cytochrome *b* and the N-terminal portion of ISP or subunit IV, located on the cytoplasmic side of the chromatophore membrane, are required for maintaining the structures of ISP and subunit IV for binding to cytochrome c_1. Thus, the mutations on the C-terminal extra fragment of cytochrome *b* induce conformational changes on ISP and subunit IV that weaken their binding affinities for cytochrome c_1. Alternatively, the binding of ISP or subunit IV to cytochrome c_1 is through cytochrome *b* and mutation of the extra fragment not only decreases the binding affinity of cytochrome *b* to cytochrome c_1, but also to ISP and subunit IV.

The Abnormality of Electrophoretic Mobilities of C-terminal Truncated Cytochrome *b* Mutants

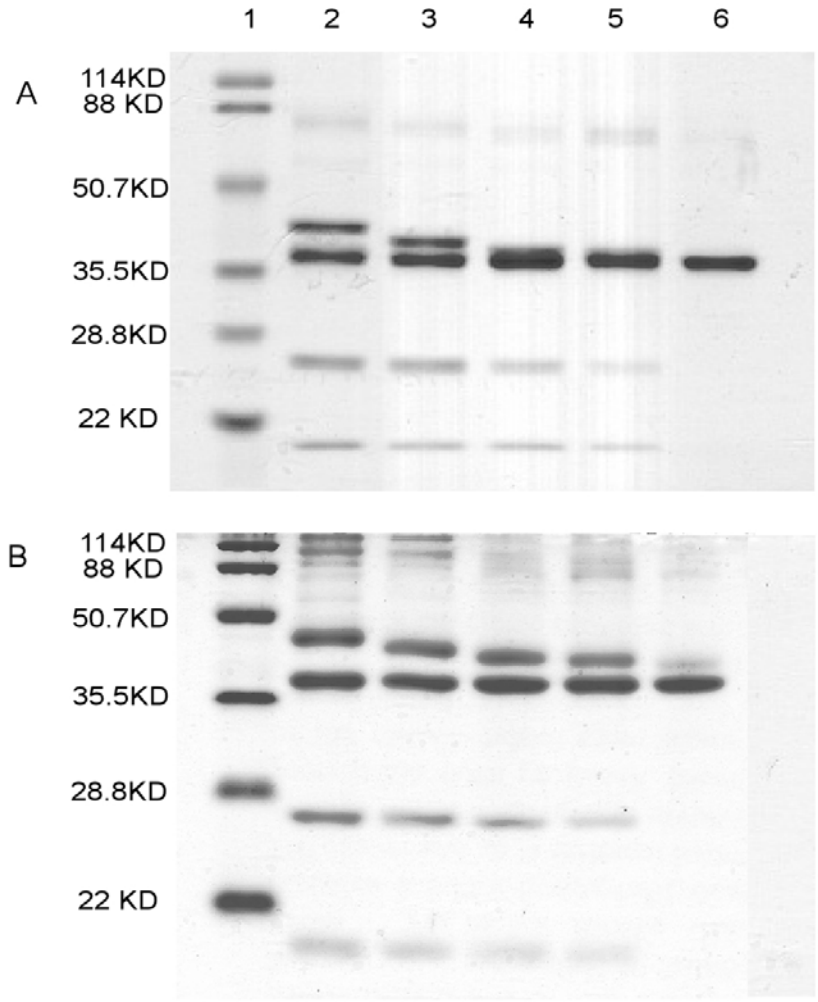

Fig.21. Comparison of electrophoretic behavior of cytochrome *b* in purified complement and mutant cytochrome bc_1 complexes under various conditions. Purified complement and mutant cytochrome bc_1 complexes (50 pmol of cytochrome c_1) were subjected to SDS-PAGE with a separation gel containing T=12.5% and C=3% (*panel A*); and T=16.5% and C=4% (*panel B*). *Lane 1*, prestained molecular weight standards; *lanes 2*-6, cytochrome *bc*1 complexes from wild-type, cyt*b*Δ(433–445), cyt*b*Δ(427–445), cyt*b*Δ(425–445), and cyt*b*Δ(421–445), respectively. T stands for the total concentration of acrylamide and bisacrylamide, C stands for cross-linker concentration.

Fig.21. shows electrophoretic mobility of wild-type and C-terminal-truncated cytochrome *b* in separation gels containing two concentrations of acrylamide (T) and bisacrylamide (C). In a separating gel having T =12.5% and C = 3%, a system used routinely for SDS-PAGE analysis of the *R. sphaeroides* bc_1 complex, wild-type and mutant bc_1 complexes of cytochrome *b* of cyt*b*Δ(433–445), cyt*b*Δ(427–445), cyt*b*Δ(425–445), and cyt*b*Δ(421–445) have R_f values of 16.2, 17.5, 18.5, 19, and 19 mm, respectively (see Fig. 21*A*). As expected, the R_f values of cytochrome c_1, ISP, and subunit IV in mutant bc_1 complexes are the same as those in the wild-type complex, because shortening the C-terminal extra fragment of cytochrome *b* should not affect the molecular masses of other subunits in the complex. The R_f values of cytochrome *b* obtained in these mutant complexes are larger than the calculated values, as the molecular mass of cytochrome *b* is decreased by 1200, 1947, 2206, 2588, respectively, from that of wild-type cytochrome *b*. It should be noted that the larger than calculated R_f values observed are not because of reduction of the molecular mass of mutant *b* proteins by proteolytic enzyme digestion, because the molecular mass of cytochrome *b* in the cyt*b*Δ(421–445) mutant complex, determined by MALDI-TOF mass analysis, is 47,264, which corresponds to the calculated value.

To further confirm that C-terminal-truncated cytochrome *b* have abnormal electrophoretic mobility in SDS-PAGE, purified wild-type and mutant cytochrome bc_1 complexes were subjected to SDS-PAGE using a separating gel having T =16% and C= 4% (see Fig. 21*B*). The electrophoretic mobility of wild-type *R. sphaeroides* cytochrome *b*, relative to cytochrome c_1, is decreased when the concentrations of T and C in a separation gel is increased. This increased distance between wild type cytochrome *b*

and c_1 enables us to obtain the R_f values for the cytochrome *b* mutants, relative to cytochrome c_1. The values are: 0.70, 0.76, 0.81, 0.84, and 0.86, respectively. These values are larger than those calculated. Thus, cytochrome *b* with decreasing lengths of the C-terminal extra fragment exhibits abnormal electrophoretic mobility in SDS-PAGE. Perhaps removal of the C-terminal extra fragment in cytochrome *b* makes cytochrome *b* protein assume a molecular shape more globular than the wild-type protein, in the presence of SDS, which moves faster in SDS-PAGE than expected.

Effect of Mutations on the Rieske Iron-Sulfur Cluster

Western blotting and SDS-PAGE analysis indicate that the amount of ISP in the purified bc_1 complex decreases as the C-terminal extra fragment of cytochrome *b* decreases; no ISP is detected in the complex with cytochrome *b* lacking this extra fragment. To see whether or not the mutations on the C-terminal extra fragment of cytochrome *b* also affect the microenvironments of the iron sulfur cluster, EPR spectra of the [2Fe-2S] cluster in complement and mutant bc_1 complexes were determined and compared (see Fig.22).

When complement and mutant complexes of cyt*b*Δ(433–445), cyt*b*Δ(427–445), cyt*b*Δ(425–445), and cyt*b*Δ(421–445), at a cytochrome *b* concentration of 230 μM, were reduced by a small excess of ascorbate, the EPR signal of the Rieske iron sulfur cluster in the complement complex is essentially the same as that previously reported for the wild-type *R. sphaeroides* bc_1 complex (8,9), with resonance at g_x=1.80, g_y=1.90, and g_z = 2.02

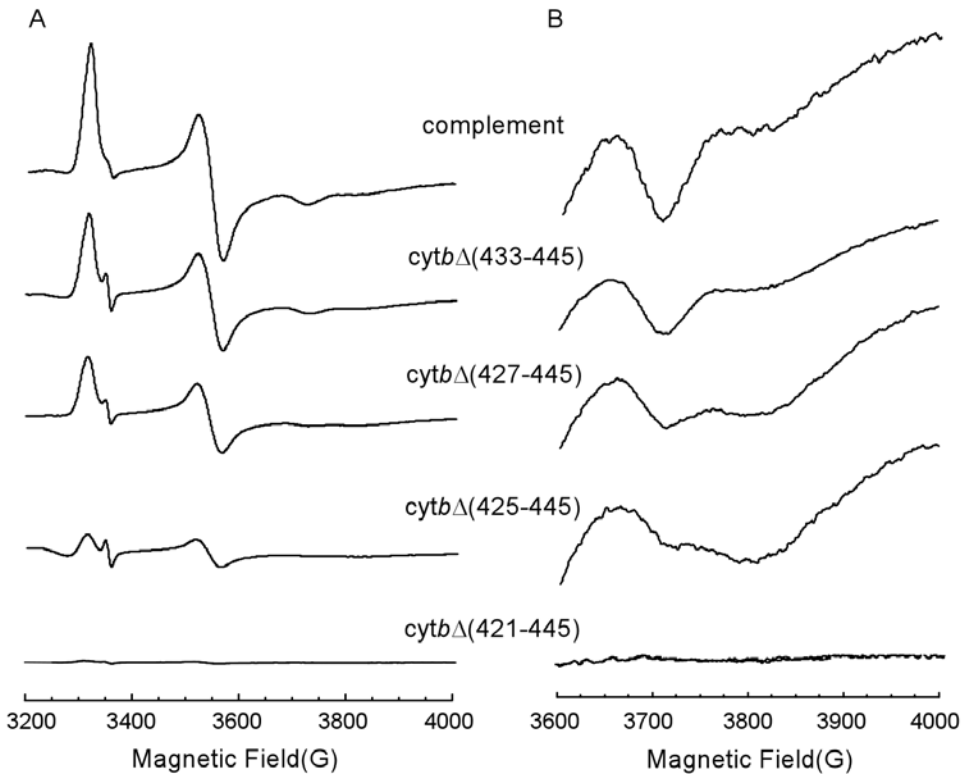

Fig.22. EPR spectra of the [2Fe-2S] cluster of the Rieske iron-sulfur protein in purified bc_1 complexes from the complement and mutants cyt*b*Δ(433–445), cyt*b*Δ(427–445), cyt*b*Δ(425–445), and cyt*b*Δ(421–445). Purified complement and mutant bc_1 complexes (230 μM cytochrome *b*) were treated with a small excess of ascorbate solution to fully reduce cytochrome c_1 and frozen in liquid nitrogen. *Panel A*, spectra obtained from samples scanning once from 3200 to 4000 G magnetic field; *panel B*, enlarged spectra at the g_x region. The g_y signal amplitude in mutant complexes have been adjusted to about the same as that in the complement complex by scanning the cyt*b*Δ(433–445), cyt*b*Δ(427–445), and cyt*b*Δ(425–445) complexes, through the magnetic field, once, twice, and five times, respectively. EPR spectra were recorded at 7 K with the following instrument settings: microwave frequency, 9.3 GHz; microwave power, 2.2 milliwatts; modulation amplitudes, 6.3 G; modulation frequency, 100 kHz; time constant, 665.4 ms; sweep time: 167.8 s; conversion time, 163.8 ms.

(see Fig. 22*A*). The signatures of g_y and g_z of [2Fe-2S] cluster in the cyt*b*Δ(433–445), cyt*b*Δ(427–445), and cyt*b*Δ(425–445) mutant complexes are the same as those detected in the complement complex, but with signal amplitudes decreasing as the C-terminal extra fragment of cytochrome *b* shortens (see Fig.22*A*). No EPR spectrum of the [2Fe-2S] cluster is detected in the cyt*b*Δ(421–445) mutant complex. These results are consistent with Western blot results showing that the amount of ISP in the bc_1 complex decreases as the C-terminal extra fragment of cytochrome *b* decreases and no ISP is detected in the complex that has cytochrome *b* lacking the entire C-terminal extra fragment.

In contrast to g_y and g_z, the g_x signal of [2Fe-2S] in mutant complexes of cyt*b*Δ(433–445), cyt*b*Δ(427–445), and cyt*b*Δ(425–445) mutant complexes change progressively from a relatively sharp peak with g=1.80 to a broadened peak with g=1.76 (see Fig.22*B*). Whereas the g_x signal from the cyt*b*Δ(433–445) mutant complex is quite sharp with g=1.80 peak, that from the cyt*b*Δ(425–445) mutant complex is broader with g=1.76 peak. These results indicate that the alteration of the microenvironments of the [2Fe-2S] cluster increases as the C-terminal extra fragment of cytochrome *b* decreases. This finding is somewhat surprising, because in the model structure of *R. sphaeroides* cytochrome bc_1 complex (5), constructed by using the coordinates of subunits from beef heart mitochondrial bc_1 complex, the Rieske iron-sulfur cluster is located at the head domain of ISP on the periplasmic side of the chromatophore membrane (positive side), whereas the C-terminal extra fragment of cytochrome *b* is located at the cytoplasmic side of this chromatophore membrane. Thus, the effect of shortening the C-terminal extra fragment of cytochrome *b* on the EPR signature of the Rieske [2F-2S] center would appear to be long range.

The line shape of the g_x signature of [2Fe-2S] clusters is thought to be sensitive to the redox state of ubiquinone present in the Qo center (8-13). The g_x of bc_1 from wild-type *R. sphaeroides* is at g=1.80 when oxidized ubiquinone is present but shifts to 1.76 and becomes much broader when ubiquinol is present. In a study of the effect of extraction of ubiquinone, from chromatophore membranes, on the iron-sulfur cluster, Ding *et al.* (13) found that the g_x signal became very broad and was located at ~1.765 upon deletion of ubiquinone from the *R. capsulatus* chromatophore membrane. Although the broadened, g_x=1.76 resonance observed in the cyt*b*Δ(427–445) and cyt*b*Δ(425–445) mutant complexes resembles the "reduced state" or the "depleted state" spectrum, it is not because of changes the redox state of Q or a decrease of Q in the mutant complex, because no EPR spectrum of [2Fe-2S cluster] is detected in these two mutant complexes without treatment with ascorbate and the amount of Q in these two mutant complexes is the same as that in the complement complex. It should also be noted that upon complete reduction by addition of dithionite, the broadened, g_x=1.76 signal observed in the mutant complexes remains unchanged, whereas the g_x=1.80 signals becomes broadened and shifts to a g_x=1.76 signal, similar to the changes observed in the complement complex (8,9).

The broadened, g_x=1.76 EPR signal observed in the cyt*b*Δ(427–445) and cyt*b*Δ(425–445) mutant complexes is similar to the g_x signal observed for the substitution of Leu for Phe-144 (F144L) in the cytochrome *b* from *R. capsulatus* (12) and of serine for Thr-160 in cytochrome *b* from *R. sphaeroides* (14). The F144L bc_1 complex in *R. capsulatus* and the T160S mutant complex in *R. sphaeroides* chromatophores were reported to have a decreased turnover rate with a broadened, redox state insensitive

g_x value at 1.765. It was suggested that these properties of the F144L and T160S complexes resulted from a reduced affinity for quinone and quinol at the Qo site of the mutated complex. One possibility, which could account for the decreased turnover rate of the cyt*b*Δ(427–445) and cyt*b*Δ(425–445) mutant complexes and their reduced state or the high field shift of the g_x EPR signal, is that shortening the C-terminal extra fragment to less than 6 residues induces conformational changes at the Qo site, which raise the effective redox potential of bound ubiquinol beyond the optimal range for transfer to the [2Fe-2S] cluster.

Effect of the Mutations on Redox potentials and EPR Characteristics of Cytochrome *b* in the bc_1 Complex

Fig. 23 shows redox titration curves of cytochrome *b* in the complement and C-terminal truncated cytochrome *b* mutant complexes. Two redox components (b_L and b_H) are resolved from each of the titration curves and their redox potentials were calculated (see Fig. 23 and Table 4). The redox potentials of b_L and b_H in the complement complex are -87 and 41 mV, respectively, similar to previously reported values (9). The redox potentials of b_L and b_H in the cyt*b*Δ(433–445) mutant complex are -73 and 49 mV, respectively, indicating that deleting 13 residues has little effect on redox potentials of cytochrome *b*. In contrast, the redox potential of b_L in mutant complexes of cyt*b*Δ(427–445), cyt*b*Δ(425–445), and cyt*b*Δ(421–445) decreases by 28, 58, and 73 mV, respectively, and that of b_H decreases by 16, 82, and 111 mV, respectively, compared with counterparts in the complement complex. Thus residues 421–432 in the C-terminal extra fragment are

essential for maintaining redox potentials of *b* cytochromes. The effect is larger in b_H than in b_L. It should be noted that the amplitudes of the reductive and oxidative titrations, shown in Figs. 23 and 25, match so well because no protein denaturation occurs during the titrations, as a freshly thawed sample from the same batch of a given bc_1 complex was used for each trial of reductive and oxidative titrations.

Fig.24 shows EPR spectra of the *b* cytochromes from the complement and mutant complexes, taken after the samples were reduced with sodium ascorbate to eliminate the overlapping signal from cytochrome c_1. The complement complex has features at g=3.53 and g=3.77 previously assigned to cytochrome b_H and b_L, respectively, in the wild-type bc_1 complex (8). The g=4.3 signal is thought to be nonspecific bound iron (III). Similar EPR spectra were reported for the mitochondrial bc_1 complex (15-18). The cytochrome b_H and b_L signals in the cyt*b*Δ(433–445) mutant complex are the same as those in the complement complex, indicating that deletion of 13 residues does not perturb the heme environments of the *b* cytochromes in the complex. A small effect on cytochrome b_L EPR signal is observed in the cyt*b*Δ(427–445) mutant complex. The positions of cytochrome b_H and b_L features in the cyt*b*Δ(425–445) and cyt*b*Δ(421–445) mutant complexes are shifted to 3.57 and 3.72, respectively, and the cytochrome b_H signals are broadened significantly. These results indicate that the first 6 residues (residues 421–426) at the N-terminal end of this C-terminal extra fragment are essential for maintaining heme environments of cytochrome *b*, especially for b_L.

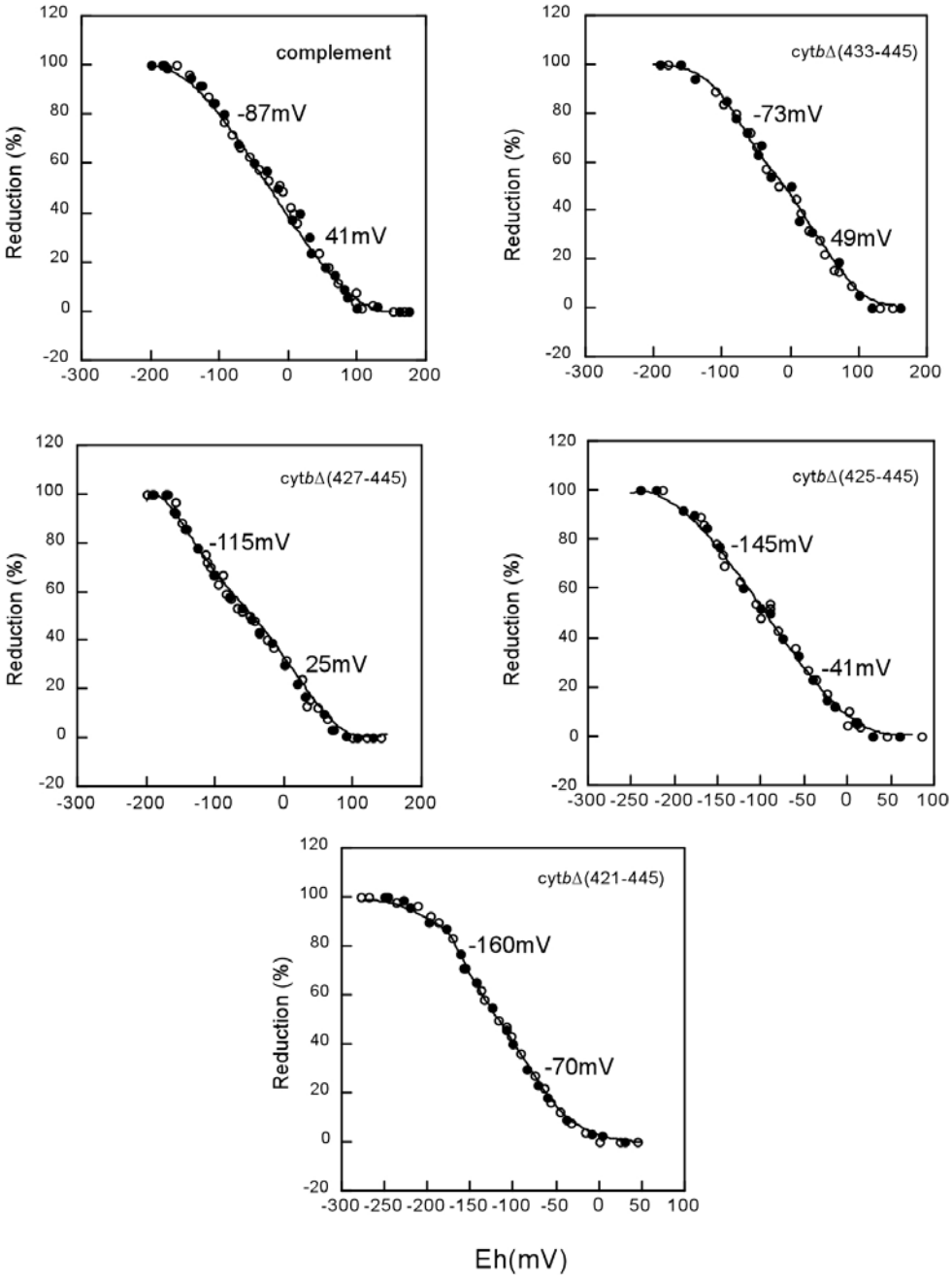

Fig.23. Potentiometric titration of cytochrome *b* in purified complement and mutant bc_1 complexes. The *filled circles* are reductive titration data and *open circles* are oxidative titration data. For each bc_1 complex two trials of oxidative and two trials of reductive titrations were performed. For each trail of reductive and oxidative titrations, a freshly thawed sample from the same batch of a given bc_1 complex was used. The data points in oxidative and reductive titration curves are average of these two trials. The *solid lines* represent the calculated n=1 redox titrations with an equal contribution from b_L and b_H having the indicated midpoint redox potentials.

Table 4. The redox potentials (mV) of cytochromes b_L, b_H, and c_1 in wild type and mutant bc_1 complexes.

Preparations	Midpoint potentials (mV)[a]		
	cytb_H	cytb_L	cytc_1
complement	41±8	-87±8	237±6
cyt$b$Δ(433-445)	49±5	-73±5	227±10
cyt$b$Δ(427-445)	25±10	-115±10	165±4
cyt$b$Δ(425-445)	-41±6	-145±6	170±7
cyt$b$Δ(421-445)	-70±5	-160±5	187±5

[a]Data on standard deviations of the mid-point potentials were obtained from four trials of titrations.

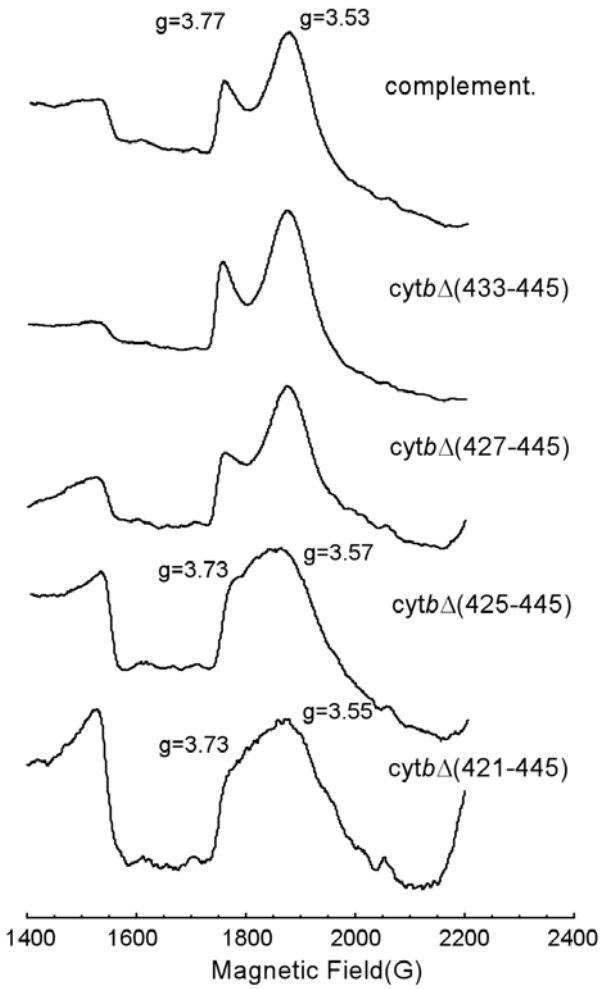

Fig.24. EPR spectra of cytochromes b_H and b_L in purified complement and mutant cytochrome bc_1 complexes. Sample preparations and instrument settings were the same as those described in the legend to Fig.22, except that the microwave power used was 108.1 milliwatts and modulation amplitude was 20 G.

Effect of the C-terminal Extra Fragment of Cytochrome *b* on Cytochrome c_1

Fig. 25 shows redox titration curves of cytochrome c_1 in complement and mutant complexes. The redox potentials of cytochrome c_1 in these bc_1 complexes, calculated to be 237, 227, 165, 170, and 187 mV, respectively (see Fig. 25 and Table 4), indicate that the redox potential of cytochrome c_1 is affected by deleting more than 13 residues from the C terminus of cytochrome *b*. In the proposed structural model of the *R. sphaeroides* cytochrome bc_1 complex, the C-terminal extra fragment of cytochrome *b* is located on the cytoplasmic side of the chromatophore membrane where N-terminal portions of cytochrome c_1, ISP, and cytochrome *b* also reside. Heme c_1 is located on the periplasmic side of the chromatophore membrane. Perhaps interactions between the first 12 residues from the N-terminal end of the C-terminal extra fragment of cytochrome *b* and residues of cytochrome *b*, cytochrome c_1, or ISP on the cytoplasmic side stabilize the structure of cytochrome c_1 and maintain its redox potential. Thus, the effect on the redox potential of cytochrome c_1 by the C-terminal extra fragment of cytochrome *b* is a long range effect. It has been previously reported that redox midpoint potentials of cytochrome c_1 are affected by substitutions in cytochrome *b* (17). Moreover, the redox potential of heme c_1, heme b_L and heme b_H of the deletion mutants cyt*b*Δ-(427-445), cyt*b*Δ-(425-445), and cyt*b*Δ-(421-445) are lower than those of the w.t.. It is well know that redox potentials are pH dependent (19). For example, the redox potential of ISP is pH dependent with a slope of *ca*. -60 mV per pH unit (20). It is possible that deletion of the first 12 residues from the

N-terminal end of the C-terminal extra fragment of cytochrome *b* would change the local pH of heme c_1, heme b_L and heme b_H. Heme is iron-protoporphyrin IX with two propionate side chains attached. The higher redox potentials of the w.t. in comparison with those of the mutants indicate that the one or both propionate might be protonated, due to the decrease of the local pH, which in turn, increases the electron affinity of the hemes.

It should be noted again that the C-terminal extra fragment of cytochrome *b* is located on the cytoplasmic side of the chromatophore membrane, yet its deletion affects redox components, such as heme b_H, iron-sulfur cluster, and heme c_1, located on the periplasmic (opposite) side of the chromatophore membrane. Therefore, these effects cannot be explained by direct interaction between the extra fragment of cytochrome *b* and the redox components or their ligands or their vicinity peptides. These long range effects are probably because of globular changes in the deleted mutant complex. That deleted cytochrome *b* proteins have electrophoretic mobilities greater than those of comparable molecular mass, in SDS-PAGE, suggests that the deleted cytochrome *b* proteins are more globular than the unaltered protein.

Very recently, our collaborator Di, X. got a new *R. sphaeroides* bc_1 crystal structure at 2.9 Å (unpublished data). In this structure the assembly of the three core subunits, cytochrome *b*, cytochrome c_1 and the iron-sulfur-protein (Fig. 26) are very similar to those in mitochondrial bc_1 (21). The iron-sulfur protein in *R. s.* bc_1 crosses over as in mitochondrial bc_1, connecting one molecule of cytochrome *b* to the adjacent one. Since *R. s.* bc_1 is structurally unsupported by supernumerary subunits (with the exception of subunit IV which appears to be too loosely associated with the core subunits

to crystallize with them), it must depend entirely on insertions and extensions both at the amino- and carboxyl termini of cytochrome *b* in order to maintain a global structure. This 3D-structure reveals that the last 15 residues are flexible and unlikely to be involved in maintaining the stability of the complex, which agrees well with our result that the fragment (residues from 432 to 445) is not essential for the function or assembly of the complex. The removal of i-helix (425-433) is expected to destabilize de-helix to which it is bound via several hydrogen bonds. The i-helix, the de-helix and the C-terminus of cytc_1 are located very close to each other, suggesting mutual structural dependence. Consequently, removal of the i-helix explains the observed reduction of cyt c_1 binding and in turn the loss of the ISP, which also agree well with our result that the first 12 residues (residues 421-432) affect ISP and cyt*b* binding affinity for cytc_1. As a whole, the new structural data about the C-terminal extra-fragment of cyt*b* are consistent with our biophysical and biochemical experimental conclusion that this extra-fragment is very important for maintaining the structure stability of cyt*b*.

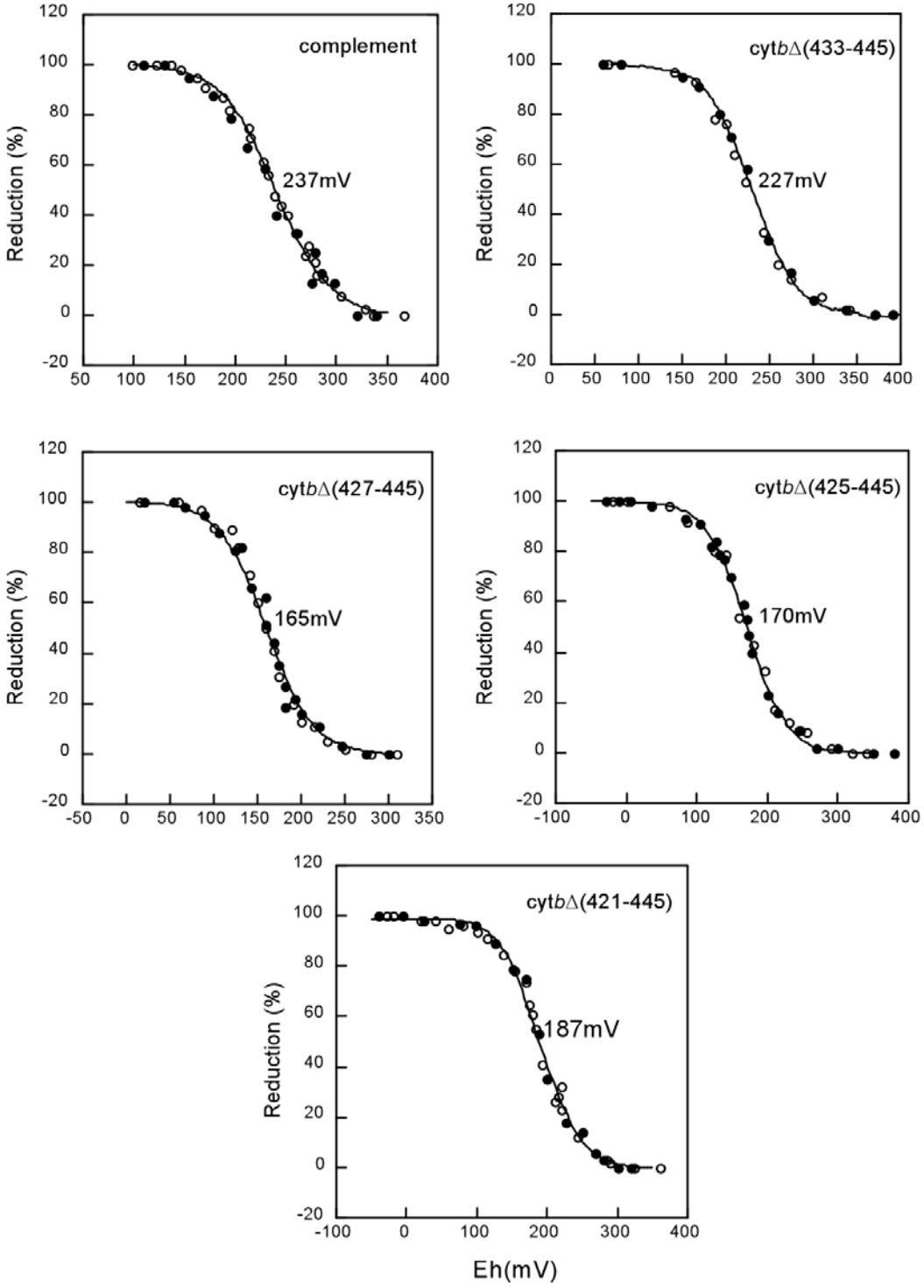

Fig.25. Potentiometric titration of cytochrome c_1 in purified complement and mutant bc_1 complexes. The *filled circles* are reductive titration data and *open circles* are oxidative titration data. The *solid lines* represent the calculated n=1 redox titrations with the indicated midpoint redox potentials.

Fig.26. The new crystal structure of *R. sphaeroides* bc_1 at 2.9Å (unpublished data). Cytochrome *b* is light green, cytochrome c_1 is blue, ISP is yellow, extra fragments are red.

References

1. Trumpower, B. L., and Gennis, R. B. (1994) *Annu Rev Biochem* **63**, 675-716
2. Ljungdahl, P. O., Pennoyer, J. D., Robertson, D. E., and Trumpower, B. L. (1987) *Biochim Biophys Acta* **891**(3), 227-241
3. Yang, X. H., and Trumpower, B. L. (1988) *J Biol Chem* **263**(24), 11962-11970
4. Phillips, J. D., Graham, L. A., and Trumpower, B. L. (1993) *J Biol Chem* **268**(16), 11727-11736
5. Yu, L., Tso, S. C., Shenoy, S. K., Quinn, B. N., and Xia, D. (1999) *J Bioenerg Biomembr* **31**(3), 251-257
6. Xiao, K., Liu, X., Yu, C. A., and Yu, L. (2004) *Biochemistry* **43**(6), 1488-1495
7. Mitchell, P. (1976) *J Theor Biol* **62**(2), 327-367
8. McCurley, J. P., Miki, T., Yu, L., and Yu, C. A. (1990) *Biochim Biophys Acta* **1020**(2), 176-186
9. Andrews, K. M., Crofts, A. R., and Gennis, R. B. (1990) *Biochemistry* **29**(11), 2645-2651
10. Matsuura, K., Bowyer, J. R., Ohnishi, T., and Dutton, P. L. (1983) *J Biol Chem* **258**(3), 1571-1579
11. Meinhardt, S. W., Yang, X. H., Trumpower, B. L., and Ohnishi, T. (1987) *J Biol Chem* **262**(18), 8702-8706
12. Robertson, D. E., Daldal, F., and Dutton, P. L. (1990) *Biochemistry* **29**(51), 11249-11260
13. Robertson, D. E., Ding, H., Chelminski, P. R., Slaughter, C., Hsu, J., Moomaw, C., Tokito, M., Daldal, F., and Dutton, P. L. (1993) *Biochemistry* **32**(5), 1310-1317
14. Mather, M. W., Yu, L., and Yu, C. A. (1995) *J Biol Chem* **270**(48), 28668-28675
15. de Vries, S., Albracht, S. P., and Leeuwerik, F. J. (1979) *Biochim Biophys Acta* **546**(2), 316-333
16. Salerno, J. C., McCurley, J. P., Dong, J. H., Doyle, M. F., Yu, L., and Yu, C. A. (1986) *Biochem Biophys Res Commun* **136**(2), 616-621
17. Hacker, B., Barquera, B., Crofts, A. R., and Gennis, R. B. (1993) *Biochemistry* **32**(16), 4403-4410

18. Orme-Johnson, N. R., Hansen, R. E., and Beinert, H. (1971) *Biochem Biophys Res Commun* **45**(4), 871-878
19. Dutton, P. L. (1978) *Methods Enzymol* **54**, 411-435
20. Link, T. A. (1997) *FEBS Lett* **412**(2), 257-264
21. Xia, D., Yu, C. A., Kim, H., Xia, J. Z., Kachurin, A. M., Zhang, L., Yu, L., and Deisenhofer, J. (1997) *Science* **277**(5322), 60-66

Chapter IV

Differential Scanning Calorimetry Study of Extra Fragment of Iron-sulfur Protein (Residues 96-107) of Cytochrome bc_1 Complex from *Rhodobacter sphaeroides*

Abstract

To confirm that the extra fragment of ISP of *R. sphaeroides* cytochrome bc_1 complex is required for protein stability, we studied the thermotropic properties of cytochrome bc_1 complexes from wild type and the mutant of ISP(96-99)A in the extra fragment of ISP by differential scanning calorimetry (DSC). When purified cytochrome bc_1 complexes from wild type and mutant were subjected to DSC analysis, they went endothermic thermodenaturation with transition temperatures (*Tm*) at 46.3 and 40.7˚C, respectively. The change of enthalpy (ΔH) (46.3 Kcal/mol) of wild type protein was much higher than that (27.5 Kcal/mol) of mutant bc_1 complex. These results further establish that the loss (or decrease) of bc_1 activity in extra fragment mutants results from a lack (or decrease) of ISP in the membrane due to ISP protein instability.

Introduction

The cytochrome bc_1 complex (also known as ubiquinol-cytochrome *c* reductase or Complex III) is an essential segment of the energy-conserving, electron transfer chain of the mitochondria and many respiratory and photosynthetic bacteria (1). This complex catalyzes electron transfer from ubiquinol to cytochrome *c* (c_2 in bacteria) and concomitantly translocates protons across the membrane to generate a membrane potential ($\Delta\Psi$) and pH gradient (ΔpH) subsequently used by the ATP synthase to produce ATP. All the cytochrome bc_1 complexes contain three core subunits, cytochrome *b*, cytochrome c_1, and Rieske iron sulfur protein (ISP), which house two *b*-type hemes (b_L and b_H), one *c*-type heme (heme c_1), and a high potential [2Fe-2S] cluster, respectively. In addition to these three core subunits, the cytochrome bc_1 complex also contains varying numbers (one to eight) of non-redox containing subunits, known as supernumerary subunits (2,3).

Although the function of supernumerary subunits in the cytochrome bc_1 complex is not yet fully understood, it has been suggested that the structure of a core subunit in the mitochondrial complex may be stabilized through interactions between a core subunit and its neighboring supernumerary subunits (4), thus keeping its redox groups in defined positions. Since the bacterial complexes contain none (or one) supernumerary subunit, maintaining the structural stability of a core subunit(s) in the bacterial complex may result from interactions between a part of a core subunit and another part of the same subunit or another core subunit. This speculation finds some support from the fact that

core subunits in bacterial complexes are generally bigger than their counterparts in the mitochondrial complex.

Sequence alignment of bacterial ISP, cytochrome *b*, and cytochrome c_1 with their counterparts in the mitochondrial complexes reveals four extra fragments in bacterial cytochrome *b* and one each in bacterial ISP and cytochrome c_1 (5). These extra fragments are modeled into the structure of *Rhodobacter sphaeroides* bc_1 complex by using coordinates from the corresponding supernumerary subunits in the mitochondrial enzyme (5). These findings encouraged us to suggest that these extra fragments may possess mitochondrial supernumerary subunit function in stabilizing the structure of the core subunits in the bacterial complex. This suggestion is further supported by the recent finding that the extra fragments of *R. sphaeroides* ISP (residues 96-107) and cytochrome *b* (residues 421-445) are found to be essential for maintaining structural integrity of the bc_1 complex (6,7) (see Fig. 16). Additionally, Xiao *et al* (8) reported that the presence of more supernumerary subunits in the mitochondrial cytochrome bc_1 complex apparently contributes to the thermal stability of the complex based on comparison of the thermotropic properties of mitochondrial bc_1 and bacterial bc_1 through the differential scanning calorimetry (DSC) study.

DSC is a thermal analysis technique which has been used to measure the energy absorbed or emitted by a sample during its thermodenaturation. When thermal transition occurs in the sample, DSC provides a direct calorimetric measurement of the transition energy at the temperature of the transition. Such measurements provide qualitative and quantitative information about physical and chemical changes that involve endothermic and exothermic processes, or changes in heat capacity. DSC can be used for a variety of

applications, such as studying stability and domain structure of proteins and nucleic acids; detecting impurity or minor components in phospholipid sample; studying protein:protein, protein:ligand or protein:lipid interaction in membrane or in the detergent dispersed form. The thermodenaturation temperature (T_m) and the change of enthalpy (ΔH) are the two parameters used to assess the thermotropic properties of the samples.

To further establish that the extra fragment of ISP of *R. sphaeroides* cytochrome bc_1 complex is required for protein stability, we studied the thermotropic properties of cytochrome bc_1 complexes from wild type and mutants in the extra fragment of ISP. Decrease in T_m and ΔH in mutant is expected. Herein, we report the procedure and results of DSC study of mutant of ISP(96-99)A in the extra fragment of ISP.

Results and Discussion

Choice of the mutant of ISP(96-99)A among the extra fragment ISP mutants

To study the role of the extra fragment of ISP in the *R. sphaeroides* bc_1 complex, several mutants expressing His-tagged cytochrome bc_1 complexes with deletion or single- or multiple-alanine substitution at various positions of this fragment (residues 96-107) were generated. They are: full deletion mutant ISPΔ(96-107), alanine substitution mutants ISP(96-107)A, ISP(96-99)A, ISP(100-103)A, ISP(104-107)A, ISP(D104A), ISP(G106A), ISP(D104A/G106A), ISP(G106L), ISP(N100A), ISP(I103A), ISP(T96A),

ISP(N97A), ISP(R99A) (6).

Because the bc_1 complex is absolutely required for the photosynthetic growth of *R. sphaeroides*, whether this ISP extra fragment is crucial to the complex can be determined by assaying photosynthetic growth. Both full deletion mutant [ISPΔ(96-107)] and full alanine substation [ISP(96-107)A] cell can not grow photosynthetically, indicating that inability to grow photosynthetically of full deletion mutant cell is due to the essentiality of the extra fragment for the bc_1 complex, not due to improper assembly or folding because of the large deletion, and this region maybe required for bc_1 complex activity. The amino acid residues, rather than the length of the extra fragment, are critical, because the alanine substituted fragment should have the same length as the wild type fragment.

To locate the critical regions of the extra fragment, three alanine substitution mutants, ISP(96-99)A, ISP(100-103)A, ISP(104-107)A, were generated. The first four residues (residues 96-99) are not critical as the ISP(96-99)A mutant grows photosynthetically at a rate comparable to that of wild type cells. Residues 100-103 may possess the supernumerary subunit's function, since the ISP(100-103)A mutant has a growth behavior similar to that of the subunit IV lacking *R. sphaeroides* (RSΔIV) cells (9), the last four residues (residues 104-107) are critical because the ISP(104-107)A mutant does not grow photosynthetically. The essentiality of the ISP extra fragment to the bc_1 complex is in the order residues 104-107>residues100-103> residues 96-99, since the ISP(96-99)A, ISP(100-103)A, and ISP(104-107)A mutant membranes have 48%, 9%, and 0% of the ubiquinol-cytochrome *c* reductase activity found in the complement chromatophores. The role played by the extra fragment of ISP is not individual amino acid specific but is a combination effect of several residues because all the single-

substitution mutant chromatophores, T96A, N97A, R99A, N100A, N10A, I103A, D104A,G106A and G106L , have ubiquinol-cytochrome *c* reductase activity similar to that found in complement chromatophores.

Absorption spectral analysis revealed that mutant membranes of ISPΔ(96-107), ISP(96-107)A, ISP(104-107)A, ISP(100-103)A, and ISP(96-99)A have cytochrome *b* and c_1+c_2 contents and spectral characteristics similar to those of complement chromatophores, indicating that the mutation in the extra fragment of ISP does not affect the assembly of cytochrome *b* and c_1/c_2 into the membrane. Western blotting analysis using antibodies against subunit IV shows that the mutations do not affect assembly of subunit IV into the membrane, as all of the mutant membranes contain the same amount of subunit IV as the complement membrane. When the cytochrome bc_1 complexes were purified from mutant membranes by dodecyl maltoside solubilization and Ni-NTA column chromatography, all but the ISP(96-99)A complex contained two subunits corresponding to cytochrome *b* and c_1. Purified ISP(96-99)A complex contains four protein subunits with ISP and subunit IV in decreased amounts compared to the purified wild-type complex. The ratio of b/c_1 in all purified mutant complexes is similar to that in the wild-type complex, which indicates that mutation does not affect the binding affinity of cytochrome *b* to cytochrome c_1, but greatly decreased the binding affinity of subunit IV to cytochrome c_1 or to cytochrome *b*. The simultaneous loss of ISP and subunit IV when the ISP extra fragment is altered may result from induced changes on subunit IV which decrease its affinity for cytochrome *b* or c_1 in the purified complex. The two-subunit bc_1 complexes purified from ISPΔ(96-107), ISP(96-107)A, ISP(100-103)A, and ISP(104-107)A are functionally active, because the activity of cytochrome bc_1

complex is almost restored after the incubation of these two subunit bc_1 complexes with subunit IV and purified ISP.

However, Western blot analysis with antibody against *R. sphaeroides* ISP revealed that mutant membranes of ISPΔ(96-107), ISP(96-107)A, ISP(104-107)A contain no detectable ISP and that the ISP(100-103)A, and ISP(96-99)A mutant membranes have 5% and 50%, respectively, of the amount of ISP found in the complement membrane, which indicate that the loss (or decrease) of cytochrome bc_1 complex activity in the ISP extra fragment mutant membranes is due to a lack (or decrease) of ISP. Although ISP(100-103)A, and ISP(96-99)A mutation cause a decrease in the amount of ISP in the membrane, they do not affect the microenvironment of the iron-sulfur cluster because the [2Fe-2S] clusters in these two mutant membranes had EPR spectral features identical to those observed in complement chromatophores. No [2Fe-2S] cluster is detected in mutant membranes of ISPΔ(96-107), ISP(96-107)A, ISP(104-107)A, since they contain no ISP.

The observation of a lack of (or decrease in) ISP in mutant membranes of ISPΔ(96-107), ISP(96-107)A, ISP(104-107)A, ISP(100-103)A, and ISP(96-99)A is due to instability of the mutant protein, not due to the instability of the mutant mRNA because all mutant cells were found to have the same amounts of ISP mRNA as complement cells. The amounts of ISP in the cell lysate, 200,000g supernatant and precipitate (membrane) fractions, from mutant cells during membrane preparation were measure and compared with those obtained from complement cells in order to further confirm that a lack (or decrease) of ISP in mutant membranes results from mutant ISP protein instability. Freshly prepared mutant cell lysates of ISPΔ(96-107), ISP(96-107)A, ISP(96-99)A, ISP(100-103)A, and ISP(104-107)A have, respectively, 10%, 10%, 50%, 30%, and 10% of the ISP

content of complement cell lysates as determined by Western blot. No ISP was found in any of the supernatant fractions after centrifugation of these cell lysates. Less than 60% and 10% of the ISPs in the ISP(96-99)A and ISP(100-103)A mutant cell lysates are recovered in the membrane fraction, respectively. No cell lysate ISP from the ISPΔ(96-107), ISP(96-107)A, ISP(104-107)A mutants is recovered in their respective membrane fractions. The low (or lack of) recovery of ISP in the membrane fractions of these mutants results from degradation of mutant ISP during centrifugation. Time course analysis revealed a progressive decrease in ISP in these mutant cell lysates, but not in the complement cell lysate.

All of these observations suggested to us that a decrease in ISP in the mutant membrane is due to the instability of assembled mutant ISP. The confirmation of this idea may be obtained from the comparison of thermotrophic properties of purified cytochrome bc_1 complexes from wild type and mutants. Among the mutants of the extra fragment of ISP, only mutant ISP(96-99)A has decreased bc_1 activity although it still has four subunits, ISP, cyt*b*, cytc_1, and subunit IV, which is the same as wild type. To unambigously establish the idea mentioned, the protein from mutant ISP(96-99)A might be the best candidate to be chosen for the further study.

Differential Scanning Calorimetry (DSC) study of ISP(96-99)A

DSC has been widely used to study protein stability. The thermodenaturation temperature (T_m) and the change of enthalpy (ΔH) are the two parameters used to assess this thermostability. Since the bc_1 complex purification involves detergents, the amount

and type of detergents used greatly affect the protein stability, for systematic comparison of protein stability, all bc_1 preparations used in these DSC studies were in 0.5% octylglucoside. When purified wild type cytochrome bc_1 complex underwent thermodenaturation, it showed endothermic thermodenaturation with a T_m at 46.3°C and ΔH of 46.3 kcal/mol. Under identical conditions the mutant ISP(96-99)A has a T_m of 40.7 °C and ΔH of 27.5 kcal/mol (see Fig. 27.). The decrease in Tm and ΔH of the mutant complex indicates that it is less stable than the wild-type complex.

From all the results mentioned above, the loss (or decrease) of bc_1 activity in these mutant membranes results from a lack (or decrease) of ISP in the membrane due to ISP protein instability and not from mutations affecting the assembly of cytochromes *b* and c_1 into the membrane, the binding affinity of cytochrome *b* to cytochrome c_1, or the ability of these two cytochromes to interact with ISP or subunit IV.

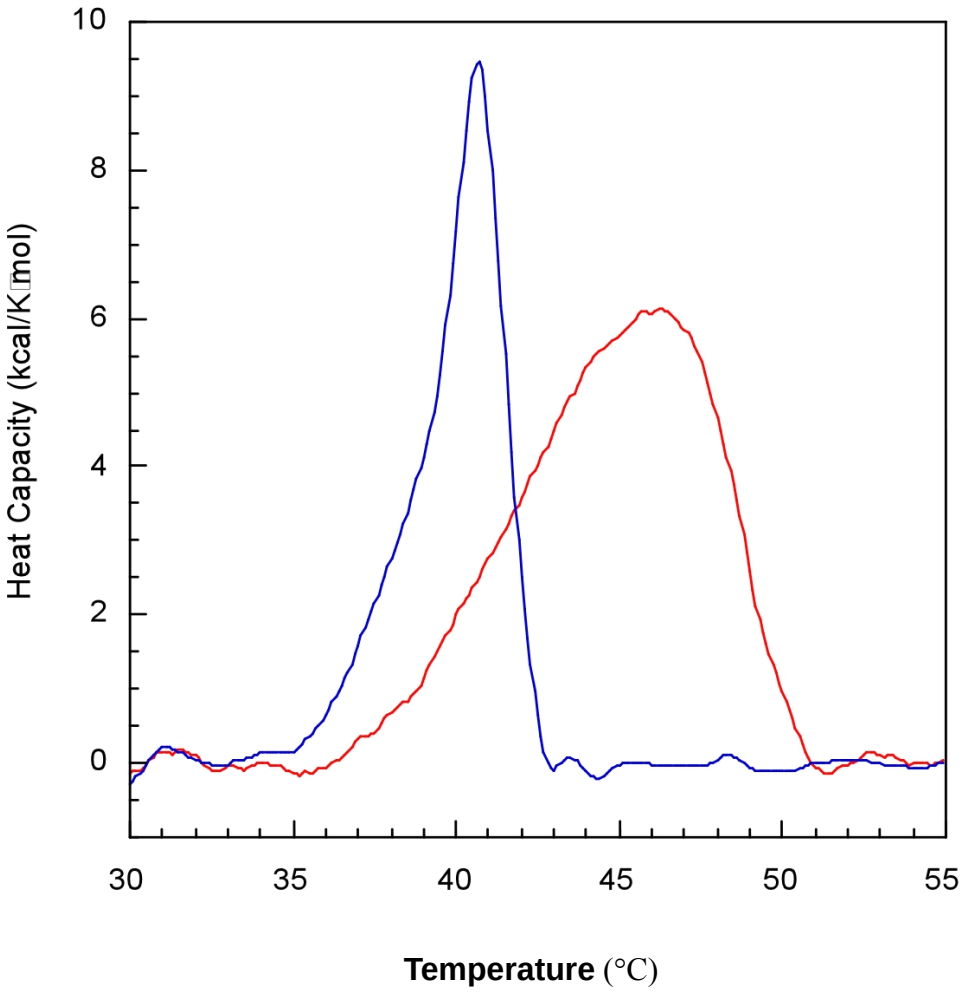

Fig.27. DSC thermograms of ISP(96-99)A and wild-type bc_1 complexes. The red line is the thermogram of wild-type cytochrome bc_1 complex. The blue line is the thermogram of ISP(96-99)A cytochrome bc_1 complex.

References

1. Trumpower, B. L., and Gennis, R. B. (1994) *Annu Rev Biochem* **63**, 675-716
2. Ljungdahl, P. O., Pennoyer, J. D., Robertson, D. E., and Trumpower, B. L. (1987) *Biochim Biophys Acta* **891**(3), 227-241
3. Yang, X. H., and Trumpower, B. L. (1986) *J Biol Chem* **261**(26), 12282-12289
4. Phillips, J. D., and Trumpower, B. L. (1993) *Yeast* **9**(1), 95-97
5. Yu, L., Tso, S. C., Shenoy, S. K., Quinn, B. N., and Xia, D. (1999) *J Bioenerg Biomembr* **31**(3), 251-257
6. Xiao, K., Liu, X., Yu, C. A., and Yu, L. (2004) *Biochemistry* **43**(6), 1488-1495
7. Liu, X., Yu, C. A., and Yu, L. (2004) *J Biol Chem* **279**(45), 47363-47371
8. Xiao, K., Chandrasekaran, A., Yu, L., and Yu, C. A. (2001) *J Biol Chem* **276**(49), 46125-46131
9. Chen, Y. R., Usui, S., Yu, C. A., and Yu, L. (1994) *Biochemistry* **33**(33), 10207-10214

Chapter V

5-Br-Q_0C_{10} Binding Site in *Rhodobacter sphaeroides* bc_1 complex

(On going project)

Abstract

The preliminary structural analysis of the low resolution of co-crystal of bovine bc_1 complex with 5-Br-Q_0C_{10} suggests that the binding site of 5-Br-Q_0C_{10} is different from Qi site and Qo site. Additionally, the crystal structure indicates that there is a channel connected to the cavity for the binding of 5-Br-Q_0C_{10}. To elucidate this novel Q binding site, two sets of *R. sphaeroides* cytochrome *b* mutants expressing His_6-tagged bc_1 complexes were generated and characterized. One set of mutants, Y399F/W400F, Y399A/W400A, M343F/L370F, are constructed to interact with 5-Br-Q_0C_{10}. Another set of mutants, I106C/V375C, Y109C/F374C, L110C/A371C, X(106,109,374,375)C, are designed to block the entrance of the putative channel. All these mutants grew photosynthetically at a rate comparable to that of wild-type cells. The bc_1 complexes prepared from these mutants have the similar activity as that of the wild type complex. The Kms for $Q_0C_{10}BrH_2$ determined with mutant chromatophores of cyt*b*-(M343F), cyt*b*-(L370F), and cyt*b*-(M343F/L370F), or with mutant complexes of cyt*b*-(Y399F/W400F),

cyt*b*-(Y399A/W400A), and cyt*b*-(M343F), are comparable with that of the wild type chromatophore or complex, respectively. Also, the 5-Br-Q_0C_{10} titration curves of all mutants showed the same pattern as that of the wild type, which is that low concentration of 5-Br-Q_0C_{10} can activate bc_1 complex, high concentration of 5-Br-Q_0C_{10} inhibits the bc_1 complex.

Introduction

The mitochondrial respiratory chain, which provides more than 90% of the energy needed for aerobic cells by oxidative phosphorylation process, a universal process that converts most of the energy provided by foodstuffs into the general energy source ATP, contains four electron transfer complexes and an ATP synthase complex (1-3). The cytochrome bc_1 complex plays a crucial role in oxidative phosphorylation. Within this process, the cytochrome bc_1 complex connects hydrophobic ubiquinol and water-soluble cytochrome *c*, transferring electrons between these two freely diffusible intermediates and thereby linking the exergonic reaction to generating a proton gradient and membrane potential for ATP synthesis by ATP synthase (4,5).

Although the study of cytochrome bc_1 has been intensive since its discovery in the early 1960s, our understanding of the bc_1 complex has been greatly enhanced by the availability of crystallographic structures (6-10). Unfortunately, none of the reported structures for cytochrome bc_1 complex shows direct ubiquinone or ubiquinol binding. The reported structures for cytochrome bc_1 complex only shows the binding of Qo site

and Qi site inhibitors (11). Because most of the Qo site inhibitors are reported to be noncompetitive inhibitors (12,13), their binding sites cannot be assumed to be the ubiquinol binding site. Although the essential role of ubiquinone in mitochondrial electron transfer is well established (14-16), the interaction between Q and protein are not yet fully understood. Establishing the nature of ubiquinol binding site is very important in the mechanistic study of this complex.

To study the ubiquinol binding site, the most direct approach is to co-crystallize the bc_1 complex with ubiquinol or ubiquinol-like compound. However, typical difficulty in co-crystallize with ubiquinol is that ubiquinol can not be seen in the crystal. To overcome this, one of the feasible methods is synthesizing Q-derivatives to enhance the diffraction signal. Recently, we synthesized 5-Br-Q_0C_{10}, whose structure is showed in Fig. 28. Due to the special property of the bromine in this Q derivative, we can locate bromine first, and then this Q-like compound can be located. More recently, we co-crystallized bovine mitochondrial bc_1 with 5-Br-Q_0C_{10} at low resolution. Surprisingly, the preliminary structural data shows that the binding site of 5-Br-Q_0C_{10} is different from putative Qo and Qi site, it also show there is a channel connected to the cavity for the binding of 5-Br-Q_0C_{10} (see Fig.29.). There was electron density among amino acid residues L357 and Y358 of helix H (Y399 and W400 in *R. sphaeroides*), residue L328 of helix G (L370 in *R. sphaeroides*), and residue L301 of helix F (M343 in *R. sphaeroides*) surrounding the putative cavity for the 5-Br-Q_0C_{10} binding. Residues I92, Y95, M96, V329, L332, L333 (I106, Y109, L110, A371, F374, and V375, respectively, in *R. sphaeroides*) are probably involved in the putative channel connected to the cavity of the binding of 5-Br-Q_0C_{10}.

5-Br-Q_0C_{10} reduced form

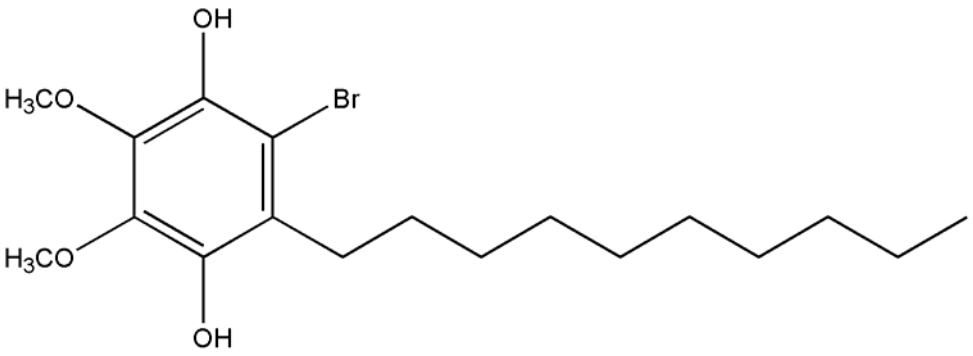

Ubiquinol

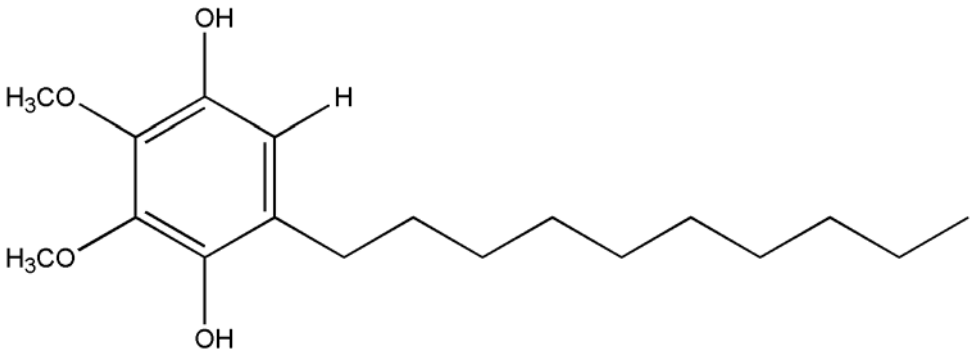

Fig.28. Structure of ubiquinol and 5-BrQ_0C_{10}

Fig.29. The relative binding location of 5-Br-Q_0C_{10} to one of Qo site inhibitor (stigmatellin), Qi site inhibitor (antimycin) and redox centers in the cytochrome bc_1 complex. Stigmatellin in green, antimycin in red, and heme b_L and b_H in yellow. The residues (Y399, W400) of helix H, residue (L370) of helix G, and residue (M343) of helix F surrounding the cavity for the 5-Br-Q_0C_{10} binding site.

An effective way to test this hypothesis is to systematically mutate the residues involved in the binding of 5-Br-Q_0C_{10} and to follow the biochemical biophysical characterization of the resulted mutant proteins. Herein, we report procedures for generating *R. sphaeroides* mutants with mutations involved in this putative Q binding site in the bc_1 complex. The photosynthetic growth behavior, cytochrome bc_1 complex activity, and Km titrations in bc_1 complexes from wild type and mutant strains were examined and compared, as were the titrations of 5-Br-Q_0C_{10}.

Experimental procedures

Materials—Cytochrome c (horse heart, type III) was from Sigma. N-Dodecyl-β-D-maltoside and N-dodecyl-β-D-glucoside were from Anatrace. Ni-NTA gel and Qiaprep Spin Miniprep kit were from Qiagen. 2,3-Dimethoxy-5-methyl-6-(10-brimodecyl)-1,4-benzoquinol ($Q_0C_{10}BrH_2$) was prepared in our laboratory as previously reported (17). All other chemicals were of the highest purity commercially available.

Growth of Bacteria—*Escherichia coli* cells were grown at 37°C in LB medium. Photosynthetic growth conditions for *Rhodobacter sphaeroides* were essentially as described previously (18). The concentration and antibiotics used were: ampicillin, 125 μg/ml; kanamycin sulfate, 30 μg/ml; tetracycline, 10 μg/ml for *E. coli*, 1 μg/ml for *R.*

sphaeroides; and trimethophrim, 100 μg/ml for *E. coli*, 30 μg/ml for *R. sphaeroides*.

Generation of R. sphaeroides Strains Expressing the His_6-tagged bc_1 Complexes With Mutations at the Binding Site of 5-Br-Q_0C_{10} and the Entrance of That Site—Mutations were constructed by using the QuikChange™ XL site-directed mutagenesis kit from Stratagene. A double-stranded plasmid pGEM7Zf(+)-*fbc*FB was used as a template and forward and reverse primers were used for PCR amplification. The pGEM7Zf(+)-*fbc*FB plasmid was constructed by ligating the *EcoR*I-*Xba*I fragment from pRKD*fbc*FBC_{6H}Q (19) into *EcoR*I and *Xba*I sites of the pGEM7Zf(+) plasmid. The primers used are given in Table 5.

There are two kinds of fragments: one is a 962-base pair *Bste*II-*Xba*I fragment, the other is a 3379-base pair *EcoR*I-*Xba*I fragment depend on the location of mutation site(s) on cytochrome *b* after mutagenesis. These two fragments were ligated into *Bste*II-*Xba*I or *EcoR*I-*Xba*I sites of pRKD418*fbc*F$B_{KmBP}C_{6H}$Q plasmid (19). Loss of kanamycin resistance was then used to screen for recombinant plasmids containing the mutant cytochrome *b* gene.

The pRKD418*fbc*FB_mC_{6H}Q plasmid in *E.coli* S17-1 cells was mobilized into *R. sphaeroides* BC-17 cells by a plate-mating procedure (19). The presence of engineered mutations was confirmed by DNA sequencing of the 962-base pair *Bste*II-*Xba*I or 3379-base pair *EcoR*I-*Xba*I fragment after photosynthetic growth as previously reported (19). DNA sequencing was performed by the Recombinant DNA/Protein Core Facility at Oklahoma State University. The primers were synthesized by Invitrogen™.

Table 5. Oligonucleotide used for site-directed mutagenesis for study the 5-Br-Q_0C_{10} binding site.

I106C(F)[a]	GCCTCGCTGTTCTTCTGCGCGGTCTATCTG
I106C(R)[a]	CAGATAGACCGCGCAGAAGAACAGCGAGGC
I109C(F)	CTTCATCGCGGTCTGCCTGCACATCTTCC
I109C(R)	GGAAGATGTGCAGGCAGACCGCGATGAAG
L110C(F)	GTTCTTCATCGCGGTCTATTGCCACATCTTCCGCGGC
L110C(R)	GCCGCGGAAGATGTGGCAATAGACCGCGATGAAGAAC
A371C(F)	CTACTTCTGGCTGCTCTGCGCGGACTTCGTGATCCTG
A371C(R)	CAGGATCACGAAGTCCGCGCAGAGCAGCCAGAAGTAG
F374C(F)	CTCGCGGCGGACTGCGTGATCCTGACCTGGG
F374C(R)	GCCAGGTCAGGATCACGCAGTCCGCCGCGAG
V375C(F)	GCTCGCGGCGGACTTCTGCATCCTGACCTGGG
V375C(R)	CCCAGGTCAGGATGCAGAAGTCCGCCGCGAGC
Y399A(F)	CATCGCATCGGCCGCCTGGTTCGCCTACTTCC
Y399A(R)	GGAAGTAGGCGAACCAGGCGGCCGATGCGATG
W400A(F)	CATCGCATCGGCCTACGCGTTCGCCTACTTCCTGGTG
W400A(R)	CACCAGGAAGTAGGCGAACGCGTAGGCCGATGCGATG
Y399F(F)	CATCGCATCGGCCTTCTGGTTCGCCTACTTCC
Y399F(R)	GGAAGTAGGCGAACCAGAAGGCCGATGCGATG
W400F(F)	CATCGCATCGGCCTACTTCTTCGCCTACTTCCTGGTG
W400F(R)	CACCAGGAAGTAGGCGAAGAAGTAGGCCGATGCGATG
M343F(F)	CGCGATCCTCGTGTTCGCGCTGGTGCCGTGGCTCG
M343F(R)	CGAGCCACGGCACCAGCGCGAACACGAGGATCGCG
L370F(F)	TACTTCTGGCTGTTCGCGGCGGACTTC
L370F(R)	GAAGTCCGCCGCGAACAGCCAGAAGTA
X(106,109)C(F)	CCTCGCTGTTCTTCTGCGCGGTCTGCCTGCACATCTTCC
X(106,109)C(R)	GGAAGATGTGCAGGCAGACCGCGCAGAAGAACAGCGAGG
X(374,375)C(F)	CTGCTCGCGGCGGACTGCTGCATCCTGACCTGGG
X(374,375)C(R)	CCCAGGTCAGGATGCAGCAGTCCGCCGCGAGCAG
X(399,400)A(F)	CTCATCGCATCGGCCGCCGCGTTCGCCTACTTCCTGGTG
X(399,400)A(R)	CACCAGGAAGTAGGCGAACGCGGCGGCCGATGCGATGAG
X(399,400)F(F)	CTCATCGCATCGGCCTTCTTCTTCGCCTACTTCCTGGTG
X(399,400)F(R)	CACCAGGAAGTAGGCGAAGAAGAAGGCCGATGCGATGAG

[a] F and R in the parentheses denote forward and reverse primers, respectively.

Enzyme Preparation and Activity Assay—Chromatophores were prepared from frozen cell paste, and cytochrome bc_1 complexes with a His_6 tag placed at the C terminus of cytochrome c_1 were purified from chromatophores as preciously reported (20). To assay the cytochrome bc_1 complex activity, chromatophores or purified cytochrome bc_1 complexes were diluted with 50 mM Tris-Cl, pH 8.0, containing 200 mM NaCl and 0.01% N-dodecyl-β-D-maltoside (DM) to a final concentration for cytochrome b of 3 μM. Appropriate amounts of the diluted samples were added to 1 ml of assay mixture containing 100mM Na^+/K^+ phosphate buffer, pH 7.4, 1 mM EDTA, 100 μM cytochrome c, and 25 μM $Q_0C_{10}BrH_2$. 30 μM potassium cyanide was added to the assay mixture when bc_1 activity in chromatophores was determined. For determination of apparent Km for $Q_0C_{10}BrH_2$, various concentrations of $Q_0C_{10}BrH_2$ were used. Activity was determined by measuring the reduction of cytochrome c (the increase of absorbance at 550 nm) in a Shimadzu UV 2101 PC spectrophotometer at 23°C, using a millimolar extinction coefficient of 18.5 for calculation. The nonenzymatic oxidation of $Q_0C_{10}BrH_2$, determined under the same conditions, in the absence of enzyme, was subtracted. Although the chemical properties of $Q_0C_{10}BrH_2$ are comparable with those of $Q_0C_{10}H_2$, it is a better substrate for the cytochrome bc_1 complex (17). The unit of specific activity is μmol of cytochrome *c* reduced/min/nmol of cytochrome *b*.

Titration of the Cytochrome bc_1 Complex Activity in Complement and Mutants Chromatophores or Proteins with Various Concentrations of $Q_0C_{10}BrH_2$ or 5-Br Q_0C_{10}. Chromatophores or purified cytochrome bc_1 complexes were diluted with 50 mM Tris-Cl, pH 8.0, containing 200 mM NaCl and 0.01% N-dodecyl-β-D-maltoside to a final

concentration for cytochrome *b* of 3μM, 3 μl of the diluted sample were added to 1 ml of assay mixture containing 100 mM Na^+/K^+ phosphate buffer, pH 7.4, 1 mM EDTA, 50 μM cytochrome c, and indicated concentrations of $Q_0C_{10}BrH_2$ or 5-Br-Q_0C_{10}.

Other Biochemical and Biophysical Techniques—The contents of cytochrome *b* (21) and cytochrome c_1 (22) were determined according to published methods.

Results and Discussion

Choice of Residues and Strategy for the Study--The low resolution co-crystal structure of bovine mitochondrial bc_1 complex with 5-Br-Q_0C_{10} showed that amino acid residues L357, Y358 of helix H, residue L328 of helix G, and residue L301 of helix F are surrounding the putative cavity for the 5-Br-Q_0C_{10} binding, and residues I92, Y95, M96, V329, L332, L333 are probably involved in the putative channel connected to the cavity of the binding of 5-Br-Q_0C_{10}. According to the sequence alignment, we picked up the correspondent residues of *R. sphaeroides* bc_1 complex to study the 5-Br-Q_0C_{10} binding site, including (Y399, W400) of helix H, residue (L370) of helix G, and residue (M343) of helix F, and the mutations blocking the entrance of the channel, including I106, Y109, L110, A371, F374, and V375.

There are mainly two ways of quinone interacting with amino acid residues, one is form hydrogen bond between the hydroxyl group of the quinol and that of amino acid

residue, the other is the interaction between the aromatic ring of quinone and aromatic ring of amino acid residues, such as W and Y. Therefore, we generated two double mutants, one is X(399,400)F to get rid of hydrogen bonding, the other is X(399,400)A to get rid of aromatic-aromatic interaction. On the other hand, the crystal structure shows that the cavity of the 5-Br-Q_0C_{10} binding is very compact, so we mutated the relative small residues, such as L370 and M343, in this cavity to the bulky residues, such as F, in order to squeeze out 5-Br-Q_0C_{10}, we generated three mutations, L370F, M343F, and X(343,370)F.

In order to blocking the entrance of the channel, we generated the mutants with double or tetra cysteine substitution, such as I106C/V375C, Y109C/F374C, L110C/A371C, X(106,109,374,375)C.

Titration of the Cytochrome bc_1 Complex Activity in Complement and Mutants Chromatophores or Proteins with Various Concentrations of $Q_0C_{10}BrH_2$—Since we hope we can extrapolate the quinol binding site by using Q-derivative compound, if the hypothesis is correct, the Km for the mutants should be different from that of the w..t.. Therefore, we titrated the cytochrome bc_1 complex activity with various concentrations of $Q_0C_{10}BrH_2$. We did following titration: X(399,400)F (Fig.30.), M343F (Fig.31.), L370F (Fig.33), X(343,370)F (Fig.34). To rule out the affect of detergent on Km, we also did titration of M343F chromatophore (Fig.32.). Because the Km of M343F chromatophore is similar to that of purified protein of M343F, the detergent affect can be omitted. As Table 6 shows, the Kms of the mutants is similar to that of the wild type.

Titration of the Cytochrome bc_1 Complex Activity in Complement and Mutants

Chromatophores or Proteins with Various Concentrations of 5-BrQ_0C_{10}—We also did 5-BrQ_0C_{10}. We titrated X(343,370)F (Fig.35), X(399,400)A (Fig.36). For X(399,400)A, although the pattern of titration curve is similar to that of w.t. (Fig.36), the value of every points is higher than that of w.t., so we incubated the X(399,400)A with endogenous Q_0C_{10}, then titrated with 5-BrQ_0C_{10} to see any difference (Fig.36). The possible explanation of the high value of every points is that X(399,400)A makes bc_1 more accessible to 5-BrQ_0C_{10}. We also did regular Km titration by using the samples at the same day, the Km and Vmax of X(399,400)A are similar to those of w.t.. We also did X(399,400)F titration, the sample was incubated with or without endogenous Q_0C_{10} (Fig.37).

We also titrated the mutants with double or tetra cysteine substitution, such as I106C/V375C (Fig.38), Y109C/F374C (Fig.39), L110C/A371C (Fig.40), X(106,109,374,375)C (Fig.41) with 5-BrQ_0C_{10}.

All of the 5-BrQ_0C_{10} titration curve of mutants show the same pattern as that of w.t., which is that low concentration of 5-BrQ_0C_{10} can active bc_1 complex, high concentration of 5-BrQ_0C_{10} inhibits the bc_1 complex. One explanation for this phenomenon is that the structural data of 5-BrQ_0C_{10} site is not accurate at all.

Table 7. Km of the different mutants.

	X(399,400)F(P)[a]	M343F(C)[b]	L370F(C)	X(343,370)F(C)
Km (μM)	1.69	1.27	1.67	1.41

a: purified protein
b: chromatophore

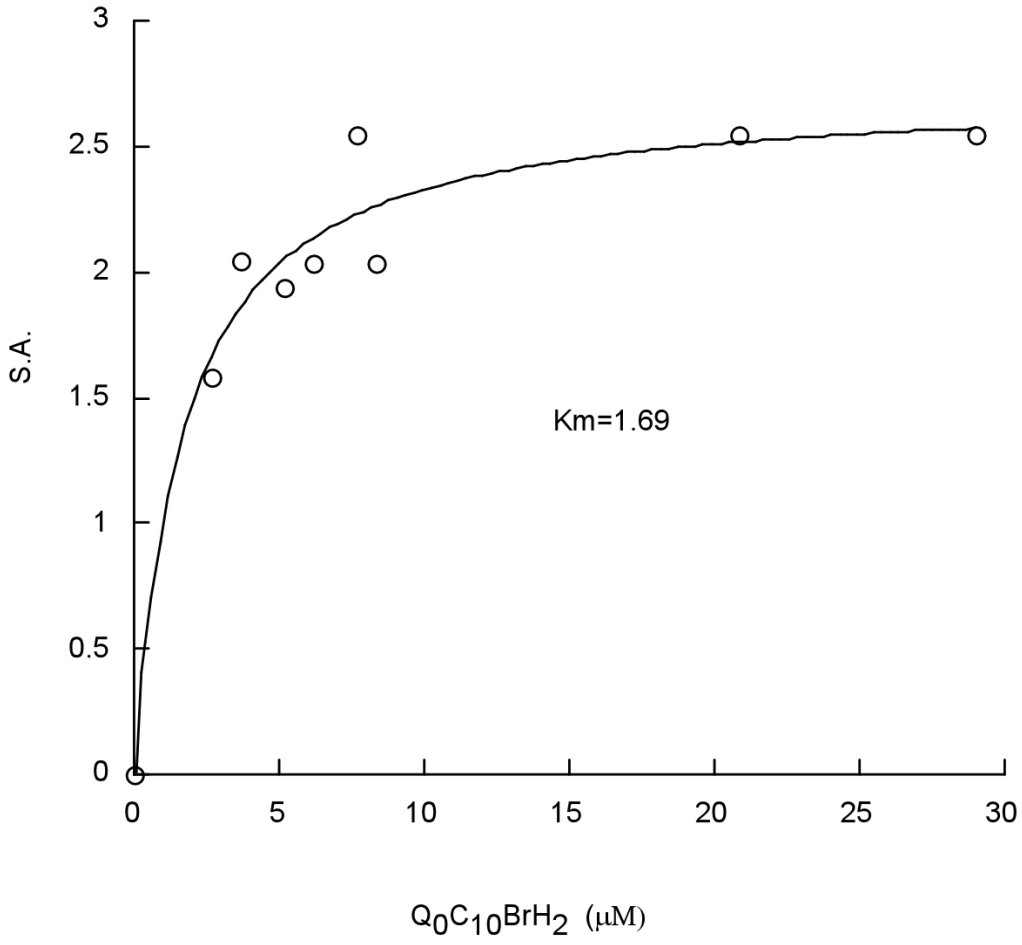

Fig.30. Km titration of X(399,400)F (purified protein).

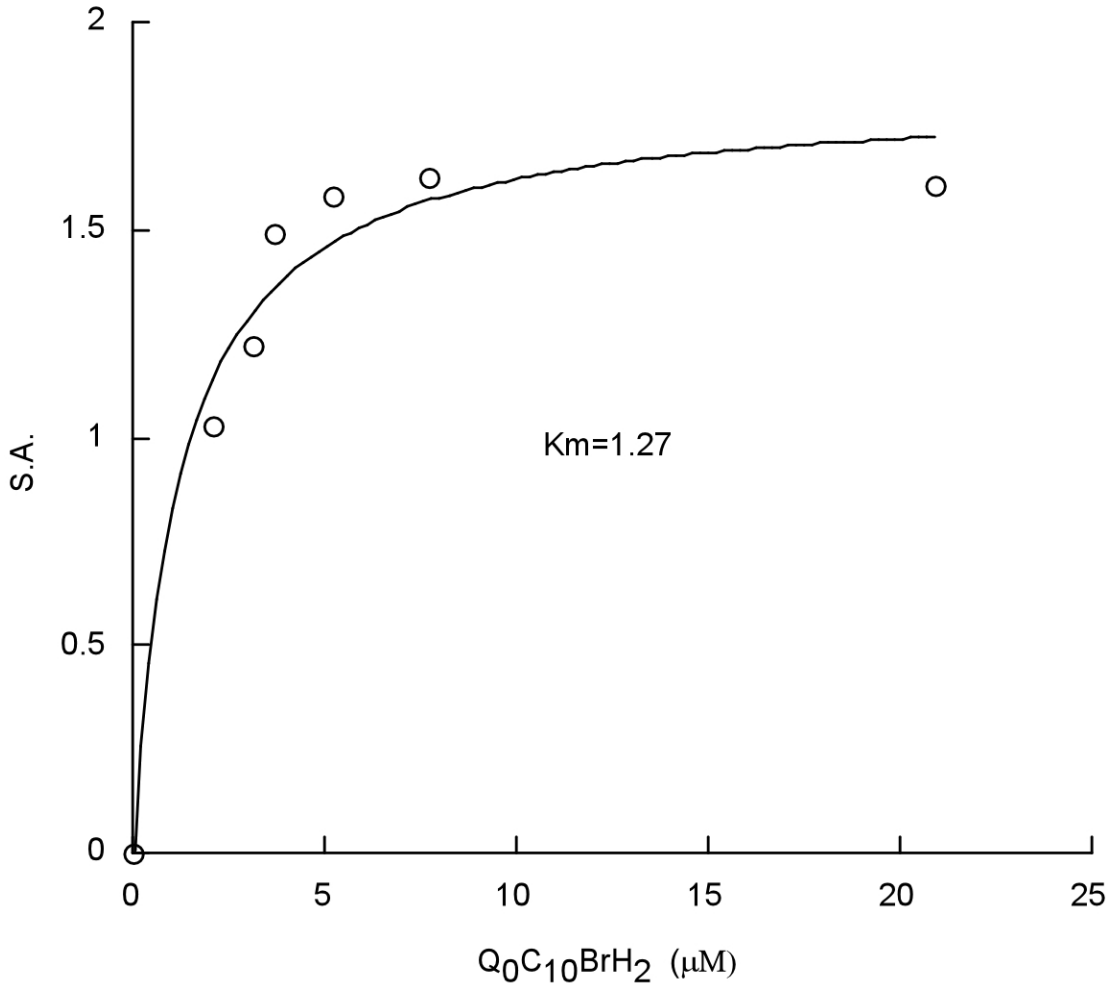

Fig.31. Km titration of M343F (purified protein).

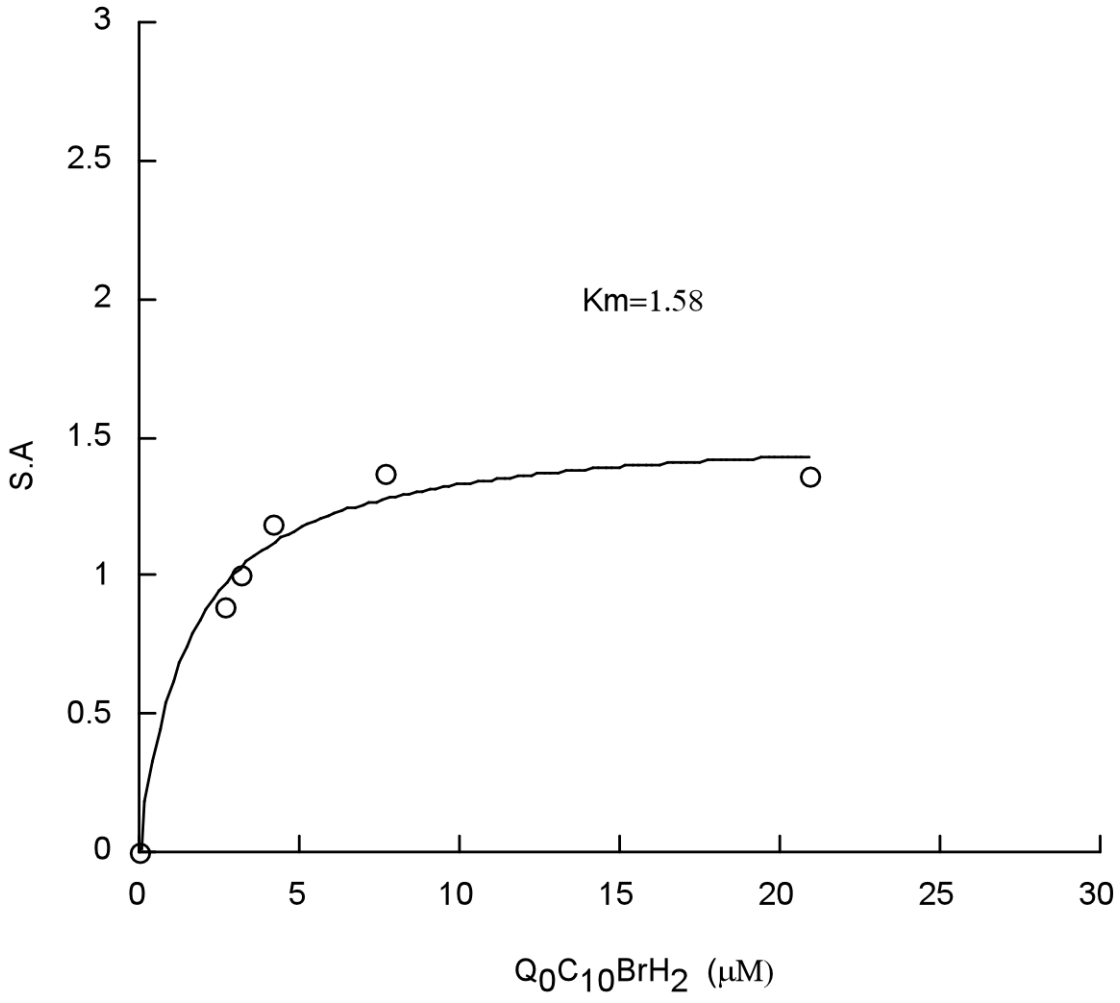

Fig.32.Km titration of M343F (chromatophore)

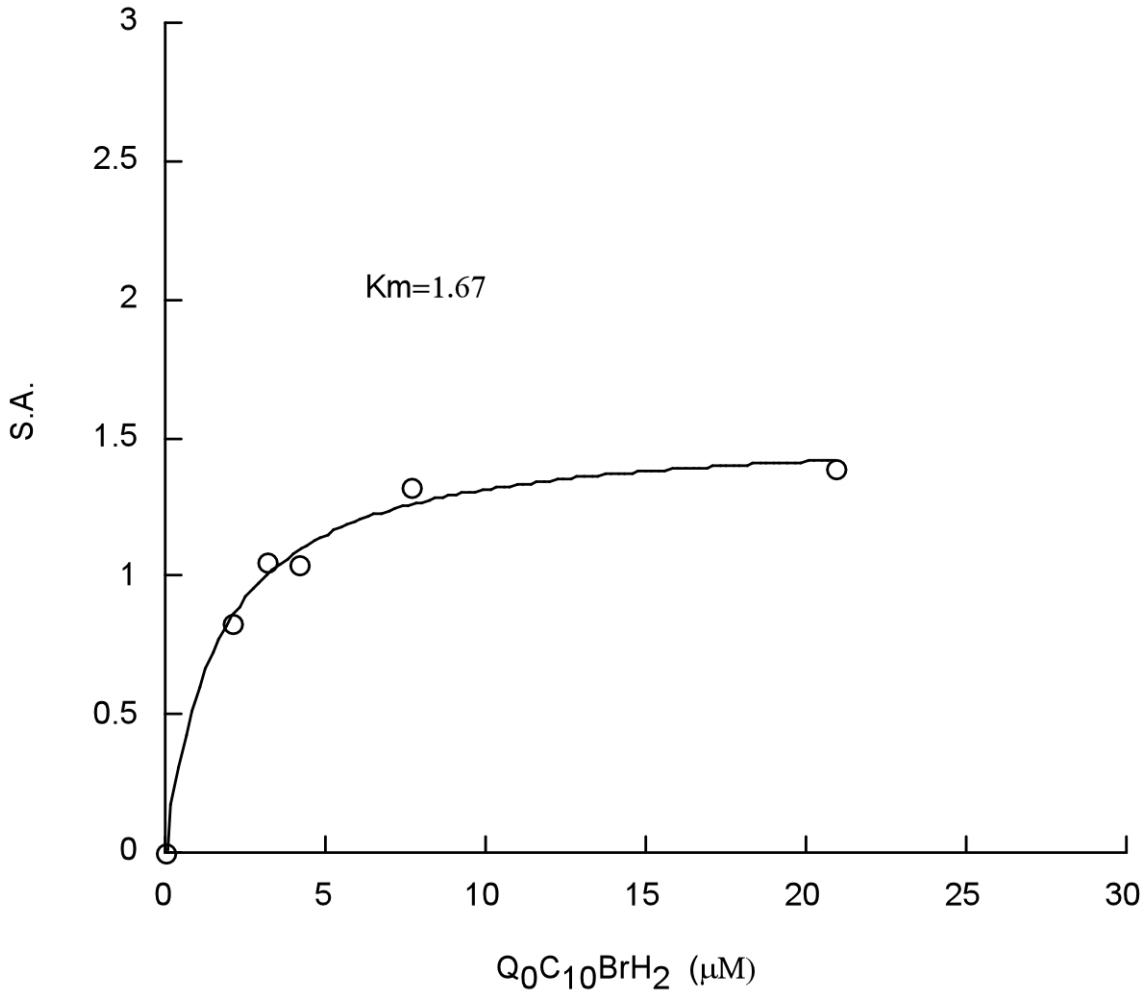

Fig.33.Km titration of L370F (chromatophore).

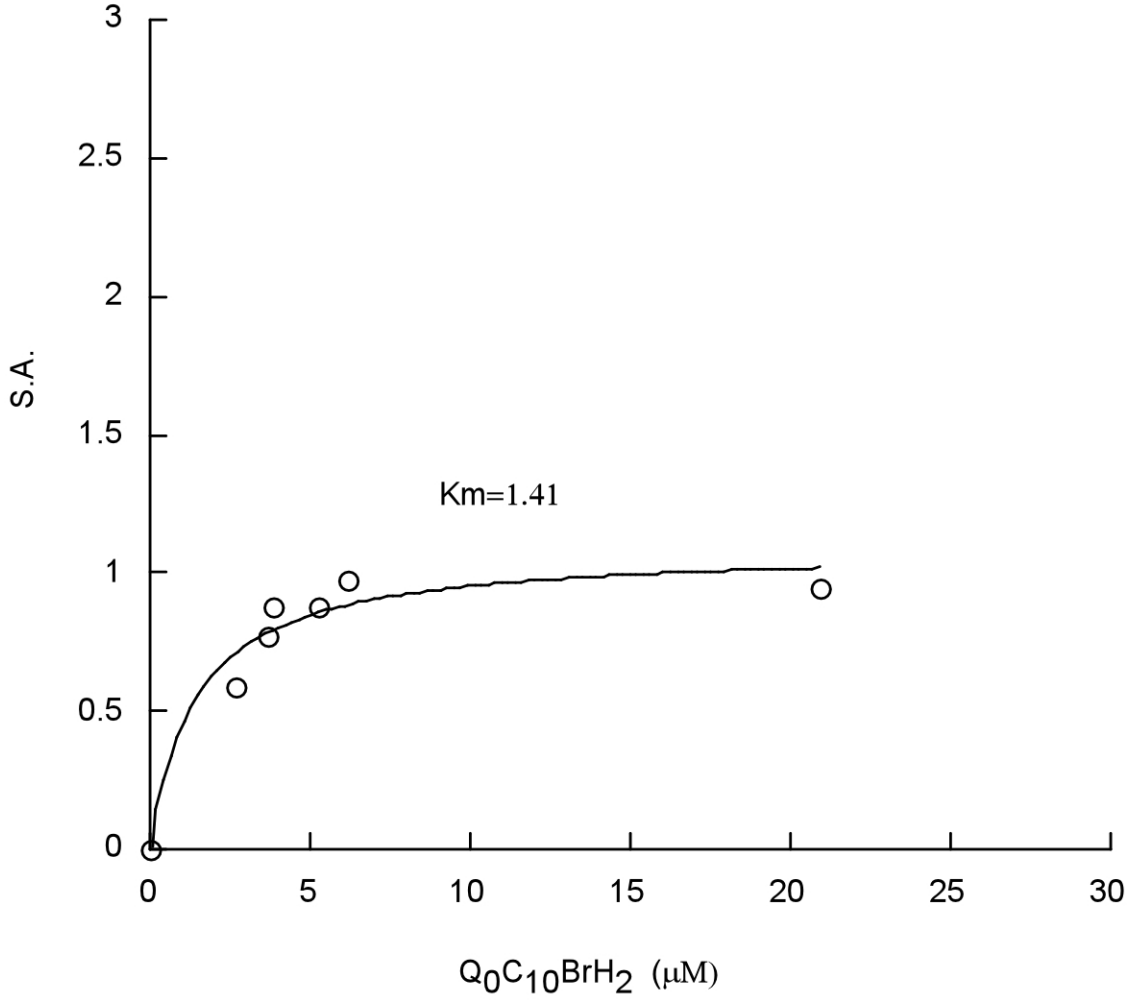

Fig.34.Km titration of X(343,370)F (chromatophore).

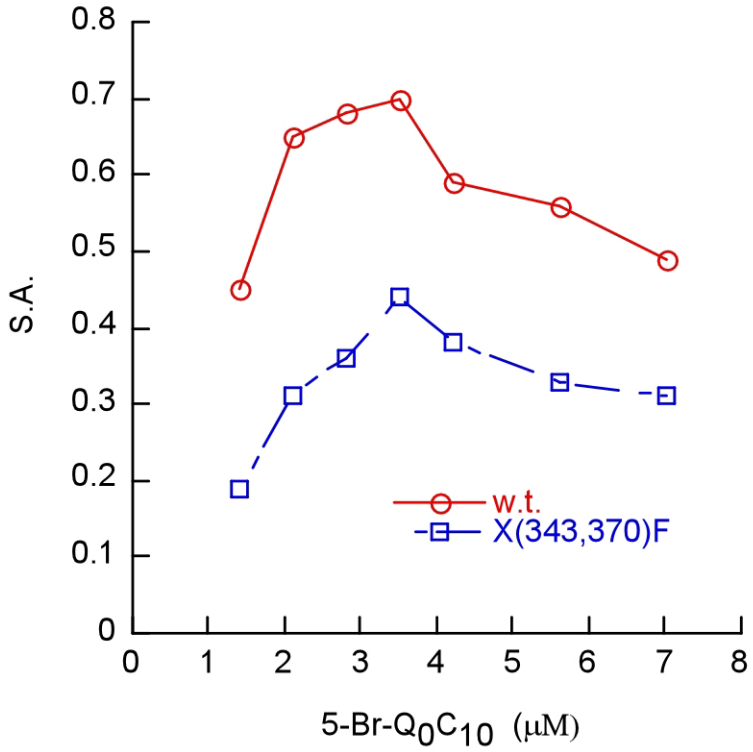

Fig.35. 5-Br-Q_0C_{10} titration of X(343,370)F (protein) compared with w.t.. (narrow range)

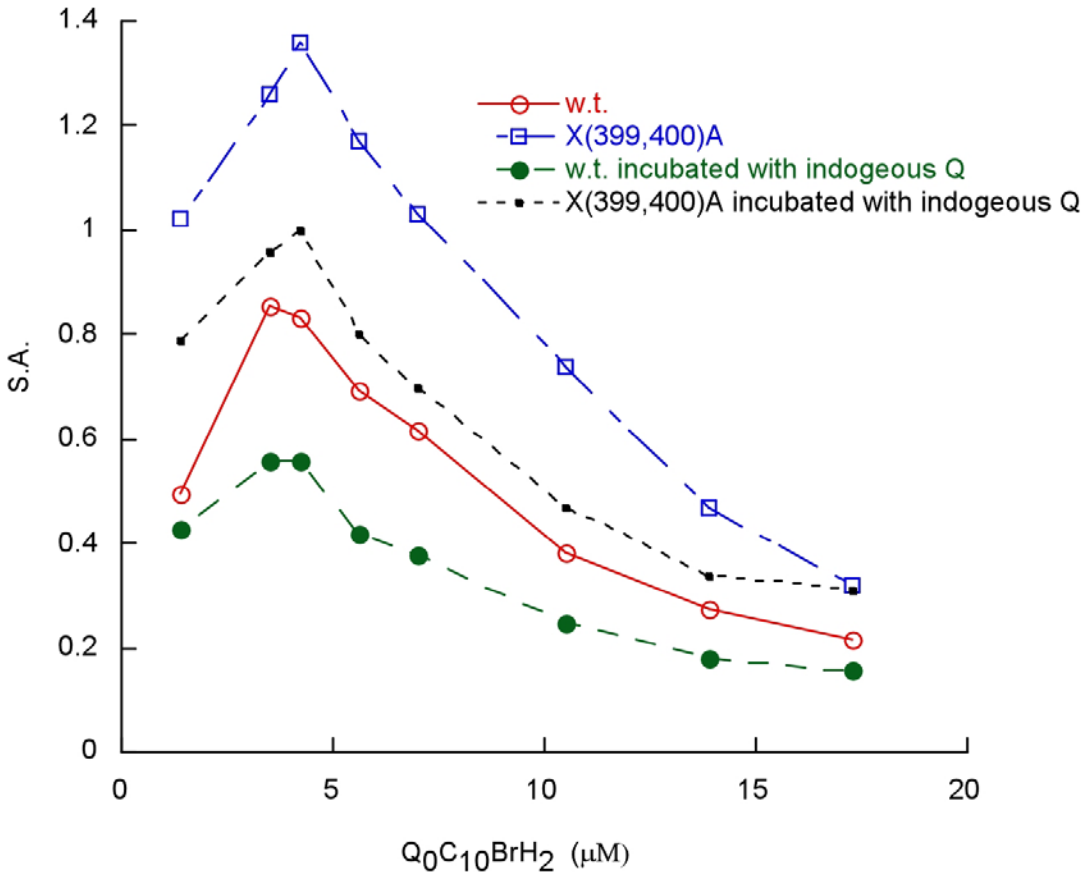

Fig.36. 5-Br-Q_0C_{10} titration of X(399,400)A compared with w.t. (the purified protein incubated w/o endogenous Q_0C_{10})

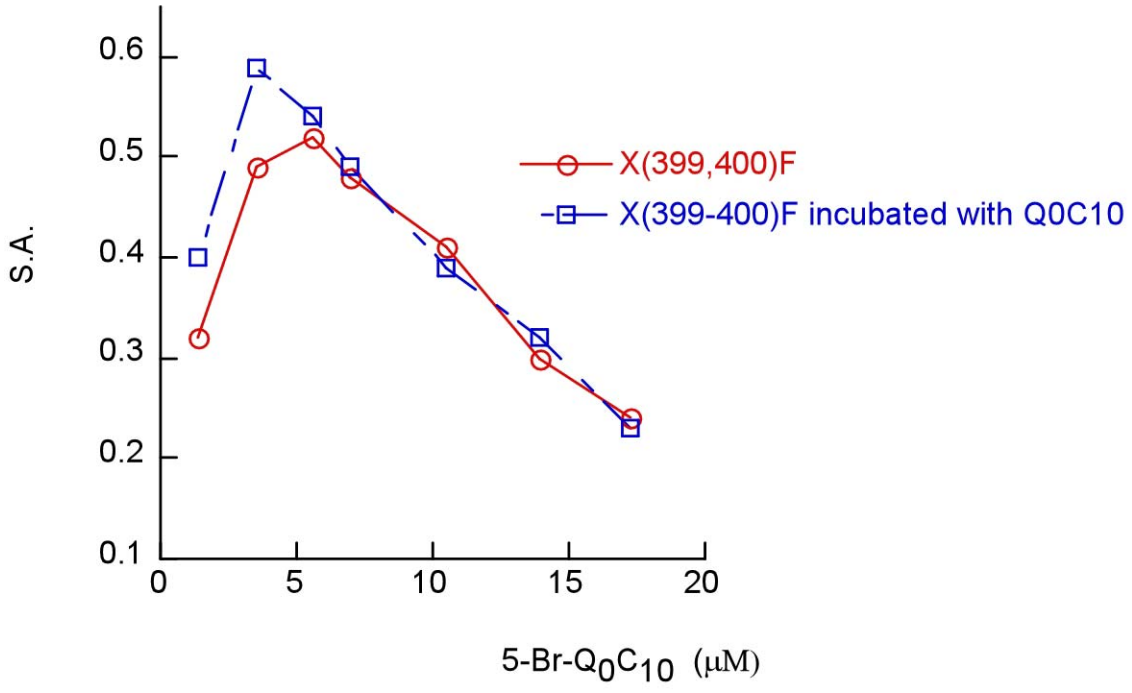

Fig.37.5-Br-Q_0C_{10} titration of X(399,400)F (purified protein incubated w/o Q_0C_{10})

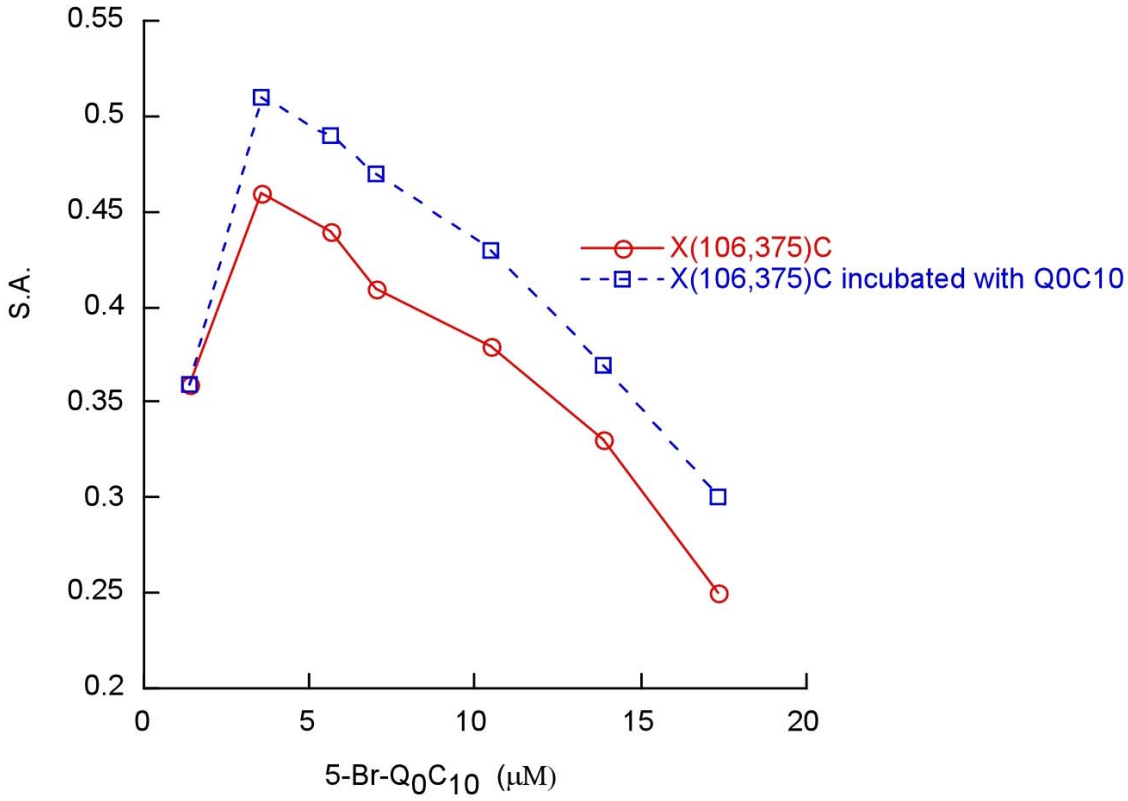

Fig.38.5-Br-Q_0C_{10} titration of X(106,375)C (purified protein incubated w/o Q_0C_{10}).

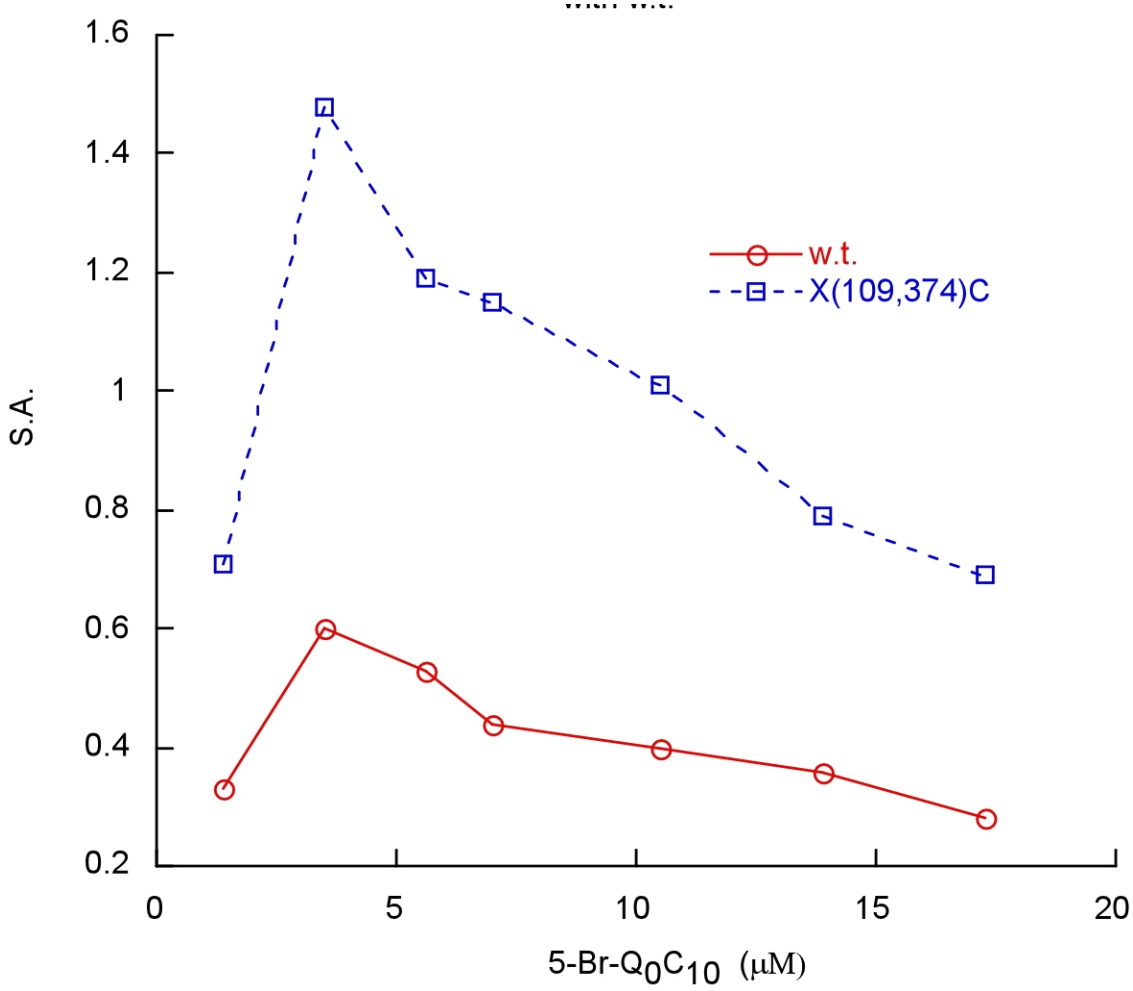

Fig. 39. 5-Br-Q_0C_{10} titration of X(109,374)C compared with w.t..

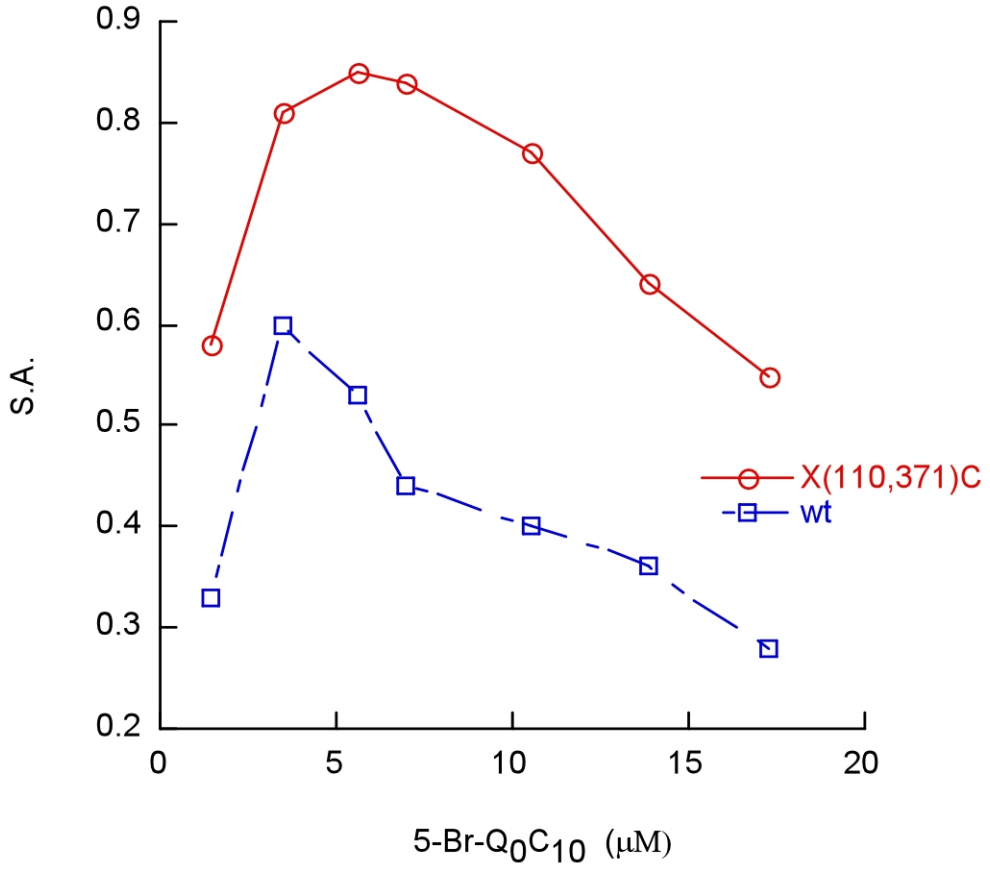

Fig. 40. 5-Br-Q_0C_{10} titration of X(110,371)C compared with w.t..

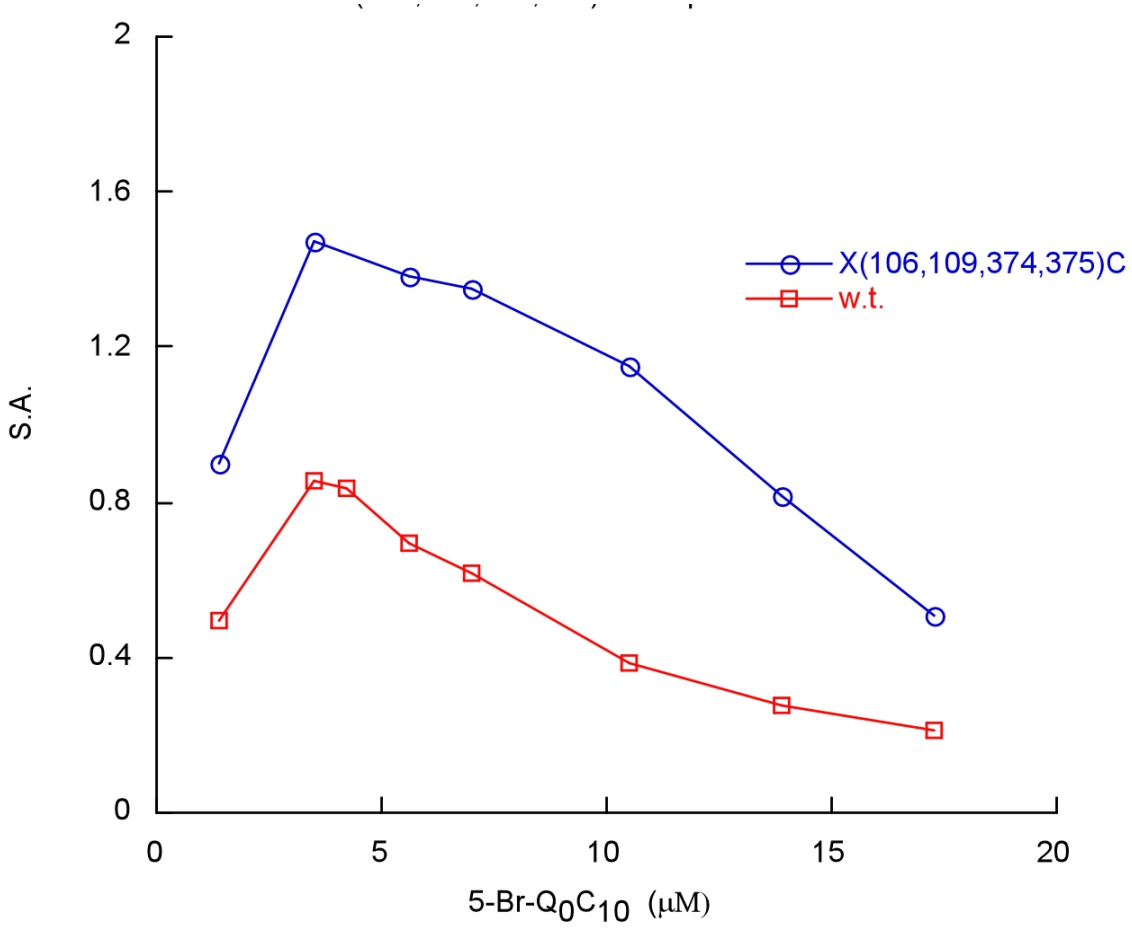

Fig. 41. 5-Br-Q_0C_{10} titration of X(106,109,347,375)C compared with w.t..

References

1. Hatefi, Y. (1985) *Annu Rev Biochem* **54**, 1015-1069
2. Y. Hatefi, i. S. P., F. Guerrieri, J.M. Tager (Eds.), Frontiers of Cellular Bioenergetics: Molecular Biology, Biochemistry, and Physiopathology,. (1999, pp.23-43)
3. P. Nicolls, i. S. P., F. Guerrieri, J. M. Tager (Eds.), Frontiers of Cellular Bioenergetics: Molecular Biology, Biochemistry, and Physiopathology,. (1999, pp. 1-20)
4. Wikstrom, M., Krab, K., and Saraste, M. (1981) *Annu Rev Biochem* **50**, 623-655
5. Trumpower, B. L., and Gennis, R. B. (1994) *Annu Rev Biochem* **63**, 675-716
6. Yu, C. A., Xia, J. Z., Kachurin, A. M., Yu, L., Xia, D., Kim, H., and Deisenhofer, J. (1996) *Biochim Biophys Acta* **1275**(1-2), 47-53
7. Xia, D., Yu, C. A., Kim, H., Xia, J. Z., Kachurin, A. M., Zhang, L., Yu, L., and Deisenhofer, J. (1997) *Science* **277**(5322), 60-66
8. Iwata, S., Lee, J. W., Okada, K., Lee, J. K., Iwata, M., Rasmussen, B., Link, T. A., Ramaswamy, S., and Jap, B. K. (1998) *Science* **281**(5373), 64-71
9. Kim, H., Xia, D., Yu, C. A., Xia, J. Z., Kachurin, A. M., Zhang, L., Yu, L., and Deisenhofer, J. (1998) *Proc Natl Acad Sci U S A* **95**(14), 8026-8033
10. Yu, C. A., Xia, D., Kim, H., Deisenhofer, J., Zhang, L., Kachurin, A. M., and Yu, L. (1998) *Biochim Biophys Acta* **1365**(1-2), 151-158
11. von Jagow, G., and Link, T. A. (1986) *Methods Enzymol* **126**, 253-271
12. Brandt, U., and Trumpower, B. (1994) *Crit Rev Biochem Mol Biol* **29**(3), 165-197
13. Brandt, U., and von Jagow, G. (1991) *FEBS Lett* **287**(1-2), 215-218
14. Yu, L., Yu, C. A., and King, T. E. (1978) *J Biol Chem* **253**(8), 2657-2663
15. Crane, F. L. (1977) *Annu Rev Biochem* **46**, 439-469
16. Gong, X., Xie, T., Yu, L., Hesterberg, M., Scheide, D., Friedrich, T., and Yu, C. A. (2003) *J Biol Chem* **278**(28), 25731-25737
17. Yu, C. A., and Yu, L. (1982) *Biochemistry* **21**(17), 4096-4101
18. Tian, H., Yu, L., Mather, M. W., and Yu, C. A. (1997) *J Biol Chem* **272**(38), 23722-23728
19. Mather, M. W., Yu, L., and Yu, C. A. (1995) *J Biol Chem* **270**(48), 28668-28675

20. Tian, H., Yu, L., Mather, M. W., and Yu, C. A. (1998) *J Biol Chem* **273**(43), 27953-27959
21. Berden, J. A., and Slater, E. C. (1970) *Biochim Biophys Acta* **216**(2), 237-249
22. Yu, L., Dong, J. H., and Yu, C. A. (1986) *Biochim Biophys Acta* **852**(2-3), 203-211

Chapter VI

Saturation Transfer Electron Paramagnetic Resonance and Differential Scanning Calorimetry Studies of the Interaction between Cytochrome *caa*$_3$ and F_1F_0-ATP Synthase from Alkaliphilic *Bacillus pseudofirmus* OF_4

Abstract

The interaction between cytochrome *caa*$_3$ and F_1F_0-ATP synthase from the alkaliphilic *Bacillus pseudofirmus* OF_4 was studied by differential scanning calorimetry (DSC) and by saturation transfer electron paramagnetic resonance (STEPR). When these two purified complexes are embedded in phospholipids vesicles individually [(*cca*$_3$) × PL, (F_1F_0) × PL)] or in combination [(*cca*$_3$+F_1F_0) × PL] and subjected to DSC analysis, they undergo exothermic thermodenaturation with transition temperatures at 69, 57, and 46/75 ˚C, respectively. The ΔH (-8.8 Kcal/mmol) of protein-phospholipid vesicles containing both cytochrome *caa*$_3$ and F_1F_0 is smaller than that (-12.4 Kcal/mmol) of a mixture of protein-phospholipid vesicles formed from each individual electron transfer complex [(*cca*$_3$ × PL) + (F_1F_0 × PL)]. These results suggest that a specific interaction between cytochrome *caa*$_3$ and F_1F_0 exists in the membrane. Further evidence for the interaction

between these two complexes is provided by STEPR studies in which the rotational correlation time of spin-labeled *caa*$_3$ (65 μs) increases significantly when the complex is mixed with F_1F_0 prior to being embedded in phospholipids vesicles (270 μs). From these results, it is concluded that at least a part of *cca*$_3$ and a part of F_1F_0 form a supermacromolecular complex in this bacterial membrane.

Introduction

The facultative alkaliphile, *Bacillus pseudofirmus* OF$_4$, grows well over a pH range extending from 7.5 to above 10.5 (1). The organism possesses a branched respiratory chain with at least two terminal oxidases, cytochrome *bd* and cytochrome *caa*$_3$ (2). Increased amounts of cytochrome *caa*$_3$ are associated with two distinct growth conditions where the bulk electrochemical proton gradient (Δp) is low: pH 10.5 (3) or pH 7.5 in the presence of protonophore carbonyl cyanide *m*-chlorophenylhydrazone (CCCP) (4). Additionally, a CCCP-resistant mutant strain was found to contain constitutively elevated levels of cytochrome *caa*$_3$ when grown at pH 7.5 (4).

Like mitochondria of eukaryotic organisms and most bacteria, alkaliphilic *Bacillus pseudofirmus* OF$_4$ synthesizes ATP using a proton-coupled F_1F_0-ATP synthase via oxidative phosphorylation (5). The widely confirmed chemiosmotic mechanism for ATP synthesis and other membrane-associated bioenergetic work requires establishment of Δp during respiration and photosynthesis. Coupling is achieved by the proton-translocating nature of the reversible F_1F_0-ATP synthase (6). Two properties of proton-coupled oxidative phosphorylation by alkaliphilic *Bacillus* species suggest that above pH

9.5, ATP synthesis utilizes a mechanism that depends upon the bulk transmembrane electrical potential, the $\Delta\Psi$, but also depends upon a sequestered transfer of protons from the respiratory chain to the ATP synthase. Firstly, the protonmotive driving force is very low at pH 10.5 and above, because the needs of pH homeostasis produce a large ΔpH, acid in. Nonetheless, the ATP synthesized, as reflected in the observed phosphorylation potential, is even greater than at pH 7.5, where the Δp is three times higher. Secondly, artificially imposed diffusion potentials fail to energize ATP synthesis at pH values above 9.5 (7).

We have hypothesized that robust alkaliphile oxidative phosphorylation at very alkaline pH values involves the required respiratory chain proton pumping to the bulk phase to establish a Δp and also involves use of one or more specific respiratory chain complexes to transfer protons to F_0 sector of the F_1F_0 ATP-synthase during dynamic protein-protein interactions (7). In this way, the proton-translocating F_1F_0-ATPase accesses protons that have not completely equilibrated with the alkaline medium, accounting for greater synthesis than anticipated from the measured bulk Δp and for the inefficacy of an imposed bulk potential. The *caa*$_3$ terminal oxidase is the best candidate for that interacting partner both because of its alkali-dependent expression and because of the observation that small mutational decreases in the level of this oxidase lead to a non-alkaliphilic phenotype on non-fermentative substrates (3,8). An alternative hypothesis that would not involve protein-protein interactions between a respiratory chain complex and the ATP synthase is that alkaliphile oxidative phosphorylation at high pH utilizes protons that are sequestered near the membrane surface in some trapped, delocalized manner (9), but such hypotheses have not been experimentlly supported and do not

account from the requirement of specific features of the alkaliphile F_1F_0-ATPase for ATP synthesis at high pH (10).

Using methods of differential scanning calorimetry (DSC) and saturation transfer electron paramagnetic resonance (STEPR), we had earlier been able to detect protein-protein interactions between the bovine heart mitochondrial cytochrome *c* oxidase and F_1F_0-ATP synthase in the native membrane state (11). Recently, we used these methods to study the interaction between cytochrome *caa*$_3$ and ATP synthase from alkaliphilic *Bacillus pseudofirmus* OF_4 in an attempt to test the hypothesis that protein-protein interactions are involved in ATP synthesis. If the assays supported such interactions, they could then be used to assess the role of specific features of the ATP synthase and oxidase. The DSC study is based on the assumption that if two lipoprotein complexes exist separately in a phospholipid vesicle, no difference in thermotropic properties will be observed between protein-phospholipid vesicles formed from a mixture of two complexes and a mixture of protein-phospholipid vesicles formed individually from each complex. Differences in the thermodenaturation temperatures and enthalpy changes would suggest formation of a physical complex between cytochrome *caa*$_3$ and ATP synthase. In the STEPR study, the formation of a physical complex between cytochrome *caa*$_3$ and ATP synthase will be indicated by an increase of rotational correlation time of spin-labeled cytochrome *caa*$_3$. Herein, we report experimental details and results of DSC and STEPR studies with cytochrome *caa*$_3$ and ATP synthase embedded in phospholipid vesicles. The results of DSC and STEPR indicate that cytochrome *caa*$_3$ does indeed interact directly with the ATP synthase in phospholipid vesicles.

Material and methods

Materials. 4-Maleimide-2,2,6,6-tetramethyl-1-piperidinyl-N-oxyl (MSL), Cytochrome c (horse heart, type III) and sodium cholate were from Sigma. N-Dodecyl-β-D-maltoside (DM) and N-octyl-β-D-glucoside were from Anatrace. Asolection was obtained from Associated Concentrates, Inc., and purified according to the procedure reported by Kagama *et. al* (12). Centriprep-30 and Centricon-30 were bought from Amicon. Other chemicals were of the highest purity commercially available.

Enzyme Preparations and Assays. Highly purified cytochrome caa_3 and F_1F_0-ATP synthase from alkaliphilic *Bacillus pseudofirmus* OF_4 were prepared and assayed essentially as reported previously (3,5).

Preparation of Maleimide Spin-Labeled (MSL) Cytochrome caa_3. Alkaliphile, *Bacillus pseudofirmus* OF_4 cytochrome caa_3, 20 mg/ml in 20 mM Tris-Cl, pH 8.0, containing 0.35 M NaCl, 1 mM EDTA, 0.1 mM PMSF, 0.05 % dodecyl maltoside, and 10 % glycerol was incubated with a 5 molar excess of 4-maleimide-2,2,6,6-tetramethyl-1-piperidinyl-N-oxyl (MSL) for 1 hour at room temperature. The stock solution of MSL (10 mM) was made in 10 mM Tris-Cl /sucrose buffer, pH 8.0, containing 20% methanol. After incubation, the unreacted MSL was removed by passage through a D-Salt™ Excellulose Desalting Column from Pierce, equilibrated with 10 mM Tris-Cl buffer, containg 0.05 % dodecyl maltoside. Fractions containing MSL-cytochrome caa_3 were pooled and concentrated by Centriprep-30 and Centricon-30 to a protein concentration of approximately 20 mg/ml. MSL-cytochrome caa_3 obtained by this method contains no free spin-label. The absence of free spin-label in the preparation was confirmed by the conventional EPR spectra.

Preparation of Cytochrome caa_3 and F_1F_0 Complex-Phospholipid Vesicles. The protein-phospholipid vesicles were prepared by the cholate-dialysis method reported by Racker (13). Cytochrome *caa*$_3$ complex, with or without MSL labeling, alone or in combination with F_1F_0, at a protein concentration of approximately 30 mg/ml, was mixed with an asolectin micellar solution (20 mg/ml in 50 mM phosphate buffer, pH 7.4) and a sodium cholate solution [20% (w/v) in water]. The final solution contained 7 mg/ml protein, 10 mg/ml sodium cholate, and 10.5 mg/ml asolectin. After incubation at 4^oC for 30 min, the solution was dialyzed overnight against 500 volumes of 50 mM phosphate buffer, pH 7.4, with four changes of buffer to form vesicles. The protein-phospholipid vesicles formed were collected as precipitated by centrifugation at 80,000 g for 1 h and were respended in 50 mM phosphate buffer, pH 7.4, to a protein concentration of suitable number. The suspensions were used for the DSC and STEPR experiments.

Differential Scanning Calorimetry. All calorimetric measurements were performed with a CSC 6100 NanoII DSC from Calorimetry Science Corp. The reference and sample solutions were carefully degassed under vacuum for 15 min prior to use. A 0.50-ml sample in 50 mM K^+/Na^+ phosphate buffer, pH 7.4, was placed in the sample capillary cell, and the same amount of buffer was placed in the reference capillary cell. All DSC scans reported in this study were run at a rate of 2^0C/min. After the first scan, the samples were cooled to the original temperature and rescanned. Since after the first scan the protein was completely and irreversibly denatured, no thermotransition peaks were observed in the second scan. Thus the second scan could be used as a baseline. All thermodynamic analyses were carried out according to the program known as CpCal from the Nano DSC program group.

EPR Measurements. All EPR measurements were made with a Bruker EMX EPR spectrometer, using an aqueous quartz flat cell. The temperature of the microwave cavity was controlled by circulation of cooled nitrogen gas from a modified variable temperature housing assembly equipped with an electric temperature sensor. Conventional EPR spectra were recorded with instrument settings as follows: field modulation frequency, 100 kHz; modulation amplitute, 8 G; microwave frequency, 9.757 GHz; microwave power, 10.78 mW; time constant, 1310.72 ms. Saturation transfer EPR spectra were recorded using the same instrument settings as those described by Thomas *et al.* (14) and Poore *et al.* (15). A field modulation of 8 G and microwave frequency of 9.757 GHz were employed with phase-sensitive detection at 100 Hz (second harmonic) 90^0 out of phase. Incident microwave power was 107.80 mW. The phase was adjusted to minimize the second harmonic signal. Approximate rotational correlation time (τ_2) was obtained from the ratio of the two field lines (L"/L). The calibration curve of Thomas *et al.* (14) derived from isotropic tumbling of MSL-labeled hemoglobin was used in the calculation.

Other Analytical Methods. Protein concentration was determined by the biuret method (16), using bovine serum albumin as the standard (assuming 1 mg/ml has an A_{279} of 0.667). Absorption spectra were measured in a Shimadzu UV-2401 PC spectrophotometer.

Results and discussion

Thermotropic Properties of Cytochrome caa_3 and F_1F_0-synthase Embedded in Phospholipid Vesicles. To unambiguously study the interaction between cytochrome caa_3

and F_1F_0-synthase from alkaliphilic *Bacillus pseudofirmus* OF_4, DSC studies were carried out with both complexes embedded in phospholipid (asolectin) vesicles, because these enzymes in protein-phospholipid vesicles should have an environment similar to that in membrane. The isolated complexes, singly or in combination, were embedded in phospholipids vesicles by the cholate dialysis method (13). A constant phospholipid to protein ratio of 1.5 was used. The ratio between F_1F_0-synthase and cytochrome caa_3 varies from 0 to 1.5. If the two lipoprotein complexes have no specific interaction, then no difference in DSC characteristics should be observed between phospholipids vesicles embedded with a mixture of two complexes and a mixture of phospholipid vesicles embedded with one or the other complex. In other words, differences in the thermodenaturation temperatures (*Tm*) and enthalpy changes (ΔH) would suggest formation of a physical complex between these two lipoproteins.

Fig. 42. show the differential scanning calorimetric curves of alkaliphilic *Bacillus pseudofirmus* OF_4 F_1F_0-synthase and cytochrome caa_3 embedded in phospholipids singly or in combination. When F_1F_0-synthase was incorporated into phospholipid vesicles and subjected to DSC analysis, an exothermic peak at 57.2 ^{0}C with the enthalpy change of -7.3 Kcal/mmol of protein was observed (see Fig. 42.A). Purified cytochrome caa_3 also shows a single transition with ΔH = -17.8 Kcal/mmol of protein and *Tm* = 68.5 ^{0}C when embedded into phospholipids vesicles as shown in Fig.42.B. As expected, when the mixture of protein-phospholipid vesicles formed individually from F_1F_0-synthase and cytochrome caa_3 was subjected to DSC analysis under the identical condition, two exothermic transient peaks at 56.8 and 68.9 ^{0}C with the ΔH of -12.4 Kcal/mmol of protein were obtained (see Fig. 43D). These data are sum of the thermotropic properties

of F_1F_0-synthase-phospholipid vesicles and cytochrome *caa*$_3$-phospholipid vesicles. However, the protein-phospholipid vesicles formed from a mixture of F_1F_0-synthase and cytochrome *caa*$_3$ have *Tm*1 = 45.5 ^{0}C and *Tm*2 = 74.6 ^{0}C with ΔH = -8.8 Kcal/mmol of protein (see Fig. 42C). These data are significantly different from those observed with a mixture of phospholipids vesicles embedded individually with F_1F_0-synthase or cytochrome *caa*$_3$, suggesting that there is some interaction between these two complexes.

Fig. 43 compares the thermodenaturation enthalpy changes of phospholipid vesicles formed with mixtures of cytochrome *caa*$_3$ and F_1F_0-synthase at various molar ratios and of mixtures of phospholipid vesicles of individual complexes. The value of the difference in ΔH increases as F_1F_0-synthase is increased. The maximum difference is obtained when approximately one mol of F_1F_0-synthase per mol cytochrome *caa*$_3$ is used. This suggests that the interaction between cytochrome *caa*$_3$ and F_1F_0-synthase is specific. The accuracy of assessment of the stoichiometry between the two complexes may have been compromised by uncertainty concerning the intactness of each complex.

As discussed earlier (11,17-19), the energy for the exothermic transition of an electron transfer complex embedded in phospholipid vesicles is derived from the collapse, upon thermodenaturation, of a strained interaction between unsaturated fatty acyl groups of phospholipids and a protein surface on the electron transfer or other lipoprotein complex which was exposed, by removal of an interacting protein from a complex or a complex from a supermacromolecular complex, during the isolation. Such an interaction occurs only when a vesicle is formed. Little exothermic transition was observed in mitochondrial or submitochondrial preparations because there is no such exposed area in the native complex or supercomplex to interact with phospholipids under

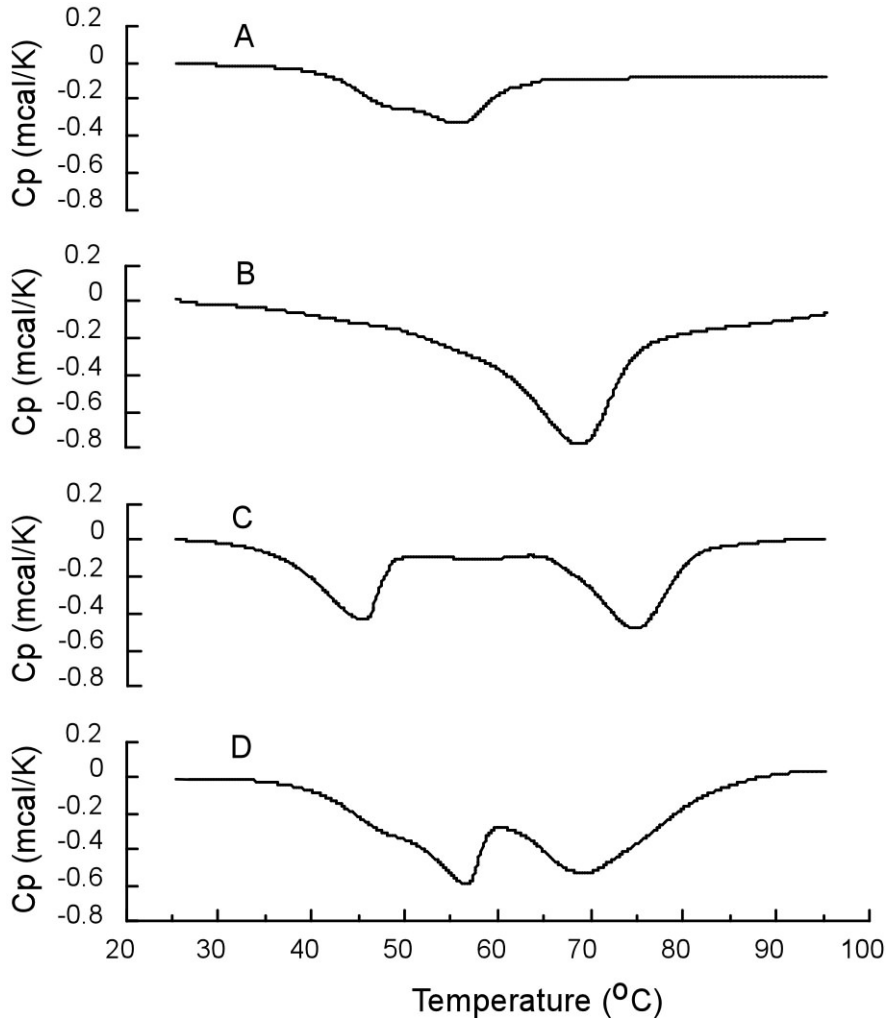

Fig.42. DSC curves of alkaliphile *B. firmus* OF_4 F_1F_0 and cytochrome caa_3 embedded in phospholipids singly or in combination. The molar ratio of F_1F_0 and caa_3 is 1 and the weight ratio of phospholipids to protein is 1.5 in all cases. These vesicles are prepared by the cholate dialysis method. Spectrum A shows the exothermic thermodenaturation of 0.5 mg F_1F_0 embedded in phospholipid vesicles. Spectrum B is the DSC thermogram of 0.105 mg/ml caa_3 embedded in phospholipid vesicles. Spectrum C is the DSC profile of phospholipid vesicle embedded with a mixture of 0.5 mg F_1F_0 and 0.105 mg caa_3. Spectrum D is a mixture of phospholipid vesicles, which include 0.5 mg F_1F_0 embedded in phospholipid vesicles and 0.105 mg caa_3 embedded in phospholipid vesicles.

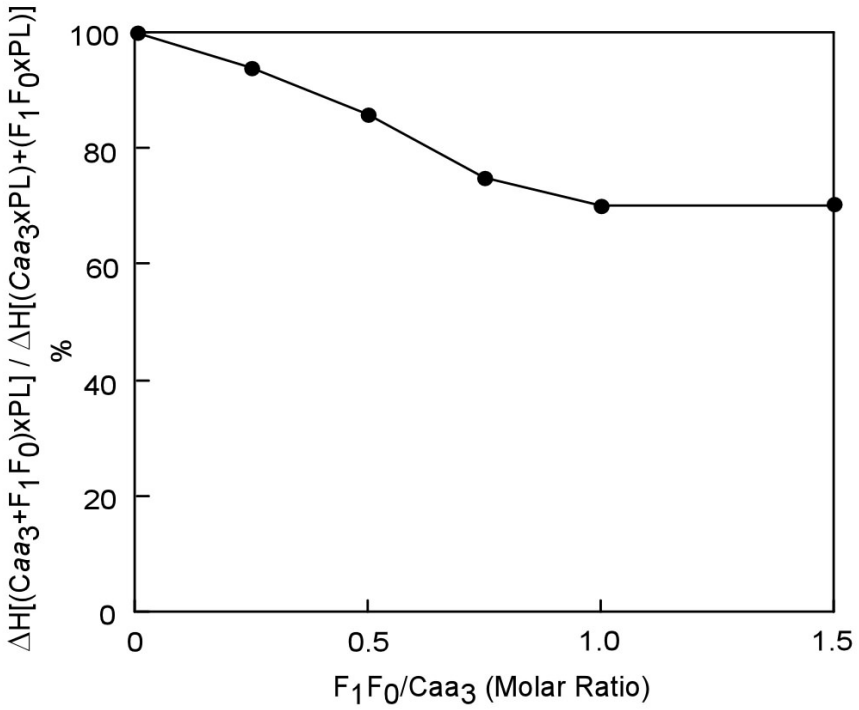

Fig.43. Comparison of thermodenaturation enthalpy changes of phospholipids vesicles formed with mixtures of cytochrome *caa*$_3$ and F_1F_0-synthase from alkaliphile *B. firmus* OF_4 at various molar ratios and of mixtures of phospholipids vesicles of individual complexes. The molecular masses used in calculation of molar ratios were 517,000 and 105, 500 daltons for F_1F_0-synthase and cytochrome *caa*$_3$, respectively. The ratio of phospholipids to protein was 1.5 by weight in all cases.

strained conditions. When two interacting complexes are mixed together before being embedded in phospholipids vesicles, the exposed area on the protein surface is greatly diminished through the protein-protein interaction. Therefore, less strained interaction occurs upon vesicle formation, and less enthalpy change of exothermic denaturation is observed. It has been reported that thermodenaturation of the mitochondrial membrane under aerobic condition is accompanied by a heat release, which was attributed to the autooxidation of iron-sulfur protein (20). This explanation is not applicable to the present study because there are no iron-sulfur proteins in either cytochrome *caa*$_3$ or F_1F_0-synthase.

STEPR Studies of Spin-labeled Cytochrome caa$_3$ Embedded in Phospholipid Vesicles in the Absence and Presence of F_1F_0-synthase. To confirm the existence of a specific interaction between cytochrome *caa*$_3$ and F_1F_0-synthase, cytochrome *caa*$_3$ was labeled with 4-maleimide-2,2,6,6-tetramethyl-1-piperidinyl-N-oxyl (MSL) as described under Materials and Methods. This MSL-cytochrome *caa*$_3$, which is enzymetically active, was embedded in phospholipids vesicles alone or together with F_1F_0-synthase. The electron paramagnetic resonance (EPR) measurements of these electron transfer complex-phospholipid vesicles show typical spin-immobilized spectra (see spectra A and B of Fig.44.). The spectra are identical regardless of whether the protein-phospholipid vesicles contained only cytochrome *caa*$_3$ or cytochrome *caa*$_3$ and F_1F_0-synthase complexes (Fig. 44.A & B). This suggests that the difference in mobility of the spin-label on cytochrome *caa*$_3$, in the absence and presence of F_1F_0-synthase, is too small to be measured by conventional EPR (14). Therefore, the protein rotational diffusion of the spin-labeled complex was measured by saturation transfer electron paramagnetic

resonance (STEPR) because ST-EPR is an excellent method for study of the motional anisotropy and dynamics of spin-labeled proteins embedded in phospholipid bilayers (21-22). The spin correlation time, τ_2, which represents the speed of motion of spin-labled proteins, can be calculated from the ratio of the low field signals (L''/L) in the ST-EPR spectrum (*e.g.*, see spectra C and D of Fig. 44) (21). The longer the rotational correlation time, the slower the protein moves (22). It was reported that the rotational correlation time of spin-labeled protein is increased when two proteins form a supermacromolecular complex (11,18). Table 5 shows the effect of additions on the rotational correlation time of spin-labeled cytochrome *caa*$_3$. When MSL-cytochrome *caa*$_3$ mixed with F_1F_0-ATP synthase before being embedded in phospholipid vesicles, a significant increase in τ_2 (270 μs) was observed in comparison with that of MSL-cytochrome *caa*$_3$ embedded in phospholipid vesicle alone (65 μs), indicating that MSL-cytochrome *caa*$_3$ does interact with F_1F_0-ATP synthase to form supermacromolecular complex. However, the τ_2 of spin-labeled cytochrome *caa*$_3$ was not affected by the addition of cytochrome *bc*$_1$ complex or ATP-synthase from bovine heart prior to the formation of vesicles; and the mixture of spin-labeled cytochrome *caa*$_3$ complex and F_1F_0-synthase phospholipid vesicles showed the same τ_2 as that of cytochrome *caa*$_3$ phospholipid vesicles alone (see Table 7), because the MSL-cytochrome *caa*$_3$ can't form complex with neither mitochondrial F_1F_0-synthase nor mitochondrial *bc*$_1$ complex.

To ensure that the observed τ_2 increase upon mixing F_1F_0-synthase with spin-labeled cytochrome *caa*$_3$ is indeed due to the specific interaction between these two complexes and the formation of a binary complex, and not due to the change of protein concentration or self-aggregation upon addition of F_1F_0-synthase, a titration of spin-

Table 7. Effect of additions on the rotational correlation time (τ_2) of spin-labeled cytochrome *caa*$_3$[1]

Preparations	L''/L	τ_2 (μs)
(MSL-*caa*$_3$ × PL)	0.70	65
[(MSL-*caa*$_3$ + bF_1F_0[2]) × PL]	1.06	270
[(MSL-*caa*$_3$ × PL) + (bF_1F_0 × PL]	0.71	70
[(MSL-*caa*$_3$ + mF_1F_0[3]) × PL]	0.71	70
[(MSL-*caa*$_3$ + m*bc*$_1$[4]) × PL]	0.70	65

[1]The molar ratio of cytochrome *caa*$_3$ to other proteins used was 1:1.

[2]The bF_1F_0 was F_1F_0-synthase from bacterial alkaliphile *B.firmus* OF_4.

[3]The mF_1F_0 was F_1F_0-synthase from bovine mitochondria.

[4]The m*bc*$_1$ was cytochrome *bc*$_1$ complex from bovine mitochondria.

labeled cytochrome *caa*$_3$ with F_1F_0-synthase was carried out. If a specific interaction between these two complexes exists, it is expected that a maximum τ_2 will be obtained when the two components complex reaches to a specific stoichiometry. As shown in Figure 45, the break point in τ_2 was obtained when the ratio of F_1F_0-synthase to cytochrome *caa*$_3$ approached one, which is in consistent with the number obtained from the DSC data.

A similar effect of succinate-Q reductase on τ_2 of spin-labeled ubiquinol-cytochrome *c* reductase (18), and of F_1F_0-synthase on τ_2 of spin-labeled cytochrome *c* oxidase from bovine mitochondria (11), has been reported from this group. It is conceivable that at least part of the observed effect resulted from a change in the fluidity of the membrane by inclusion of protein complexes other than the spin-labeled complex. Also, it should be mentioned that the rotational correlation time obtained from STEPR is only an approximate value; it is based on the calibration curve derived from the isotropic motion of spin-label. The values obtained, however, agree with those obtained by other methods, such as flash photolysis (23). Although in this study our main concern is with the relative τ_2 of spin-labeled cytochrome *caa*$_3$ in the absence and presence of the F_1F_0-synthase from alkaliphilic *Bacillus pseudofirmus* OF_4, the τ_2 values obtained are in agreement with the DSC data.

From the results of DSC and STEPR experiments, we conclude that cytochrome *caa*$_3$ and F_1F_0-synthase from alkaliphilic *Bacillus pseudofirmus* OF_4 may exist as a supermacromolecule complex in the membrane. This conclusion differs significantly from the free diffusible model of electron transfer complexes derived from results of membrane fusing (24) and fluorescence recovery, after photobleaching, measurements

(25). However, it has been clearly established that some mitochondrial electron-transfer complexes specifically interact to form supermolecular structures called supercomplexes from the work on the yeast *Saccharomyces cerevisiae* (26,27), beef (11,18,27,28), and plants (29-32). Similar supermolecular structures were also described for the respiratory chains of bacteria (33-37). The roles that have been attributed to respiratory supercomplexes are substrate-channeling, catalytic enhancement, sequestration of reactive intermediates (27), stabilization of protein complexes (38), increasing the capacity of the inner mitochondrial membrane for protein insertion (26), and generating mitochondrial cristae morphology (39). Furthermore, the dynamic formation of such supercomplexes is speculated to serve some regulatory function in the energy generation in mitochondria from plants (29) and beef (11,29). Similarly, the formation of a supermacromolecule complex between cytochrome caa_3 and F_1F_0-synthase from alkaliphilic *Bacillus pseudofirmus* OF_4 may help control energy generation in this alkaliphilic bacterium. The formation of supermacromolecule complexes from some electron transfer and F_1F_0-synthase complexes indicates that some of these complexes do not follow the random diffusion model, even though they are capable of doing so.

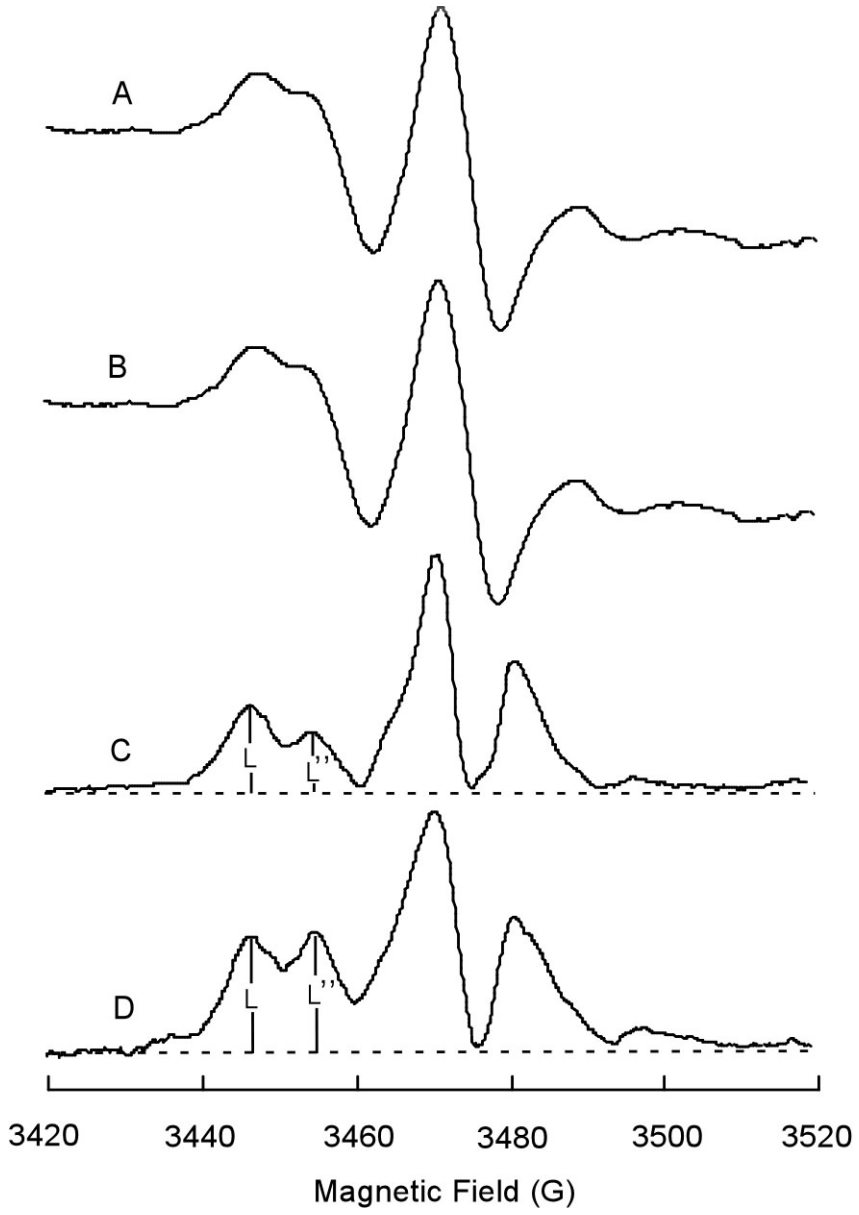

Fig.44. EPR spectra of spin-labeled alkaliphile *B. firmus* OF_4 cytochrome caa_3 in the absence and presence of OF_4 F_1F_0-synthase complex. Spectra A and B are conventional EPR spectra of spin-labeled OF4 cytochrome caa_3 embedded in phospholipid vesicles in the absence or presence of OF_4 F_1F_0-synthase complex. Spectra C and D are the saturation transfer EPR spectra of the same samples. The protein concentrations were 6 and 36 mg/ml for caa_3 and (caa_3 + F_1F_0) vesicles, respectively.

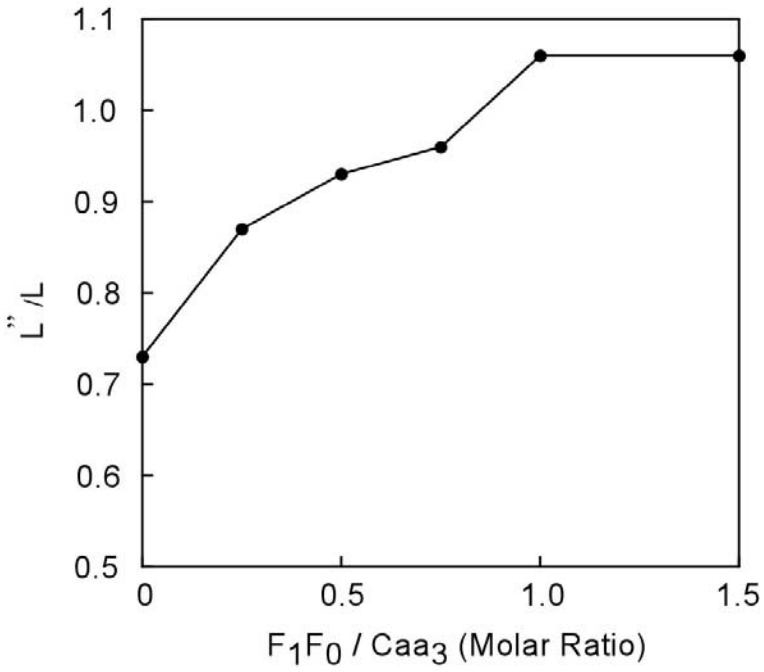

Fig.45. Effect of F_1F_0-synthase on STEPR of spin-labeled cytochrome *caa*$_3$. Increasing amounts of F_1F_0-synthase were added to a constant amount of spin-labeled cytochrome *caa*$_3$. The solutions were incubated for 60 min at 4 ^{o}C before embedded in phospholipids vesicles. 1.5 mg of phospholipid/mg of protein was used. L''/L was calculated from the saturation transfer EPR spectra of each sample. Instrument settings are given under Materials and Methods.

References

1. Krulwich, T. A., Ito, M., Gilmour, R., Hicks, D. B., and Guffanti, A. A. (1998) *Adv Microb Physiol* **40**, 401-438
2. Gilmour, R., and Krulwich, T. A. (1997) *J Bacteriol* **179**(3), 863-870
3. Quirk, P. G., Hicks, D. B., and Krulwich, T. A. (1993) *J Biol Chem* **268**(1), 678-685
4. Quirk, P. G., Guffanti, A. A., Plass, R. J., Clejan, S., and Krulwich, T. A. (1991) *Biochim Biophys Acta* **1058**(2), 131-140
5. Hicks, D. B., and Krulwich, T. A. (1990) *J Biol Chem* **265**(33), 20547-20554
6. Mitchell, P. (1961) *Nature* **191**, 144-148
7. Krulwich, T. A. (1995) *Mol Microbiol* **15**(3), 403-410
8. Krulwich, T. A., Ito, M., Gilmour, R., Sturr, M. G., Guffanti, A. A., and Hicks, D. B. (1996) *Biochim Biophys Acta* **1275**(1-2), 21-26
9. Cherepanov, D. A., Feniouk, B. A., Junge, W., and Mulkidjanian, A. Y. (2003) *Biophys J* **85**(2), 1307-1316
10. Wang, Z., Hicks, D. B., Guffanti, A. A., Baldwin, K., and Krulwich, T. A. (2004) *J Biol Chem* **279**(25), 26546-26554
11. Qiu, Z. H., Yu, L., and Yu, C. A. (1992) *Biochemistry* **31**(12), 3297-3302
12. Kagawa, Y. (1971) *Tanpakushitsu Kakusan Koso* **16**(9), 775-786
13. Racker, E. (1972) *J Membr Biol* **10**(3), 221-235
14. Thomas, D. D., Dalton, L. R., Hyde, J. S., . (1976) *J. Chem. Phys.* **65**, 3006
15. Poore, V. M., Fitzsimmon, J. T. R., and Ragan, C. I. (1981) *Biochim. Biophys. Acta* **693**, 113-124
16. Gornall, A. G., Barwawill, C. J., and David, M. M. (1949) *J. Boil. Chem.* **177**, 751-766
17. Gwak, S. H., Yu, L., and Yu, C. A. (1985) *Biochim Biophys Acta* **809**(2), 187-198
18. Gwak, S. H., Yu, L., and Yu, C. A. (1986) *Biochemistry* **25**(23), 7675-7682
19. Yu, C. A., Gwak, S. H., and Yu, L. (1985) *Biochim Biophys Acta* **812**(3), 656-664
20. Tsong, T. Y., and Knox, B. E. (1984) *Biophys. J.* **45**, 296a

21. Hemminga, m. A., Faber, A. J., . (1986) *J. Magn. Reson.* **66**, 1-8
22. Adhikari, B., Hideg, K., and Fajer, P. G. (1997) *Proc Natl Acad Sci U S A* **94**(18), 9643-9647
23. Cherry, R. J. (1979) *Biochim Biophys Acta* **559**(4), 289-327
24. Schneider, H., Lemasters, J. J., Hochli, M., and Hackenbrock, C. R. (1980) *J Biol Chem* **255**(8), 3748-3756
25. Gupte, S., Wu, E. S., Hoechli, L., Hoechli, M., Jacobson, K., Sowers, A. E., and Hackenbrock, C. R. (1984) *Proc Natl Acad Sci U S A* **81**(9), 2606-2610
26. Arnold, I., Pfeiffer, K., Neupert, W., Stuart, R. A., and Schagger, H. (1998) *Embo J* **17**(24), 7170-7178
27. Schagger, H., and Pfeiffer, K. (2000) *Embo J* **19**(8), 1777-1783
28. Schagger, H., and Pfeiffer, K. (2001) *J Biol Chem* **276**(41), 37861-37867
29. Eubel, H., Jansch, L., and Braun, H. P. (2003) *Plant Physiol* **133**(1), 274-286
30. Eubel, H., Heinemeyer, J., and Braun, H. P. (2004) *Plant Physiol* **134**(4), 1450-1459
31. Krause, F., Reifschneider, N. H., Vocke, D., Seelert, H., Rexroth, S., and Dencher, N. A. (2004) *J Biol Chem* **279**(46), 48369-48375
32. Dudkina, N. V., Eubel, H., Keegstra, W., Boekema, E. J., and Braun, H. P. (2005) *Proc Natl Acad Sci U S A* **102**(9), 3225-3229
33. Esser, L., Quinn, B., Li, Y. F., Zhang, M., Elberry, M., Yu, L., Yu, C. A., and Xia, D. (2004) *J Mol Biol* **341**(1), 281-302
34. Sone, N., Sekimachi, M., and Kutoh, E. (1987) *J Biol Chem* **262**(32), 15386-15391
35. Iwasaki, T., Matsuura, K., and Oshima, T. (1995) *J Biol Chem* **270**(52), 30881-30892
36. Niebisch, A., and Bott, M. (2003) *J Biol Chem* **278**(6), 4339-4346
37. Stroh, A., Anderka, O., Pfeiffer, K., Yagi, T., Finel, M., Ludwig, B., and Schagger, H. (2004) *J Biol Chem* **279**(6), 5000-5007
38. Acin-Perez, R., Bayona-Bafaluy, M. P., Fernandez-Silva, P., Moreno-Loshuertos, R., Perez-Martos, A., Bruno, C., Moraes, C. T., and Enriquez, J. A. (2004) *Mol Cell* **13**(6), 805-815

39. Paumard, P., Vaillier, J., Coulary, B., Schaeffer, J., Soubannier, V., Mueller, D. M., Brethes, D., di Rago, J. P., and Velours, J. (2002) *Embo J* **21**(3), 221-230

Vita

Xiaoying Liu

Candidate for the Degree of

Doctor of Philosophy

Thesis: STUDIES OF EXTRA FRAGMENTS OF CYTOCHROME bc_1 COMPLEX FROM *RHODOBACTER SPHAEROIDES* AND THE INTERACTION BETWEEN CYTOCHROME CAA_3 AND F_1F_0-ATP SYNTHASE FROM ALKALIPHILIC *BACILLUS PSEUDOFIRMUS* OF_4

Major Field: Biochemistry and Molecular Biology

Biographical:

Education: Graduated from the first High School of Lanzhou, Gansu, China in July 1992; received Bachelor of Science degree and Master of Science degree in Chemistry from Lanzhou University, Gansu, China in July 1996 and July 1999, respectively. Completed the requirements for the Doctor of Philosophy degree with a major in Biochemistry and Molecular Biology at Oklahoma State University in May, 2006

Experience: Employed as a research assistant by College of Chemistry and Chemical Engineering, Lanzhou University from September 1996 to July 1999; employed by Oklahoma State University, Department of Biochemistry and Molecular Biology as a graduate research assistant from August 1999 to present.

Publications: 1. Liu, X., Yu, C. A., and Yu, L. (2004) The role of extra fragment at the C-terminal of cytochrome *b* (residues 421- 445) in the cytochrome bc_1 complex from *Rhodobacter sphaeroides*, *J. Biol. Chem.* **279**, 47363- 47371;

2. Xiao, K., Liu, X., Yu, C. A., and Yu, L. (2004) The extra fragment of iron-sulfur protein (residues 96-107) of *Rhodobacter sphaeroides* cytochrome bc_1 complex is required for protein stability, *Biochemistry* **43**, 1488-1495.

Name: Xiaoying Liu Date of Degree: May, 2006

Institution: Oklahoma State University Location: Stillwater, Oklahoma

Title of Study: STUDIES OF EXTRA FRAGMENTS OF CYTOCHROME bc_1 COMPLEX FROM *RHODOBACTER SPHAEROIDES* AND THE INTERACTION BETWEEN CYTOCHROME caa_3 AND F_1F_0-ATP SYNTHASE FROM ALKALIPHILIC *BACILLUS PSEUDOFIRMUS* OF_4

Pages in Study:161 Candidate for the Degree of Doctor of Philosophy

Major Field: Biochemistry and Molecular Biology

Scope and Method of Study: Although bacterial enzymes have simpler subunit composition than their mammalian counter parts, the sizes of core subunits (cytochrome *b*, ISP and cytochrome c_1) are generally larger. Are these extra fragments required for bacterial bc_1 complex? To answer this question, we studied two of these extra fragments through the molecular genetic manipulation of *Rhodobacter sphaeroide* (*R.S.*) bc_1 complex at various positions of residues 421- 445 in cytochrome *b* and residues 96-107 in ISP. bc_1 activity assay, SDS-PAGE, western-blotting, DSC, and EPR, were used to characterize the mutants. To elucidate the quinone binding site of the bc_1 complex, we generated and characterized some mutants in *R.S.* bc_1 complex based on the structural analysis of the low resolution of co-crystal of bovine bc_1 complex with 5-Br-Q_0C_{10}. There is a hypothesis alkaliphile oxidative phosphorylation at very alkaline pH values involves the required respiratory chain proton pumping to the bulk phase to establish a membrane potential and also involves the use of one or more specific respiratory chain complexes to transfer protons to F_0 sector of the F_1F_0 ATP-synthase during dynamic protein-protein interaction. To test this hypothesis, the interaction between cytochrome caa_3 and F_1F_0-ATP synthase from alkaliphilic *Bacillus pseudofirmus* OF_4 was studied by using DSC and saturation transfer EPR.

Findings and Conclusions: Our data demonstrated that both extra fragments are required for bacterial bc_1 complex. The first 12 residues (residues 421- 432) of the C-terminal extra fragment of cytochrome *b* in the cytochrome bc_1 complex from *Rhodobacter sphaeroides* are essential for maintaining structural integrity of the bc_1 complex. The ISP extra fragment (residues 96-107) is found to be required for the structural stability of ISP in this bacterial bc_1 complex. Both of these findings suggest that these two extra fragments possess the supernumerary subunit function in stabilizing the structure of the bacterial complex. Quinone binding site is an ongoing project, we haven't got very good results yet. From the results of DSC and ST-EPR experiments, we concluded cytochrome caa_3 and F_1F_0-synthase from alkaliphilic *Bacillus pseudofirmus* OF_4 exist as a supermacromolecular complex in the membrane.

ADVISER'S APPROVAL: Chang-an Yu